Acknowledgements

Contents list

Chapter 1 Introduction

1.1 Background and motivation

Laser was invented in the year 1960, the time just passes half century from then, but laser has dramatically changed our world. Some of the laser applications are well known in our daily life like CD and fiber optical internet; some of the applications are far from ordinary people and at the cutting edge of scientific research like attosecond science and National Ignition Facility. With non-stopping intensive research and development in recent decades, more and more applications go out of laboratory: laser manufacturing, medical surgery, metrology, data storage, communications, displays, spectroscopy, microscopy, energy technology, scientific and military applications. No matter you know them or not, laser has a close relation with everyone. Nowadays, the development of laser is faster and faster and people are trying to study more to control the "special light" to change our world.

The past decades has witnessed the revolution in the types and performance of solid-state lasers. Especially after the narrow-band powerful pump source laser diodes became widely available[1]. Compared with traditional lamp pump source, diodes promise high efficiency, intensive and small size for various laser ions. Another major advantage is that diode pump methods can improve the mode-matching between pump beams and laser beam to increase the laser efficiency. The penetrations of diode pumped solid-state laser (DPSSL) in commercial market lead to compact, low cost, reliable and long life laser system for various requirements of applications. In laboratory, researchers are still pursuing high-energy, high-peak power DPSSLs. Like the unique edge-pump face-cooling microchip laser is good candidate for high power solid-state laser system because of the good heat transport geometry and efficient

cooling method. Besides, it separates the pump, cooling and lasing directions making the design much easier for each term. With the flexibility of pump design, the pump can be controlled to realize different kinds of pump shape to fit transverse modes. Like the widely popular end-pump Gaussian-like pump shape, which is critical for fundamental mode generation, can be realized by multi-direction edge-pump scheme by the design of pump overlapping.
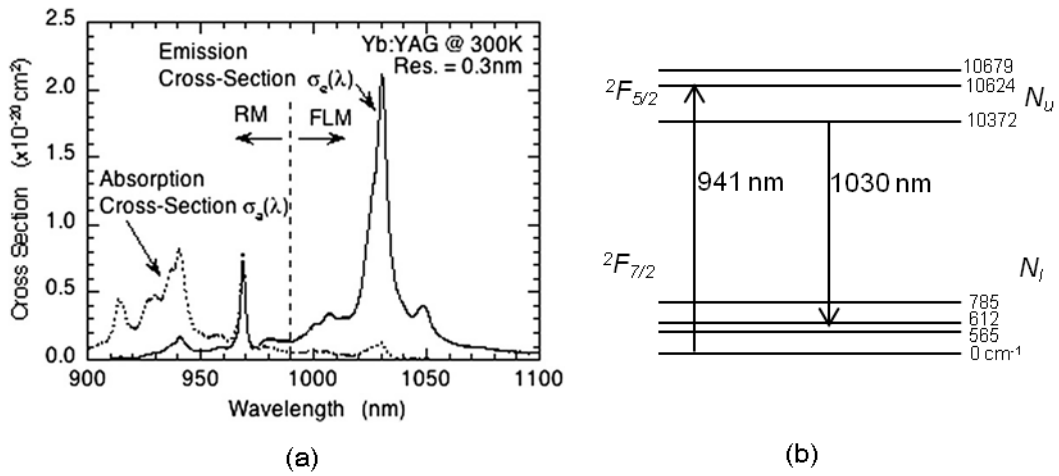
Figure 1.1 (a) room temperature Yb:YAG absorption and emission spectrum (b) relevant energy level.

Consider about the gain media, a trivalent-ytterbium-ion (Yb^{3+}) doped YAG is very promising for high power, high efficiency and short pulse operation[2,3]. Figure 1.1 shows (a) room temperature Yb:YAG absorption and emission spectrum[4] and relevant energy level[5]. The absorption spectral region lies between 900 nm to 980 nm, which is suitable for emission of InGaAs laser diodes. Usually, the pump of Yb:YAG is performed at 941 nm at the peak of the second strong and relatively broad bandwidth ~18 nm. The emission bandwidth is ~8 nm at 1030 nm, which is enough for sub-picosecond pulses generation. Yb:YAG has a small quantum defect of 9%, which dramatically decrease the thermal load compared with 24% of Nd:YAG. The longer upper state lifetime of ~1 ms prolongs the energy storage lifetime. Yb^{3+} ion has very simple two $4f$ manifolds, no undesirable loss processes such as excited-state

absorption and up-conversion. As a result, Yb:YAG has several advantages relative to Nd: YAG for diode laser pumping and ultrafast lasers. In 1991 and 1993 T. Y. Fan demonstrated the room temperature diode pumped Yb:YAG CW laser[6] and Q-switched pulsed laser[7]. The power scaling of single crystal Yb:YAG was soon demonstrated over kilo watts CW output power[8,9] in end and side pump rod and face pump disk laser[10]. By far the highest average power 275 W and highest pulse energy 41μJ pluses laser were achieved by passive mode-locked thin disk Yb:YAG laser[11,12].

Yb:YAG laser has peak emission at 1030 nm due to the transition between the lowest Stark level of $^2F_{5/2}$ manifold at 10372 cm^{-1} and the Stark level of $^2F_{7/2}$ manifold at 612 cm^{-1}. At room temperature, the latter Stark level contains a thermal population equal to 4.2% of Yb ions in the $^2F_{7/2}$ manifold. Thus, near room temperature, Yb:YAG laser exhibits quasi-four-level character, at least 5.6% of all Yb ions must be pumped into the upper manifold to achieve gain media transparency, compared with four-level laser like Nd:YAG laser the number is almost 0. As a consequence, the un-pumped laser medium causes re-absorption loss at the laser wavelength; this can be used for soft-aperture or loss. As the nature of quasi-four-level laser material, the re-absorption loss is particularly useful in aiding transverse mode shaping and selection, which is an additional advantage when Yb:YAG comes to generate high order transverse modes.

Yb:YAG has been demonstrated as a promising candidate for high power DPSSLs. However, difficulties in growing large-sized crystals and their poor thermo mechanical properties are preventing their further progress, especially for power scaling. Recently, transparent polycrystalline ceramics are making an impact in the development of solid-state lasers because of their numerous advantages over melt growth methods, like faster production times, large size, lower cost, better optical homogeneity and better mechanical properties[4,13]. One obvious advantage is the composite structure ceramic, which can be used for thermal dissipation, doping design, pump waveguide and suppression of amplified spontaneous emission (ASE).

For a long time people pay attention only on the diffraction-limited fundamental Gaussian beam because of the good beam quality and high-brightness. Just in recent year, great interest has been shown in the generation of high-order beams including paraxial wave family: Hermit-Gaussian modes (HG) and Laguerre-Gaussian modes (LG). The new properties of laser beam were brought out by these high-order modes to generate new physics phenomena. Like in the optical trapping science, normal transparent particles with higher refractive index than the surrounding environment can be trapped near the focal area of fundamental mode beam[14]. But, for these particles with low index or metal target and heat strongly absorbed ones it is difficult to deal with[15,16] because of unbalanced resultant force or heating effect. In these cases, circle density laser beam dark trapping are required. People find that the vortex beam (like high-order LG modes) possesses the orbital angular momentum mixed with phase singularity can transfer[17] these properties to micro-partials or atoms for trapping, guiding and manipulating[18,19,20,21]. Not only limited in scalar beam, the vector beam (radial or azimuthal polarized) has more applications in super-resolution microscopy and laser processing[22,23]. Even HG_{mn} modes have the potential application in multiple trapping laser tweezers[24]. Vortex arrays modes could be applied for dark optical two-dimensional trapping as new class of optical tweezers for physics, chemistry biology and medical science application. In spite of so many exciting applications, most of researches are only limited in end-pump Nd^{3+} lasers[25,26]; the high-order modes are limited in HG_{m0} modes and single vortex modes; the power is as low as several mW which is not enough for the applications.

While Yb:YAG ceramic has been proving itself as a potential gain media, until now there are not too many research on Yb:YAG high-order modes generation. In addition, there is no research to bring it into the study of mode control based on edge-pumped microchip towards high-power; especially we found the importance of re-absorption loss mechanism in quasi-four-level material for mode-selection process. We have studied on the mode-control theory in both fundamental mode and

high-order modes towards high-power. We experimentally demonstrated various high-order modes generation especially the HG_{mn} and vortex arrays with relative high power of W level.

Recently, high brightness diode lasers enable to pump solid-state laser directly without any optical coupling device, which we introduce lens-less edge-pumped microchip scheme in this thesis. The scheme dramatically decreases the size of DPSSL, simplifies the system and increase the reliability of solid-state laser. It is the goal of our research to make DPSSL more compact, more powerful and easy-operation of transverse mode.

1.2 Content of this thesis

In chapter 2, we introduce the design principle of edge-pumped laser module based on the composite ceramic Yb:YAG and diode pump source. We also study the pump shape in our current 4-direction diode stacks edge-pumped microchip laser. We simulate the mode selection between TEM_{00} mode and TEM_{01} mode under different pump shape. The simulation results indicate that Gaussian-like pump shapes are preferable for high-power TEM_{00} mode generation; contrarily, top-hat shape and basin shape are easy to break into multi mode oscillation.

In chapter 3, we design the lens-less edge-pumped microchip laser, which is directly pumped by single-emitter diode chips from multi-direction. The lens-less design is compact and efficient for the coupling of pump beam; the multi-direction pump scheme can realize the desired pump shape by pump manipulation. As the experimental result, the 9-direction edge-pumped laser module was successfully assembled. The measured fluorescence image shows us the Gaussian-like pump shape, which is greatly agreed with our calculation. We also propose the optimized pump shape by simulation towards uniform ideal shape for high-power TEM_{00} mode generation.

The mode control study does not only rest on fundamental mode, because of the

booming high-order modes researches. Chapter 4 focuses on the high-order Hermit-Gaussian (HG) modes and vortex modes generation. Compare with traditional end-pumped scheme, which is only limited in HG_{n0} modes and several mW level, the edge-pumped microchip laser with big gain aperture shows the advantage both in power scaling and desired mode generation. The pump design can realize complex pump shape concerning with high-order mode. It is easy to scale the HG_{n0} to HG_{nm} by the method of two-dimensional pump manipulation. In addition, the re-absorption loss of Yb:YAG can suppress un-wanted mode competition. By using our 9-directions edge-pumped microchip laser module and V-type laser cavity, we experimentally realized the generation of HG_{n0} modes with the highest index number n=22 and HG_{nm} modes with index number $1<n, m<7$. The continuous wave output power of these HG modes is from mW to several W. Next, we demonstrated the vortex beam and vortex arrays generation directly from the laser oscillator, as vortex modes can be simply represented by a superposition of HG mode pairs with locked phase shift of $\pi/2$. By carefully selecting the mode areas across the gain aperture on microchip, we got 7 W of doughnut shape vortex beam and hundred mW to several W vortex array modes.

The theory study and experimental demonstration in chapter 4 show us, it is promising to design the laser module for the generation of desired transverse mode towards efficient and high power. In chapter 5, we propose the laser module design to achieve hundred-W-level doughnut mode as an example of high-order mode selection and power scaling. By numerically calculation, we can achieve 150 W output power with 24.2% optical-optical conversion efficiency by using a 4.25 mm diameter Yb:YAG microchip. The re-absorption loss plays the important role for mode-selection and scale about 2 times output power of selected doughnut mode. Since most of the mode-selection experiments are based on Nd^{3+} doped laser material, in our case, purer mode and better mode selectivity will be expected. Moreover, not only limited in HG modes and vortex modes generation, we expect edge-pump system will show the advantage in high-power Laguerre-Gaussian scalar modes, even vector

beams generation in soon.

In chapter 6, there is a conclusion.

---

[1] Jankiewicz, Z., and K. Kopczynski. "Diode-pumped solid-state lasers." Opto-Electron. Rev 9.1 (2001): 19-33.

[2] Dominik Bauer, Ivo Zawischa, Dirk H. Sutter, Alexander Killi, and Thomas Dekorsy, "Mode-locked Yb:YAG thin-disk oscillator with 41 µJ pulse energy at 145 W average infrared power and high power frequency conversion," Opt. Express 20, 9698-9704 (2012)

[3] Clara J. Saraceno, Florian Emaury, Oliver H. Heckl, Cyrill R. E. Baer, Martin Hoffmann, Cinia Schriber, Matthias Golling, Thomas Südmeyer, and Ursula Keller, "275 W average output power from a femtosecond thin disk oscillator operated in a vacuum environment," Opt. Express 20, 23535-23541 (2012)

[4] Taira, Takunori. "Ceramic YAG lasers." *Comptes Rendus Physique* 8.2 (2007): 138-152.

[5] Takunori Taira, William M. Tulloch, and Robert L. Byer, "Modeling of quasi-three-level lasers and operation of cw Yb:YAG lasers," Appl. Opt. 36, 1867-1874 (1997)

[6] P. Lacovara, H. K. Choi, C. A. Wang, R. L. Aggarwal, and T. Y. Fan, "Room-temperature diode-pumped Yb:YAG laser," Opt. Lett. 16, 1089-1091 (1991)

[7] T. Y. Fan, S. Klunk, and G. Henein, "Diode-pumped Q-switched Yb:YAG laser," Opt. Lett. 18, 423-425 (1993)

[8] Bruesselbach, Hans, and David S. Sumida. "A 2.65-kW Yb: YAG single-rod laser." Selected Topics in Quantum Electronics, IEEE Journal of 11.3 (2005): 600-603.

[9] Sumida, David S., et al. "High-power Yb: YAG rod oscillators and amplifiers." Optoelectronics and High-Power Lasers & Applications. International Society for Optics and Photonics, 1998.

[10] Yuan Han Peng, Yu Xian Lim, James Cheng, Yipei Guo, Yan Ying Cheah, and Kin Seng Lai, "Near fundamental mode 1.1 kW Yb:YAG thin-disk laser," Opt. Lett. 38, 1709-1711 (2013)

[11] Dominik Bauer, Ivo Zawischa, Dirk H. Sutter, Alexander Killi, and Thomas Dekorsy, "Mode-locked Yb:YAG thin-disk oscillator with 41 µJ pulse energy at 145 W average infrared power and high power frequency conversion," Opt. Express 20, 9698-9704 (2012)

[12] Clara J. Saraceno, Florian Emaury, Oliver H. Heckl, Cyrill R. E. Baer, Martin Hoffmann, Cinia Schriber, Matthias Golling, Thomas Südmeyer, and Ursula Keller, "275 W average output power from a femtosecond thin disk oscillator operated in a vacuum environment," Opt. Express 20, 23535-23541 (2012)

[13]Taira, Takunori. "RE $^{3+}$-Ion-Doped YAG Ceramic Lasers." Selected Topics in Quantum Electronics, IEEE Journal of 13.3 (2007): 798-809.

[14]A. Ashkin, J. M. Dziedzic, J. E. Bjorkholm, and Steven Chu, "Observation of a single-beam gradient force optical trap for dielectric particles," Opt. Lett. 11, 288-290 (1986)

[15]Shu-Chun Chu, Takayuki Ohtomo, and Kenju Otsuka, "Generation of doughnutlike vortex beam with tunable orbital angular momentum from lasers with controlled Hermite-Gaussian modes," Appl. Opt. 47, 2583-2591 (2008)

[16]Heckenberg, N. R., Friese, M. E. J., Nieminen, T. A., & Rubinsztein-Dunlop, H. (2003). Mechanical effects of optical vortices. arXiv preprint physics/0312007.

[17]Simon Parkin, Gregor Knöner, Timo A. Nieminen, Norman R. Heckenberg, and Halina Rubinsztein-Dunlop, "Measurement of the total optical angular momentum transfer in optical tweezers," Opt. Express 14, 6963-6970 (2006)

[18]E. Santamato, A. Sasso, B. Piccirillo, and A. Vella, "Optical angular momentum transfer to transparent isotropic particles using laser beam carrying zero average angular momentum," Opt. Express10(17), 871–878 (2002).

[19]Y. Song, D. Milam, and W. T. Hill III, "Long, narrow all-light atom guide," Opt. Lett.24(24), 1805–1807 (1999).

[20]W. M. Lee, X.-C. Yuan, and W. C. Cheong, "Optical vortex beam shaping by use of highly efficient irregular spiral phase plates for optical micromanipulation," Opt. Lett. 29, 1796-1798 (2004)

[21]A. T. O'Neil and M. J. Padgett, Axial and lateral trapping efficiency of Laguerre-Gaussian modes in optical tweezers, Opt. Commun. 193, 45-50 (2001)

[22]Qiwen Zhan, "Cylindrical vector beams: from mathematical concepts to applications," Adv. Opt. Photon. 1, 1-57 (2009)

[23]M. Meier, V. Romano, and T. Feurer, "Material processing with pulsed radially and azimuthally polarized laser radiation," Appl. Phys. A 86, 329–334 (2007).

[24]Rene Eriksen, Vincent Daria, and Jesper Gluckstad, "Fully dynamic multiple beam optical tweezers," Opt. Express **10**, 597-602 (2002)

[25]Y. F. Chen, T. M. Huang, K. H. Lin, C. F. Kao, C. L. Wang, and S. C. Wang, "Analysis of the effect of pump position on transverse modes in fiber-coupled laser-diode end pumped lasers," Opt. Commun.136(5-6), 399–404 (1997).

[26]Shu-Chun Chu, Yun-Ting Chen, Ko-Fan Tsai, and Kenju Otsuka, "Generation of high-order Hermite-Gaussian modes in end-pumped solid-state lasers for square vortex array laser beam generation," Opt. Express 20, 7128-7141 (2012).

Chapter 2

Edge-pumped Yb:YAG ceramic microchip laser

Related paper:

W. Kong and T. Taira, "Lens-less edge-pumped high power microchip laser," Appl. Phys. Lett., vol. 100, no. 14, pp. 141105-1-4 (2012).

2.1 Introduction

This chapter is the basic and theory of high-power DPSSL module design. We begin with properties of rate equation, laser material, pump source, pump scheme and cooling method. Based on above, mode selection in edge-pumped system is explained theoretically.

2.2 Solid-state laser

The world has changed a lot, since the first experimental demonstration of LASER (**L**ight **A**mplification by **S**timulated **E**mission of **R**adiation) in 1960[1]. Even for normal people, we enjoy a lot of "lasers" in our daily life, such as DVD players, laser printers, laser TV and barcode scanners. Furthermore, the laser can be used in medical surgery, material processing, metrology, spectroscopy, microscopy, communications, lighting displays, scientific applications and so on[2]. Until today, more and more useful applications are developing in the labs based on the flexible characteristics of lasers.

The laser system provide the various output parameters including: average output power, peak power, pulse width, pulse repetition rate, line width, spectral range and spatial beam characteristics[3]. Based on different applications, it is possible to design the laser system to optimize the performance. The history of laser is the development history of laser material and laser pump source as well as the laser engineering. The trend is towards high power, room temperature cooling, better electrical-optical conversion efficiency and all-solid state. For the pump schemes and laser configuration, compact, reliability, low cost and easy operation are favourable.

The design of a laser system is started from laser module design followed by laser configuration or resonator design. The laser module design includes: (a) the choice of the laser material: the size, shape, gain, energy storage and spectral properties; (b) pump source, pump scheme and thermal dissipation method. The laser configuration and resonator design are related to different application, aiming to various output parameters: such as mode-locked laser, Q-switched laser, HG (harmonic generation), OPO (optical parametric oscillator), OPA (optical parametric amplifier), CPA (chirped pulse amplifier) and so on. The pump schemes need to consider several aspects: the efficiency, the optical design and energy distribution. Under the condition of acceptable absorption efficiency and the relevant simple and low cost optical design, the energy distribution is quite important, because that the distribution governs spatial overlap of mode, uniformity, divergence and optical distortions. Depending on the shape of active material and the position of pump source, side-, edge-, end- and face-pumped schemes are named. For high-power laser, side- or end-pumped rod, side-pumped slab, face-pumped disk and edge-pumped microchip are common schemes. The key issue of high-power laser is the method of thermal dissipation under the condition of enough energy absorption. For the rod and slab type, the energy gain (also the heat generation) volume and cooling area are lengthened for enough absorption and cooling. Obviously, it is more difficult for bulk (rod or slab) laser to scale up the power in a limited pump geometry volume.

Normally they become very big when power scaling. In the disk and microchip type, the gain aperture is enlarged (>1 mm) for power scaling and the thickness is minimized (normally less than 300 μm) to shorten the cooling path[4].The disk laser applies multi-pass face pump and microchip laser applies waveguide edge-pump for efficient absorption.[5]

2.3 Rate equation of Yb:YAG

In the quasi-four-level laser system, the lower level is very close to the ground state, a finite population exists at the Stark level of lower manifold. So, re-absorption on the laser wavelength will happen in the non-pumped area of laser material, which requires high-intensity pumping, high-brightness pump source and good thermal dissipate method. The transparency can be reached as soon as the pumping reaches certain intensity.

As a typical example of quasi-four-level laser, the energy level diagram of Yb:YAG and transition cross-section spectrum are shown if Fig 1.1. Yb^{3+} ion has only two $4f$ manifolds, the ground state $^2F_{7/2}$ and excited state $^2F_{5/2}$. The energy level of upper and lower level separate about 10000 cm^{-1}. Spectral band is available for pump at wavelength around 941 nm with relative strong peak and broad bandwidth as well as around 969 nm with strongest peak and narrow bandwidth. Emission bandwidth is ~8 nm at 1030 nm, broad enough suitable for sub-picosecond pulse operation. The quantum defect is only 9%. The energy level is so simple that no additional $4f$ energy levels compared with other trivalent rare earths. By neglecting all processes such as excited state absorption and upstate conversion, the simplified energy levels then become two with the populations N_u of upper state and N_l of lower state respectively. The total population number is $N_t = N_l + N_u$.
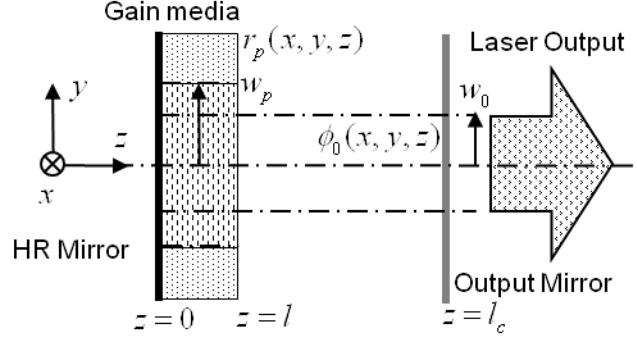
Figure 2.1 Scheme of solid state laser system.

Figure 2.1 shows the scheme of solid state laser system, considering the spatial distribution of the pump energy $r_p(x,y,z)$ and the spatial distribution of the laser photons $\phi_0(x,y,z)$. The x, y, z axis in Fig.2.1, where x and y are the transverse coordinate and z is the coordinate along the laser output. The radius of laser material is bigger than the radius of pump w_p. The radius of laser is w_l. The laser system has a cavity length of l_c and the laser material has a thickness of l. By neglecting the depletion of the ground state, the distribution of the population inversion density is given by the equation: $\Delta N(x,y,z) = N_u(x,y,z) - N_l(x,y,z)$. The rate equations for a solid state laser system by a certain pump scheme can be started from a steady state $d\Delta N(x,y,z)/dt = 0$ and $d\Phi/dt = 0$ [6].

$$\frac{d\Delta N(x,y,z)}{dt} = (f_u + f_l)Rr_p(x,y,z) - \frac{\Delta N(x,y,z) - \Delta N^0}{\tau_f}$$
$$- \frac{(f_u + f_l)c\Delta N(x,y,z)}{n}\Phi\phi_0(x,y,z) \qquad (2.1)$$

$$\frac{d\Phi}{dt} = \iiint\limits_{laser\,material} \Delta N(x,y,z)\Phi\phi_0(x,y,z)dv - \frac{\Phi}{\tau_c} \qquad (2.2)$$

Where the $\Delta N^0 = N_u^0 - N_l^0 \approx -N_l^0$ is the un-pumped population-inversion density, τ_f is the fluorescence lifetime, c is the light speed in the vacuum, n is the refractive index of laser material, σ is the laser transition cross section, $\tau_c = 2l_c/cL_{i,T}$ is the

cold-cavity life-time. $L_{i,T} = L_i + T$ is the round-trip cavity loss including the intrinsic

cavity loss L_i and the output transmission loss T. The diffusion of the excited state

ions is neglected. The total pump rate can be given by: $R_p = \eta_p \eta_a P_p / h v_p$, The total

number of photons inside the cavity is given by $\Phi = 2l_c P_0 / cTh v_l$. Where P_p is the

incident pump power, P_0 is the output laser power, h is the Planck constant, v_p

and v_l are the pump and laser emission frequencies respectively. η_p is the pump

quantum efficiency which is the number of ions in upper manifold created by one

absorbed photon, in the case of Yb:YAG approximate to 1, η_a is the absorption

efficiency.

By using $\iiint\limits_{Laser\,material} r_p(x, y, z) dv = 1$ and $\iiint\limits_{Cavity} \phi_0(x, y, z) dv = 1$, the special

distribution of pump and photons are normalized inside the laser material volume and

laser cavity volume. Define the effective mode volume as:

$$V_{eff} = \frac{1}{\iiint\limits_{Laser\,material} \phi_0(x, y, z) r_p(x, y, z) dv} \qquad (2.3)$$

which considering the overlap of pump $r_p(x, y, z)$ and laser mode $\phi_0(x, y, z)$.

It is easy to derive the threshold of pump power when $\Phi = 0$ and

$R_{th} = \eta_p \eta_a P_{th} / h v_p$:

$$P_{th} = \frac{h v_p V_{eff} L_{i,T,r}}{2\eta_a \eta_p l (f_u + f_l) \sigma \tau_f} \qquad (2.4)$$

Where $L_{i,T,r} = L_i + T + 2N_l^0 \sigma l$ is the total loss including re-absorption term $2N_l^0 \sigma l$

of quasi-four-level laser material.

2.4 Edge-pumped scheme and power scalability

The edge-pumped microchip scheme is shown in Fig.2.1. The shape of the laser material is round shape generally in order to get the uniform pump shape. The position of pump is changed to *x-y* coordinate instead of along the *z* axis, so called edge-pumped scheme. In order to give more space for pump arrangement, the waveguide is introduced. The pump power enters the waveguide and is delivered by total internal reflection. The shape of waveguide could be round or polygon
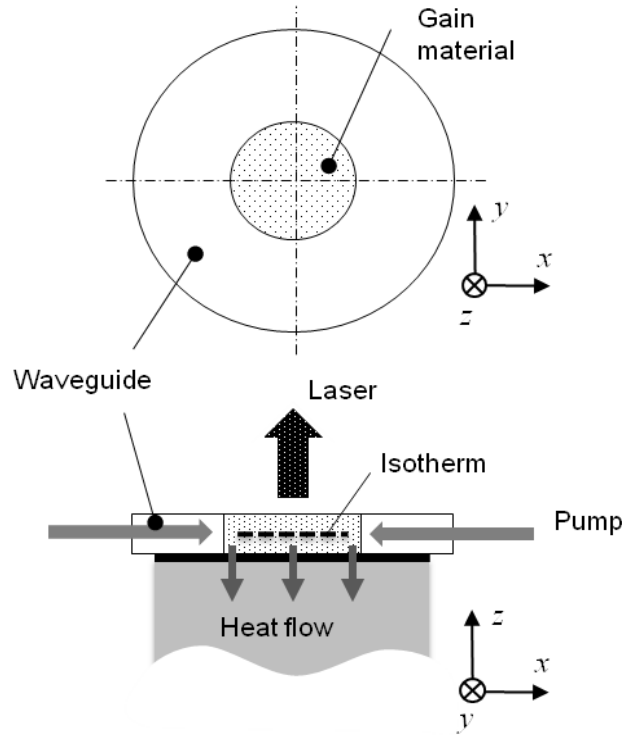
Figure 2.2 The scheme of edge-pumped solid state laser.

depending on the pump source and optical coupling method. The heat is generated inside the laser material. Use R, r and l to define the radius of waveguide, radius of laser material and thickness of laser material. When $r >> l$, under the condition of uniform pumping and face cooling, the heat will flow almost one dimensional to the heat-sink. This will dramatically reduce the transversal temperature gradient and phase distortions transferring to the laser direction. All the thermal-lens effects can be minimized by the reduction of l. Different from the pump method of thin disk laser, the absorption efficiency only depends on the r; it is possible to minimize the l without

considering the absorption efficiency, the limitation is only technique: the fabrication method of a thinner microchip and preventing from break.

The edge-pumped method realizes the separation of the pump, cooling and laser interface. The separation of pump and cooling dramatically simplify the solid state laser module design, offering flexibility for both pump system and cooling system. In engineering consideration, people could design the pump and cooling separately. The separation of pump and laser offer another possibility for intra-cavity applications, such as second-harmonic generation[7], passively Q-switched laser[8] and secondary material inserted without worry about the block of pump beam.

The power scalability of edge-pumped microchip laser promises high average power operation without significant optical distortion and thermal fracture. Consider the pump situation in laser material; the transparent pump power P_{th} is the laser threshold that decided mainly by the volume and doping ratio. One limitation of the power scaling is the stress fracture of the laser material if the volume is given. To define the power scaling figure of merit as: $\Upsilon = P_F / P_{th}$, where P_F is the fracture damage pump power caused by stress. The Υ of face pumped thin disk laser can be expressed by[9]:

$$\Upsilon_{face-disk} = (\frac{12R_s\tau_f\sigma}{\eta_h h\nu_p})(\frac{f_l+f_u}{f_l})\frac{1}{\ln\frac{1}{1-\eta_{min}}}\frac{N}{l} \qquad (2.5)$$

Where R_s is the material tensile factor, which is proportional to the tensile stress at the fracture damage, R_s it only has relationship with the material property. η_{min} is the minimum absorption efficiency acceptable for practical design. Similarly, the Υ of edge-pumped microchip can be written as:

$$\Upsilon_{edge-microchip} = (\frac{12R_s\tau_f\sigma}{\eta_h h\nu_p})(\frac{f_l+f_u}{f_l})\frac{1}{\ln\frac{1}{1-\eta_{min}}}\frac{2r}{l^2} \qquad (2.6)$$

Where r is radius of the microchip core. Compare Υ of the two pump method. Use

$\Upsilon_{edge} / \Upsilon_{face} = 2r / Nl$, r=1.5 mm and l=0.2 mm. The edge-pumped scheme is almost equal to N=15 passes pump beam of thin disk laser. Edge pumped scheme could make the microchip thinner, for example l=0.1 mm, which equal to N=30 passes of pump beam in thin disk laser. The power scalability is same as thin disk laser by increasing the size of r. Edge-pumped scheme has the advantage to minimize the thickness to scale the figure of merit. The thermal problem and optical distortion are also minimized. In addition, the simplified pump scheme, compact structure and low fabrication cost make it suitable for cascade active mirrors without significant optical distortion accumulation.

2.5 Yb:YAG composite ceramic microchip

Yb:YAG is very promising for high power short pulse generation. Because it has the small quantum defect leading to less thermal load; lacking of excited state absorption and up-conversion are suitable for intensive pump; the broad absorption bandwidth is good for absorption and against pumping wavelength shift; sufficient emission bandwidth is available for sub-picosecond pulse generation.

Transparent ceramic laser material was firstly developed in the year of 1995 by Ikesue[10] and became very attractive because several advantages compared with single crystal. The ceramic material can be mass produced with lower cost, shorter time and bigger size compared with single crystal. Nowadays, the optical quality of ceramic YAG has been much improved to compare with single-crystal, in addition, the mechanical toughness, hardness and the stress resistance are better than single crystal[11]. In 2007, Tsunekane and Taira of our group demonstrated the diode edge-pumped microchip laser by using composite structure all-ceramic Yb:YAG microchip, which taking place of the single crystal core and surrounding ceramic waveguide microchip, achieving 414 W cw output power[12]. In the case of all-ceramic microchip, the boundary loss between laser material and waveguide is avoided, the different material mismatch of thermal expansion also eliminated. This demonstrate

the promising Yb:YAG composite ceramic for high-power solid-state lasers. In addition, the composite ceramic material offers a big flexibility in design of the shape and optical properties (doping area, doping gradient and doping material). The easy shape-forming is good for various pump methods. The doping design could be used for ASE absorber[13], pump shape control and mode-selection, which is another topic for our future research.
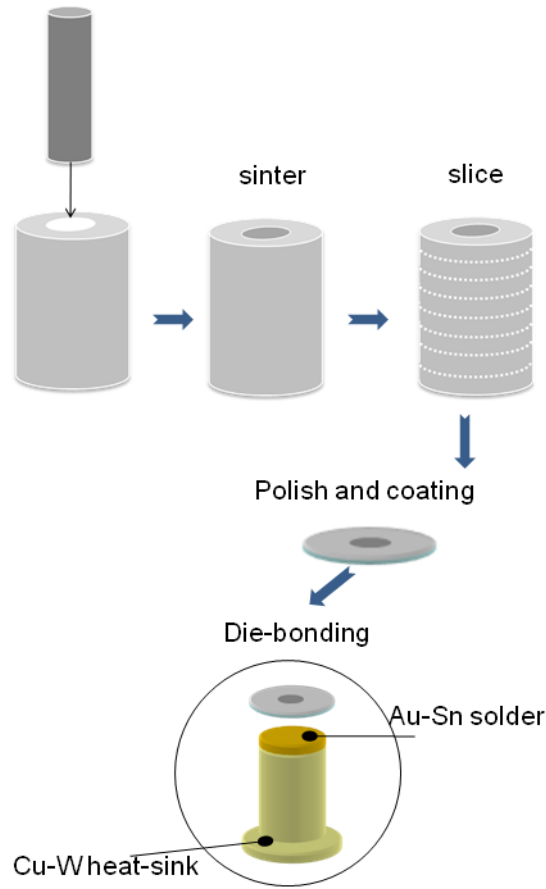
Figure 2.3 The fabrication procedure of all-ceramic microchip bonding on water-cooling heat-sink

As an example of our microchip fabrication method[14], Fig 2.3 shows the procedure from the rough material until hundreds watts available water-cooling all-ceramic microchip. Firstly, the doped core rod is inserted to the un-doped clad and shape-formed by sintering[15]. Secondly, the composite rod is sliced to chips, followed by polishing, optical coating and metallization. Finally, the microchip is die-bonded to

prepared heat-sink[16] by gold-tin solder; the material of heat-sink is CuW, which has the similar thermal expansion coefficient with YAG ceramic.

For all of the available microchips in our laboratory, which will be used in this thesis, are summarized as in Tab.2.1. The quality of every microchip is slightly different depending on the material, processing, coating and bonding. But all of them are available for 100 W multimode operations without break.

It is worthy pointing that the practical limitation of the waveguide diameter size is less than 9 mm. Because the current facility of ceramic maker only fabricate the composite rod with the diameter of 10 mm efficiently, it can be sliced to over ten pieces; but the rod with the diameter over 10 mm only can be sliced into a few, so the price becomes very high. This is only the problem for small quantity of experiment, if large quantity is needed; the price could be very low compared with single crystal. After cutting and polishing the 10 mm rough material, the finished microchips become 8~9 mm size.

Table 2.1 The available microchip specification

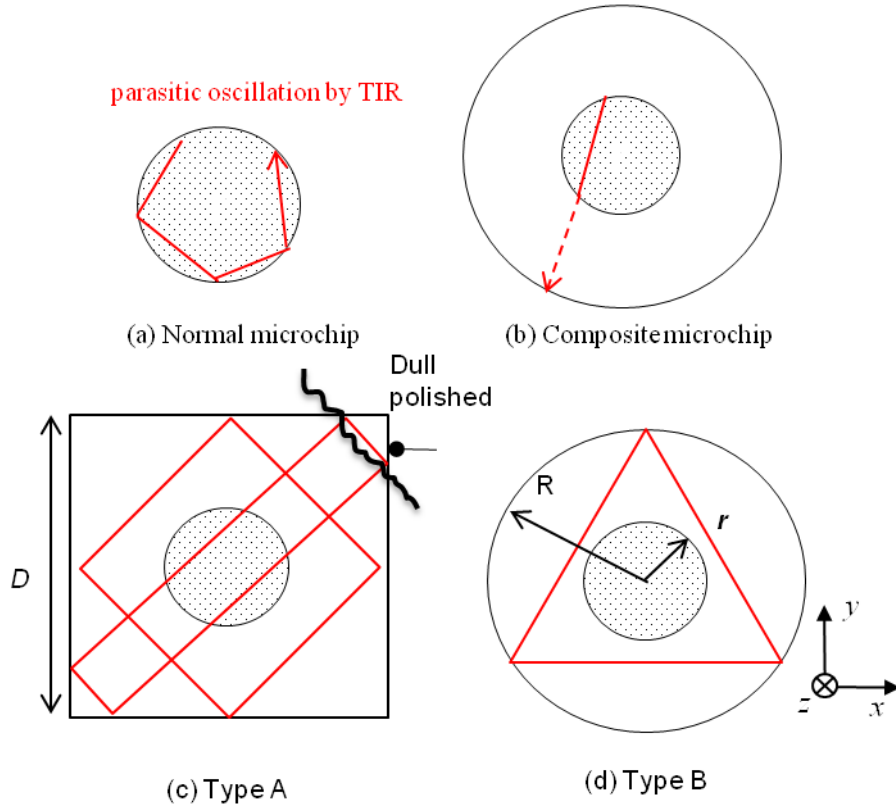| Specification	Unit	Microchip type	
		Type A	Type B1; Type B2
Yb^{3+} doping rate	at. %	9.8	9.8
Core shape, radius r	mm	Round, 1.5	Round, 1.5 ;1.9
Clad shape, size	mm	Square, side length D=8	Round, R=4.26
Thickness l	μm	200	200
Treatment		Edge-polished	Edge-polished

Figure 2.4 The sketch of parasitic oscillation in the microchip.

Compared with traditional microchip (in Fig.2.4 (a)), the composite microchip avoids most of the possible total internal reflection (TIR) parasitic oscillation (as described in Fig.2.4 (b) dash line). The treatment of edge-polished microchip is good for the coupling of pump power, but it will still exist several type of parasitic oscillation inside the microchip as shown in Fig.2.4 (c) and (d) corresponding to the microchip of Type A and Type B. The method of eliminating parasitic oscillation that we used is to carefully design the size of the waveguide to eliminate the possible paths of parasitic oscillation inside the gain area.

In type A microchip, the parasitic oscillation happens in two ways showed by red lines: the square one and the rectangular one. To eliminate the square one, which means to keep the square dash line outside the gain area, we obtain $r < \sqrt{2}D/4$. To eliminate the rectangular one, it is necessary to dull polish the length $\sqrt{2}r$ around the corners or cut along the hand-drawing line and dull polish the corner.

In type B, it is much easier: only keep the regular triangle dash line outside the gain area. We can obtain $r < R/2$.

2.6 Pump source of diode lasers

It is no doubt that the most efficient pump source for solid-state laser is semiconductor diode lasers. The diodes have the high electrical-optical generation efficiency, very narrow emission bandwidth which completely matching the absorption band of a particular laser material. The diodes own extreme small dimension but very high output power, which is suitable for high-power, intensive pump and flexible for all kinds of pump scheme. Laser diodes exhibit long lifetime, which dramatically increases the reliability of the total solid state laser system. During last two decades significant progress has been made in developing laser diode. Now, the available commercial laser diodes can cover the range of the wavelength from 375 nm to 2000 nm. The output power can over CW 100 W/cm for Nd^{3+} and Yb^{3+} laser with the efficiency above 50%. As Yb:YAG laser pump source, InGaAs-GaAs diode is quite suitable at the wavelength 915-980 nm with a spectral width about 3~4 nm and wavelength shift 0.3 nm/K. Many type of diodes including: diode chips, diode bars, diode stacks, vertical-cavity surface-emitting diode and fiber coupled diode, are available for different kind of pump scheme.
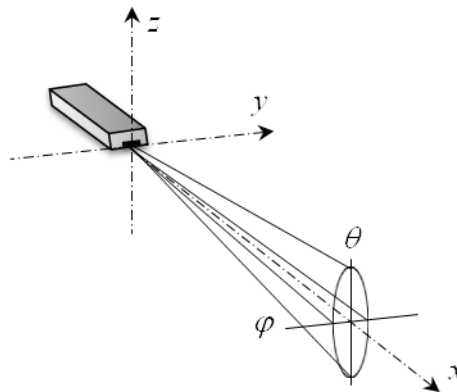

Figure 2.5 The radiation generated by single emitter diode

The laser diodes emit optical radiation with the dimension of emitter around

1μm×100μm in high and in wide respectively. Fig 2.5 shows the optical radiation generated by a single emitter of laser diode. Apparently, the beam let of diode radiation in *z* and *y* axis are not symmetric. The typical divergence in the fast axis *z* is around 30 deg. and in slow axis *y* is around 10 deg. at the full-width half –maximum intensity (FWHM). The single emitter diode normally can emit 1~10 W. Recently, the company of Optoenergy Inc.[17] offers high-brightness single emitter diode chips with the output power over 15 W. The power is enough for achieving over hundreds watts pump by using 10 pieces diode chips or more. The advantage of these chips is: the emitter is pretty small that can be coupled directly inside the waveguide without any focus. Table 2.2 shows the specification of the diode chips offered by Optoenergy Inc. The parameters are used for our calculation and analysis in this thesis.

The far field of spacial intensity profile of the single emitter output can be approximately defined by the equation[18]:

$$P_{chip}(x, y, z) = \frac{P_0}{\pi w^2 \varphi \theta} \exp[-\left(\frac{y - y_s}{x\varphi}\right)^2 - \left(\frac{z}{x\theta}\right)^2] \quad (2.7)$$

Where, the P_0 is the total output power, the (y_s, 0, 0) is the location of the emitter. The θ and φ are the far-field perpendicular FWHM divergence angels of the fast axis and slow axis showed in Fig.2.5. The relationship between FWHM width and $1/e^2$ width can be given by: $w_{FWHM} = w_{1/e^2}\sqrt{2Ln(2)}$.

The diode bar is consisted by several of diode emitter in linear array. Normally, the number of the emitter is 5~20. The commercial diode bar typically can supply the total power over 100 W in CW operation around 940 nm with the emitter number around 12. The aperture size is about 12mm×0.125mm, if use these bars as edge-pumped source, the lens is needed for the collimation and coupling corresponding the smaller core size. One special type diode mini bars are offered by Optoenergy. Inc. The mini bare has the aperture size about 3.5mm×0.125mm with the total power of 80 W from 7 emitter. This size is small enough to pump into the microchip without any focus by lens.

Table 2.2 The specification of single emitter diode chip

Parameters	Unites	Value
Operating light output	W	15
Canter wavelength	nm	938±5
Emitter size	μm×μm	1×100
Aperture size	μm×μm	500×125
Cavity length	mm	6
Spectral width, $\Delta\lambda$	nm	3
Spectral shift, $d\lambda/dt$	nm/K	0.29
Far-field perpendicular FWHM θ; φ	deg.	26; 9
Operating Temperature	$°C$	20

The far field intensity distribution of a beam generated by the diode bar can be described by:

$$P_{bar}(x, y, z) = \frac{1}{2y_0} \int_{-y_0}^{y_0} P_{chip} dy_s \qquad (2.8)$$

where the $2\,y_0$ is the length of the bar aperture. Figure.2.6 shows the far-filed intensity profile generated by one mini bare mentioned above. In the picture show the intensity profile at distances of, $0.2y_0$ $0.5y_0$ and y_0.Using the parameters: θ_{1/e^2} and

φ_{1/e^2} with the number of 39.6 deg. and 15.1 deg. respectively. The intensity profile becomes uniform after the distance y_0.

In many cases, the diode bars are stacked so called diode stacks in order to emit very high output power, over several hundred watts or even thousand watts. The pump power is pretty high and with good pre-collimation of micro-lens. In our laboratory, we have the 4 diode stacks pumped type A microchip laser modules, each of the diode stacks can emit over 250 W at CW operation by 6 diode bars stacked. The pump intensity profile after collimation and focusing is roughly a top-hat shape.
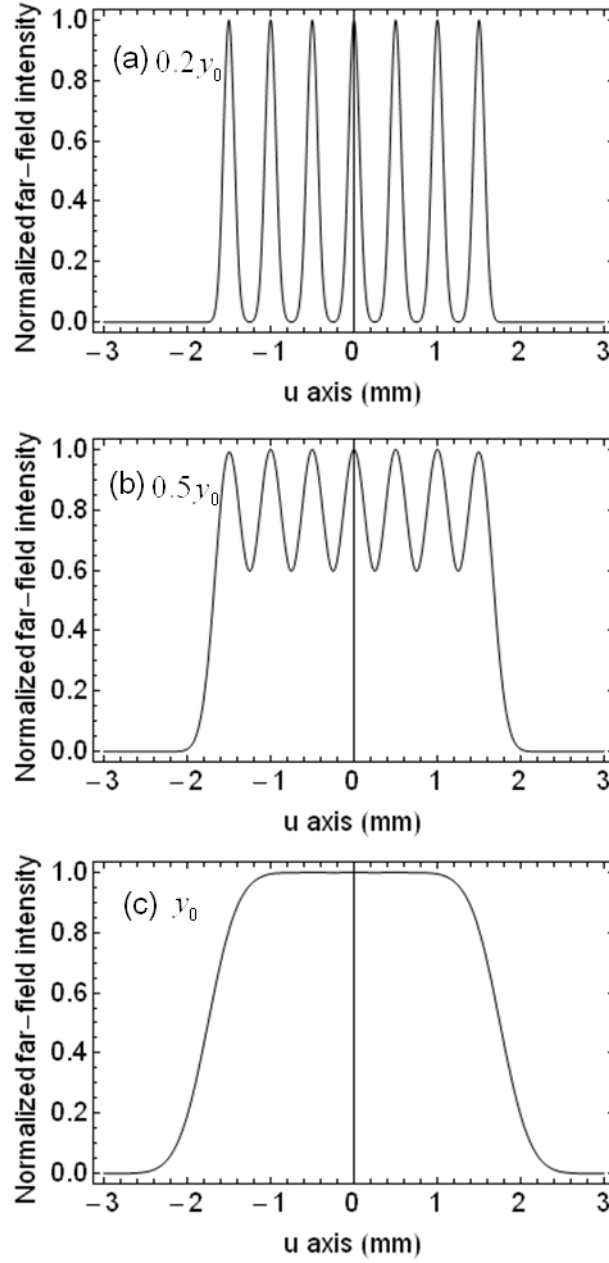
Figure 2.6 The normalized far-field intensity profile of the mini bar at different distance from the emitter aperture plane.

2.7 Absorption efficiency

One of the advantages for edge-pumped scheme is that the absorption efficiency is independent on the laser material thickness. It avoids making the complex multi-pump setup like in thin disk laser module. To increase absorption efficiency, only need to increase the diameter of the laser material, the thickness along the cooling direction can be minimized. The absorption efficiency is written by:

$\eta_a = \eta_c \eta_{abs}$, where the η_c is the coupling efficiency described by $\eta_c = P_{in} / P_p$, the ratio of the power coupling inside the laser material with the total pump power. $\eta_{abs} = 1 - \exp(-\alpha d_p)$, α is the absorption coefficient and d_p is the propagation distance of pump beam inside laser material. In the edge-pumped microchip situation, the pump beam propagate in the laser materials by total internal reflection, the thickness l far less than the diameter of laser material $2r$. It could be approximately replace the d_p by $2r$ for the most simple case. As the shape of laser core is round shape, the d_p varies in different incident position. We use d for the width of top-hat pump beam (the laser stacks or laser bar situation), by neglecting the φ_{1/e^2} (for micro lens collimated stacks, only less than 1 deg. and the beam path in the laser material only several millimetres) η_{abs} can be written as:

$$\eta_{abs,T} = \frac{\int_{-y_s}^{y_s} (1 - e^{-2\alpha\sqrt{r^2 - y^2}})dy}{d} \qquad (2.9)$$
$$(d \le 2r, \; y_s = d/2; \; d > 2r, \; y_s = r)$$

the coordination follows that in Fig.2.4 and incident direction is along the -x axis. Figure.2.7 shows the absorption efficiency η_a as a function of the absorption coefficient α. We assume $\eta_c = 1$ and the Type A microchip situation, which $r=1.5$ mm under the condition of different pump width $d=0$ mm, $d=1$ mm, $d=2$ mm, $d=2.5$ mm. $d=3$mm and $d=4$mm. Base on the result, it is easy to find if the pump width d is same or bigger than the diameter $2r$, the absorption efficiency is not so good. It is better to keep the ratio $r/d>0.6$,
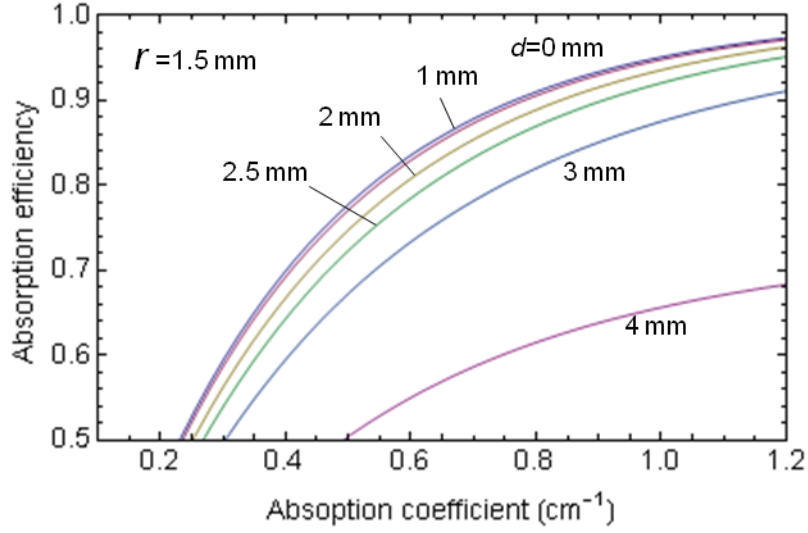
Figure 2.7 The absorption efficiency as a function of the absorption coefficient when the d=0, 1, 2, 2.5, 3, 4 mm, under the condition r=1.5.
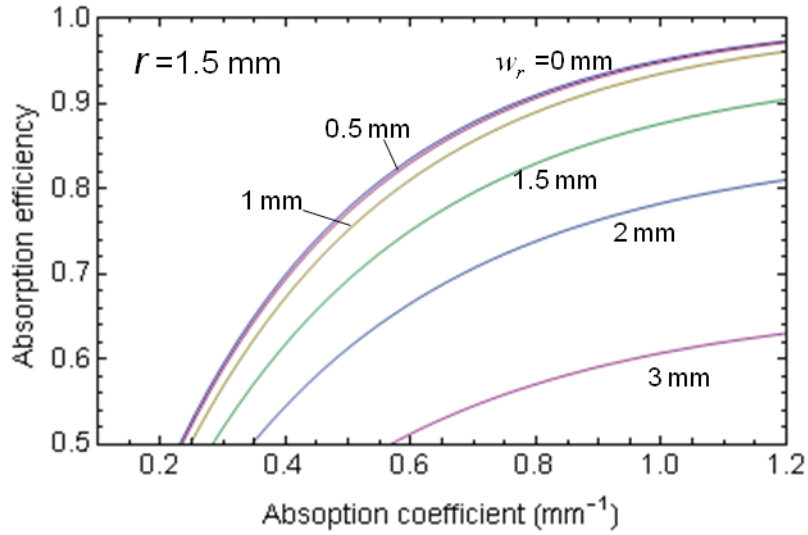

Figure 2.8 The absorption efficiency dependent on the absorption coefficient when the w_r=0, 0.5, 1, 1.5, 2, 3 mm, under the condition r=1.5.

For Gaussian pump (diode chip situation), use w_r for the beam waist at the edge of laser material, w_r corresponds to the intensity fall to $1/e^2$ of the maximum Gaussian shape. By neglecting φ_{1/e^2}, η_{abs} can be written as:

$$\eta_{abs,G} = \frac{\int_{-r/2}^{r/2}(1-e^{-2\alpha\sqrt{r^2-y^2}})Exp[-\frac{2y^2}{w_r^2}]dy}{\int_{-\infty}^{\infty}Exp[-\frac{2y^2}{w_r^2}]dy} \qquad (2.10)$$

The coordination follows that in Fig.2.5 and incident direction is along the -x axis. Fig.2.8 shows the absorption efficiency η_a as a function of the absorption coefficient

α. We assume $\eta_c=1$ and the Type B microchip situation, which $r=1.5$ mm under the condition of different pump waist $w_r=0$ mm, $w_r=0.5$ mm, $w_r=1$ mm, $w_r=1.5$ mm. $w_r=2$ mm and $w_r=3$mm. Base on the result, it is easy to find if the pump waist is same or bigger than the diameter r, the absorption efficiency is not so good. It is better to keep the ratio $r/w_r>1.5$,

If the edge of microchip is un-coated, the coupling efficiency η_c can be simply calculated by $\eta_c=1-(n-1)^2/(n+1)^2$, where the n is the refractive index of YAG. By using $n=1.82$, the calculation result is about 91.5%. In reality, the η_c is strongly depends on the optical design and collimated technique. As an example of diode stacks pump module for microchip Type A, the pump scheme is shown in Fig.2.9, the pump source is a 6 bar stacked diode with the fast-axis collimation microlens (made by JENO OPTIK). The full beam divigence angle after the microlens is $\varphi_{1/e^2}=0.5°$ and $\theta_{1/e^2}=12°$ for the slow and fast axis at the $1/e^2$ intensity. The focus lens unit including a slow-axis (SA) lens and a fast-axis (FA) lens with the focus length of 30 mm and 8.5 mm respectively. These lenses are specially designed aspheric cylindrical lenses, which can foucs the pump beam to the size around 100 μm in the direction of axis z and 2~2.5 mm size in the direction of axis y with the typical distance in the Fig.2.9. This is small enough to coupling inside the $l=200$ μm thickness of microchip. By carefully adjust the distance and hights of the lens unit, it possible to coupling inside the microchip with $\eta_c>90\%$ ideally. In fact, the measurement result is around

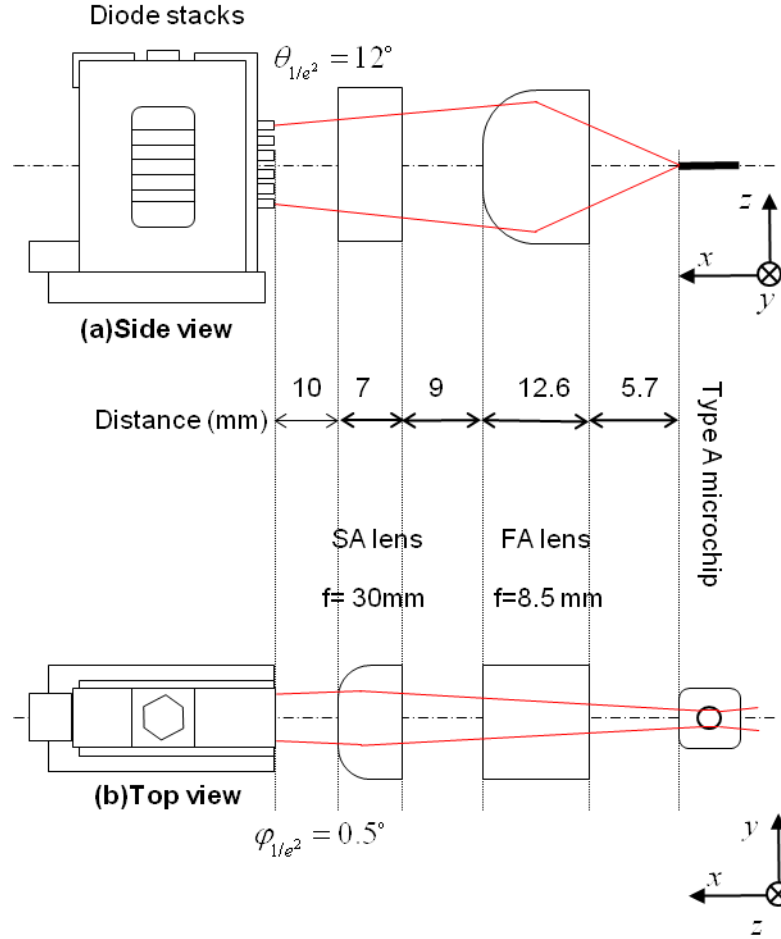81.3% at 20 W pump level. Considering about the reflection of the secondary edge face, it becomes reasonable.

Figure 2.9 The optical coupling scheme for diode stacks edge-pump microchip laser, the red line is the pump light sketch from diode stacks.

2.8 Pump shape distribution

It is always a headache of the edge-pumped scheme that the pump uniformity, because the edge absorption is always higher than the centre if there was only one pump direction. Depends on different absorption coefficient α, the slop will be different. Fig.2.10 shows the he absorption non-uniformity depends on different absorption coefficient α and core radius r. Since α is proportional to the doping rate. As soon as decide the core size and α to achieving enough absorption efficiency as mentioned in last section, it is import to consider the uniformity.
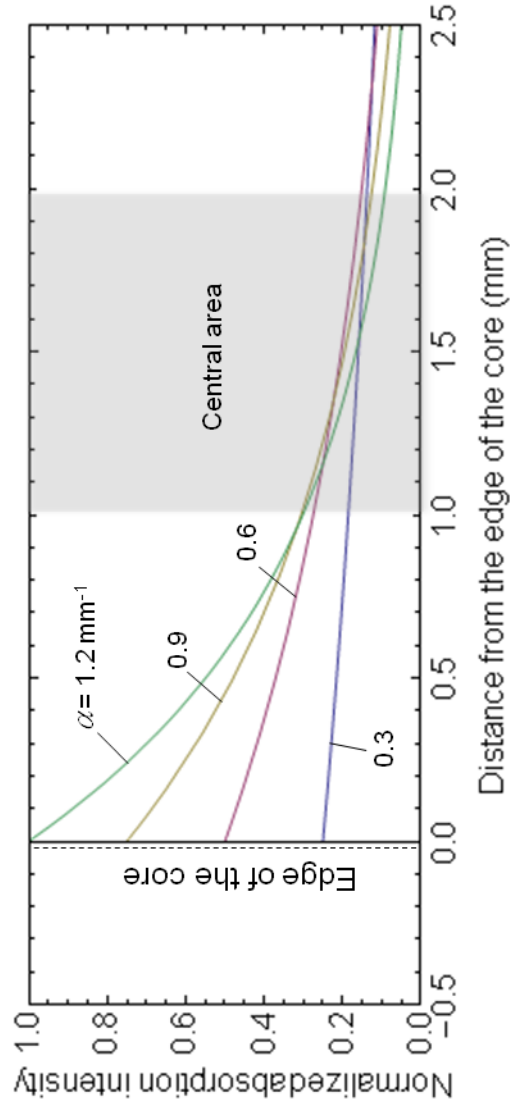
27

Figure 2.10 The absorption intensity as a function of distance from the edge, the absorption intensity is normalized to show the un-uniformity of the absorption at the edge and central area.

Typically, the solution is to apply multi-direction pump to solve the uniform problem. As an example of our 4-dirctions pump module for microchip Type A, the pump shape distribution can be calculated by the ray-trace method, assume the pump beam is top-hat pump with the total power of P_p, and $P_p\eta_c$ reach the edge of the core. We assume that the pump only travels once in the laser material and the refraction effect is not considered, the pump width is d, the absorption coefficient is α, for z-axis the pump is uniform. The density of absorption (W/mm^3) can be written as[19]:

$$D(x,y,z) = \frac{P_p \eta_c Exp[-\alpha l_g(x,y)]}{d \, l}, \quad (2.11)$$

where the $l_g(x,y) \approx \left| \sqrt{r^2 - y^2} - x \right|$ is the absorption length, l is the thickness of microchip. Figure 2.11 shows the relative density of absorption indicating the pump shape with the key parameter: d=2 mm, r=1.5 mm and α =0.9 mm^{-1}. It is easy to see the non-uniformity under the condition of limited pump direction. The shape is top-hat like, but the central part is lower than the edge. This calculated result is great agreement with our experiment result.
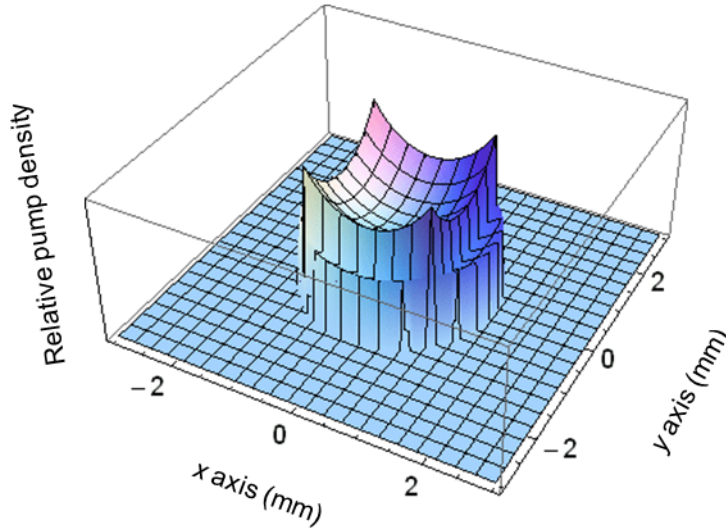

Figure 2.11 The pump shape of 4-direction diode stacks edge-pumped microchip laser with the parameter α=0.9 mm^{-1}, d=2 mm and r=1.5 mm.

We used to use this laser module for high-power mode-locked experiment, the result is that it was difficult to generate fundamental mode with high power. This is one of the motivations for us to study on mode selection of TEM$_{00}$ mode towards high-power.

2.9 Mode selection theory

We start from the rate equation in section 2.3, the $P_{th} \propto V_{eff}$, assuming a given pump position and pump beam waist w_p, the transverse mode with the minimum

threshold can oscillate at first. As the pump power increase, the secondary mode finally reaches the threshold and become mix-mode oscillation.
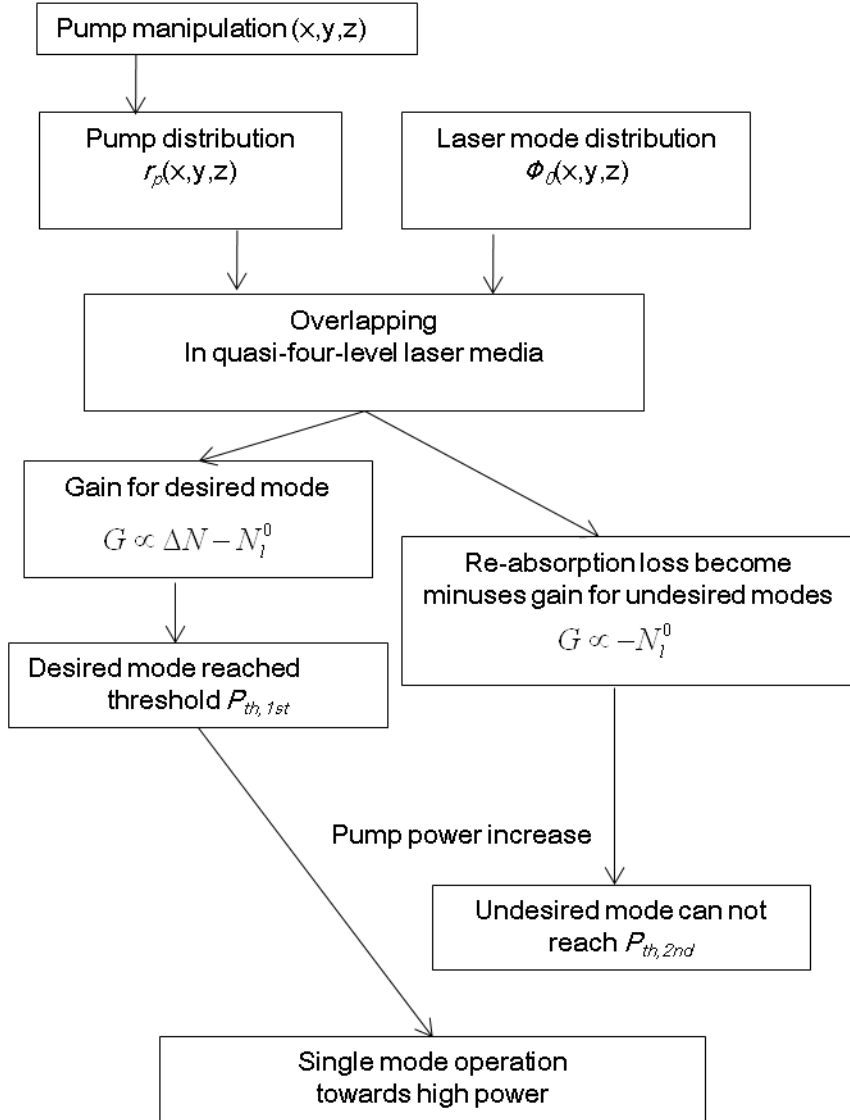

Figure 2.12 The flowchart of mode selection theory in quasi-four-level laser media, the re-absorption loss as minuses gain in non-pumped area

Define the relative pump power [20] as: $r_{in} = P_{th,TEM_{2nd}} / P_{th,TEM_{1st}}$; loss factor: $\Gamma = L_{i,T}^{TEM_{2nd}} / L_{i,T}^{TEM_{1st}}$. The loss $L_{i,T}$ for certain mode includes the intrinsic cavity loss and output mirror loss. Normally, people try to increase the loss factor Γ by the method of cavity design and hard aperture, to increase diffraction loss for the suppression of undesired mode oscillation and scaling up the output power of desired mode. From the rate equation, it is easy to get the relationship between pumping rate

R and total laser cavity photo number Φ to analyse the mode competition as the equation below:

$$\frac{2\sigma l_c}{n} \iiint \frac{(f_u + f_l)\tau_f R r_p(x,y,z) - N_l^0}{1 + \dfrac{(f_u + f_l)\tau_f c\sigma}{n}\Phi\phi_B(x,y,z)}\phi_A(x,y,z)dv = L_{i,T} \qquad (2.17)$$

Where $\phi_B(x,y,z)$ is normalized spatial distribution of the 1st mode (1st mode oscillated mode in laser cavity). $\phi_A(x,y,z)$ is normalized spatial distribution of the 2nd mode (2nd oscillated mode in laser cavity). In quasi-four-level laser material, the $-N_l^0$ is re-absorption loss term, which is important to prevent the secondary mode reaching threshold. By numerically solve the equation 2.17, we can figure out the mode selection details including the threshold, input and output power. For better understanding of mode control theory, the flowchart of mode selection in quasi-four-level laser material is given in Fig.2.12.

Take the fundamental mode TEM$_{00}$ selection as an example, the normalized spatial distribution of the laser photons $\phi_0(x,y,z)$ for TEM$_{00}$ and TEM$_{10}$ mode can be given by:

$$\phi_{00}(x,y,z) = \frac{2}{\pi w_l^2 l}\exp[-\frac{2(x^2 + y^2)}{w_l^2}] \qquad (2.12)$$

$$\phi_{10}(x,y,z) = \frac{1}{\pi w_l^2 l}\exp[-\frac{2(x^2 + y^2)}{w_l^2}]\cdot H_1^2(\frac{\sqrt{2}x}{w_l}) \qquad (2.13)$$

Where H_n is the Hermite polynomial with the order n, we assume the w_l is beam waist of laser, which is approximately constant in the z-axis, because the thickness of microchip l is very small. Several normalized spatial distribution of the pump energy $r_p(x,y,z)$ can be expressed as:

$$r_T(x,y,z) = \frac{1}{\pi w_p^2 l}, \quad r \le w_p \qquad \text{(for top hat)} \quad (2.14)$$

$$r_G(x,y,z) = \frac{2}{\pi w_p^2 l} \exp[-\frac{2(x^2+y^2)}{w_p^2}] \quad \text{(for Gaussian)} \quad (2.15)$$

$$r_{SG}(x,y,z) = \frac{1}{2\pi w_p^2 l} \exp[-2\left(\frac{x^2+y^2}{w_p^2}\right)^{q/2}] \frac{4^{1/q}}{Gamma[2/q]} \quad \text{(for Super-Gaussian)} \quad (2.16)$$

Where the q is the super-Gaussian factor[21] and when $q=2$, it becomes Gaussian shape and when q increases to ∞, it becomes the top-hat shape. *Gamma* is the Euler Gamma function.
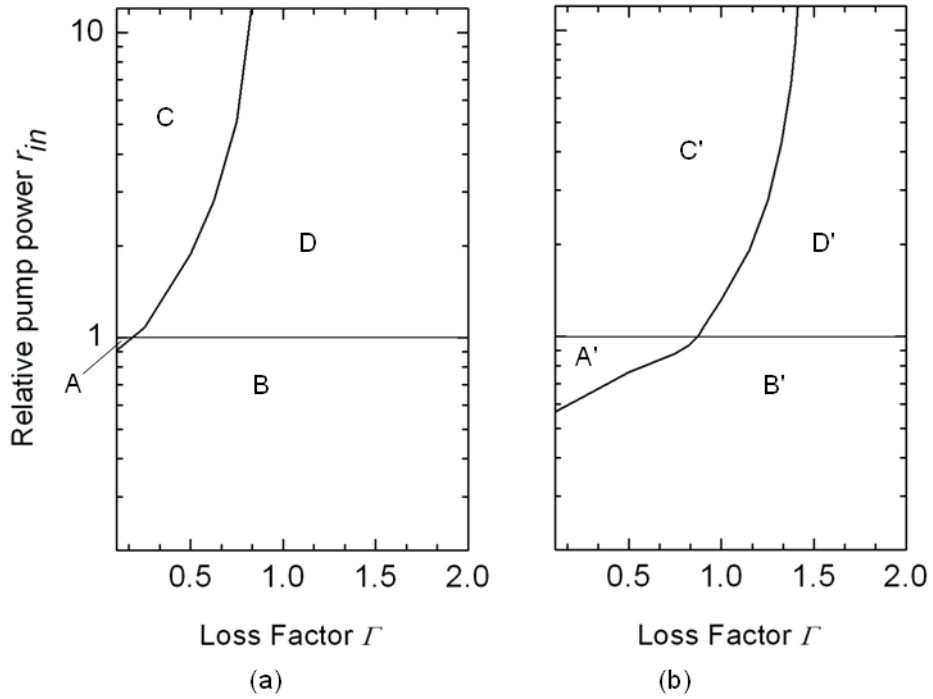

Figure 2.13 The TEM$_{00}$ mode scalability to prevent from the TEM$_{10}$ mode break into oscillation. The line the relative threshold as function of loss factor. A and A' areas are TEM$_{10}$ mode oscillation area, D and D' are TEM$_{00}$ mode oscillation area. C and C' are TEM$_{00}$+TEM$_{10}$ mode oscillation area. B and B' are below threshold area. (a) is under Gaussian shape pump; (b) is under Top-hat shape pump.

Let us consider the simplified situation only for top-hat pump and Gaussian pump. Figure 2.13 shows the TEM$_{00}$ mode scalability to prevent from the TEM$_{10}$ mode reaches the threshold, the numerical calculation is under the condition of $w_p/w_l=a=1.1$, $\alpha=3.3\times10^{-20}$ cm^{-2}, $\tau_f=0.951$ ms, $f_u=0.7$, $f_l=0.046$, $L_{TEM_{00},i}=0.01$ and $L_T=0.03$. The transverse line $r_{in}=1$ is $P^G_{th,TEM_{00}}/P^G_{th,TEM_{00}} = P^T_{th,TEM_{00}}/P^T_{th,TEM_{00}} = 1$, where $P^G_{th,TEM_{00}}$ is the threshold of TEM$_{00}$ mode under the condition of Gaussian pump shape

(the left figure (a)); $P_{th,TEM00}^{T}$ is the threshold of TEM_{00} mode under the condition of top-hat pump shape (the right figure (b)). For the area $r_{in} < 1$, the calculation is made by $\Phi = 0$, and, $\phi_{A}(x, y, z) = \phi_{10}(x, y, z)$ which means no cavity mode reaches the threshold before TEM_{10} mode. The result of the line date means if the loss of TEM_{10} mode is much smaller than TEM_{00} mode, TEM_{10} mode is possible to oscillate firstly before TEM_{00} mode. In most of the Gaussian pump case; it is quite difficult to realize this as shown in the left figure A area. This is also the reason that why traditional pump method is difficult to realize efficient high-order mode oscillation. In the right figure (b) A' area, it is much easier to realize TEM_{10} mode as $r_{in} < 1$.

For the area $r_{in} > 1$, the calculation is made by $\Phi > 0$, $\phi_{A}(x, y, z) = \phi_{10}(x, y, z)$ and $\phi_{B}(x, y, z) = \phi_{00}(x, y, z)$, which means TEM_{00} mode reaches the threshold before TEM_{10} mode and make single transverse mode oscillation as in the area D and D'. The area D and D' show us the scalability of TEM_{00} mode in certain cavity. By the given cavity with the given loss factor $\Gamma < 1.3$, the top-hat shape pumping has the difficulty in power scaling compared with Gaussian shape pump. Because soon it will reach the C and C' area, which means the TEM_{10} will reach the threshold and become multi-mode oscillation. For example, as $\Gamma = 1.25$, the TEM_{10} will reach the threshold as the pump power is 2.78 times of the threshold pump. In the Gaussian pump situation, this number almost infinite. The meaning of result in this figure is limited, only in the condition of not high-power and ideal pump shape like Gaussian or Top-hat.

In the condition of high power laser, for example of thin disk mode-locked laser, the Gaussian pump shape is too sharp and it will lead to thermal problems: such as optical distortion and thermal-induced stress, we will discuss it in next chapter. Normally, the fiber coupled high-power diode produce a supper-Gaussian pump shape with the factor q=4~6. The experienced pump size is a=1.1. Then we modify the

result in Fig.2.14 and make it have more practical significance. The black line is Gaussian pump shape, the black dot lines are super-Gaussian pump shape (left q=4, right q=6). The red line is top-hat pump shape, the dash red lines are the pump shape in Fig.2.11. (left α =0.6 mm^{-1} and right α =0.9 mm^{-1}).It shows us that it is very easy to reach the threshold of TEM$_{10}$. A Gaussian shape is good for TEM$_{00}$ mode selection against high-order mode generation when the low power operation; a supper-Gaussian is preferable when it turns out to be high-power operation. The q number don't change too much compared with ideal Gaussian pump shape, when $r_{in}<1$, all of them can scale up to 10 times of threshold pump power. It is clear that, for TEM$_{00}$ mode generation, it is better to move the pump power to the centre and it is not good to have a edge-peak pump shape.
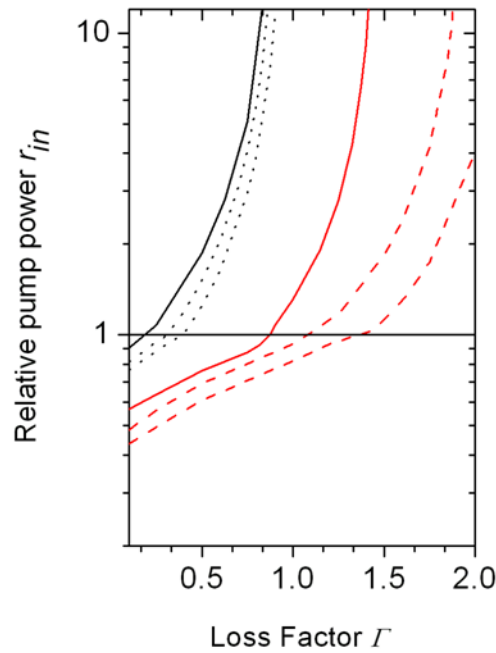

Figure 2.14 The TEM$_{00}$ mode scalability to prevent from the TEM$_{10}$ mode break into oscillation under different pump shape.

2.10 Conclusion

In this chapter, we introduced the basic of high-power solid state laser module design. We use the quasi-four level laser rate equation to explain the mode-selection

theory based on various pump shape. We use TEM_{00} mode selection as an example for better understanding and solving our practical research problems. Now it is clear that the intensive edge absorption goes against the fundamental mode generation and power scaling. In order to overcome this difficulty, we will study on the pump distribution design in edge-pumped scheme in the following chapter.

[1]T. H. Maiman, "Stimulated optical radiation in ruby", Nature 187, 493 (1960)

[2]http://www.rp-photonics.com/laser_applications.html.

[3]W. Koechner, Solid-State Laser Engineering, 4th ed. (Springer, 1996).

[4]Giesen, A., et al. "Scalable concept for diode-pumped high-power solid-state lasers." Applied Physics B 58.5 (1994): 365-372.

[5]Rutherford, Todd S., et al. "Edge-pumped quasi-three-level slab lasers: design and power scaling." Quantum Electronics, IEEE Journal of 36.2 (2000): 205-219.

[6]Taira, Takunori, William M. Tulloch, and Robert L. Byer. "Modeling of quasi-three-level lasers and operation of cw Yb: YAG lasers." *Applied optics* 36.9 (1997): 1867-1874.

[7]Saikawa, Jiro, et al. "Tunable frequency-doubled Yb: YAG microchip lasers." Optical Materials 19.1 (2002): 169-174.

[8]Hiroshi Sakai, Hirohumi Kan, and Takunori Taira, ">1 MW peak power single-mode high-brightness passively Q-switched Nd3+:YAG microchip laser," Opt. Express 16, 19891-19899 (2008)

[9]Rutherford, Todd S., et al. "Edge-pumped quasi-three-level slab lasers: design and power scaling." Quantum Electronics, IEEE Journal of 36.2 (2000): 205-219.

[10]Ikesue, Akio, et al. "Fabrication and Optical Properties of High Performance Polycrystalline Nd: YAG Ceramics for Solid State Lasers." Journal of the American Ceramic Society 78.4 (1995): 1033-1040.

[11]Kaminskii, A. A., et al. "Micro hardness and fracture toughness of Y_2O_3 and $Y_3Al_5O_{12}$ based nanocrystalline laser ceramics." Crystallography Reports 50.5 (2005): 869-873.

[12]Tsunekane Masaki, and Takunori Taira. "High-power operation of diode edge-pumped, composite all-ceramic Yb:$Y_3Al_5O_{12}$ microchip laser." Applied physics letters 90 (2007): 121101.

[13]Azrakantsyan, M., et al. "Yb3^{+}: YAG crystal growth with controlled doping distribution." Opt. Mater. Express2 (1) (2012): 20-30.

[14]Masaki Tsunekane and Takunori Taira, "300 W continuous-wave operation of a diode edge-pumped, hybrid composite Yb:YAG microchip laser," Opt. Lett. 31, 2003-2005 (2006)

[15]Pawlowski, Edgar, et al. "Yb: YAG composite ceramic laser." Proceedings of SPIE.Vol. 7578. 2010.

[16]Tsunekane, Masaki and Takunori Taira. "Design and performance of compact heatsink for high-power diode edge-pumped, microchip lasers." Selected Topics in Quantum Electronics, IEEE Journal of 13.3 (2007): 619-625.

[17]http://www.optoenergy.com/global/index.html.

[18]Copeland, Drew A., and John Vetrovec. "Gain tailoring model and improved optical extraction in CW edge-pumped disk amplifiers." SPIE LASE. International Society for Optics and Photonics, 2012.

[19]Nicola Coluccelli, "Nonsequential modeling of laser diode stacks using Zemax: simulation, optimization, and experimental validation," Appl. Opt. 49, 4237-4245 (2010)

[20]Kubodera, Kenichi, and Kenju Otsuka. "Single transverse mode $LiNdP_4O_{12}$ slab waveguide laser." Journal of Applied Physics 50.2 (1979): 653-659.

[21] Shealy, David L., and John A. Hoffnagle."Beam shaping profiles and propagation."Optics & Photonics 2005. International Society for Optics and Photonics, 2005.

Chapter 3

Compact multi-direction edge-pumped laser module

Related paper:

3.1 Introduction

There are several key techniques for high-power mode-locking laser, such as cavity design, semiconductor saturable absorber mirror (SESAM), chirped mirror and so on[1]. Before that, the first step is to build the compact laser module suitable for TEM_{00} mode generation. The edge-pumped scheme exhibits advantages for high-power compact DPSSL module, but it also has the drawback that non-uniformity of pump and edge-peak pump shape. At the end of last chapter, the reason has been explained that top-hat or basin pump shape is not suitable for fundamental mode generation and power scaling. The aim of this chapter is trying to change the pump shape towards Gaussian or Super-Gaussian by theory manipulation and experimental proof.

3.2 Pump distribution design

We choose the diode chips as our pump source. The specification of diode bare-chip is shown in Talbe2.1. The output distribution is shown in equation 2.7. We assume that the pump only travels once in the laser material; refraction and scatting

are not considered at the boundary between the core and the clad of microchip; along

z-axis the pump and absorption are uniform. The simulation of absorbed pump

density (W/mm^3) distribution is defined by:

$$D(x, y, z) = \frac{\exp\{-\alpha \cdot l_g(x, y)\}\alpha I(x, y)}{l} \qquad (3.1)$$

Where α is the absorption coefficient, $l_g(x, y) \approx \left|\sqrt{r^2 - y^2} - x\right|$ is the absorption

length, l is the thickness of microchip and r is the radius of microchip core. $I(x, y)$ is

the input power per unit length with the unit of W/mm at the edge of the microchip

core. $I(x, y)$ can be written as:

$$I(x, y) = \sqrt{\frac{2}{\pi}} \frac{P_p \eta_c}{w(x)} \exp\{-\frac{2y^2}{w(x)^2}\} \qquad (3.2)$$

We assume the pump beam with the total power of P_p, and $P_p \eta_c$ reach the edge of the

core. $w(x) \approx (R - x)\tan(\frac{\varphi_{1/e^2}}{2})$, R is the clad radius of microchip, φ_{1/e^2} is the

divergence angle inside the microchip. Figure 3.1 shows the pump shape by the

number of (a) N=1, (b) N=3, (c) N=9 diodes from multi-directions by using the key

parameter: R=4.26 mm, r=1.9 mm, α =0.3 mm^{-1} and φ_{1/e^2}=8.54 deg. It could be

intuitively understand the concept of pump distribution design in Fig.3.1. It is the

gain-guiding to realize the desired pump shape. The basic concept is to overlap the

energy at the centre of microchip, which change the basin shape to the Gaussian shape.

To evaluation the central peak, a very simple method is to make the comparison of the

density at the centre and the core-edge of microchip, corresponding to

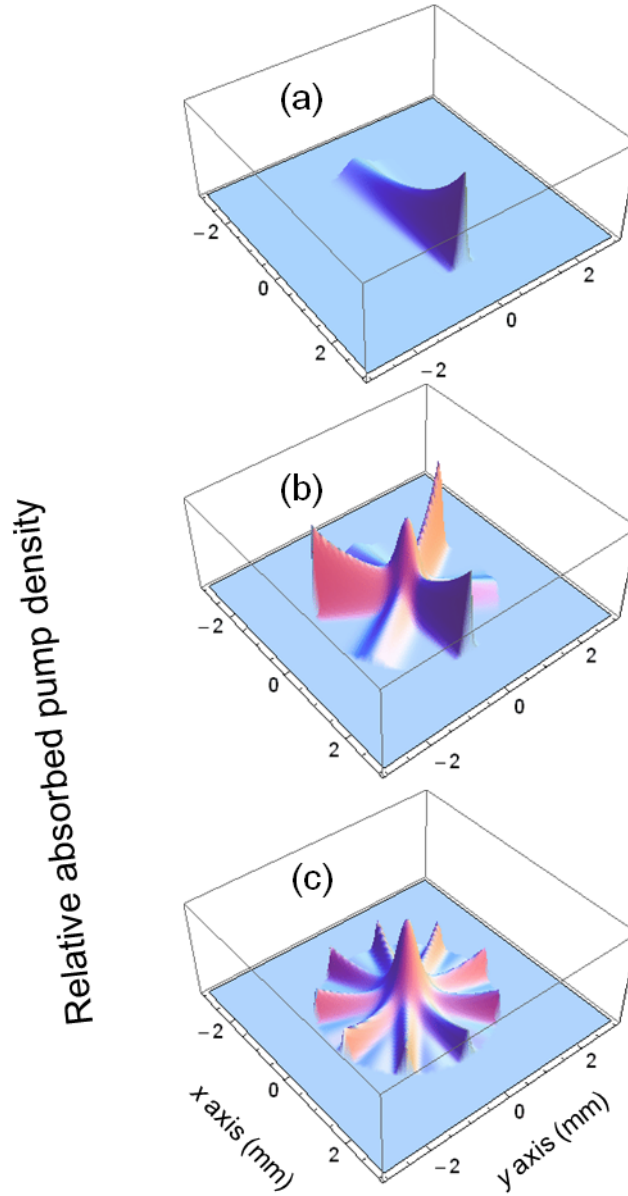$D(0, 0, z) / D(r, 0, z)$. The calculated result for Fig.3.1 (a) (b) (c) is 0.31, 0.94, 2.8,

respectively.

Figure 3.1 The pump shape of edge-pumped microchip laser by
(a) 1, (b) 3, (c) 9 diodes from multi-directions with the parameter
α=0.3 mm^{-1}, R=4.26 mm and r =1.9 mm.

3.3 Lens-less diode pump

The lens-less coupling design benefit from the small emitter size and high-brightness of diode laser, it was the prediction that no optical coupling device is needed for future laser system since the first diode laser pumped solid-state laser was invented. The idea has been realized in end-pump scheme. It has significant to apply in edge-pumped microchip to make microchip laser more compact.
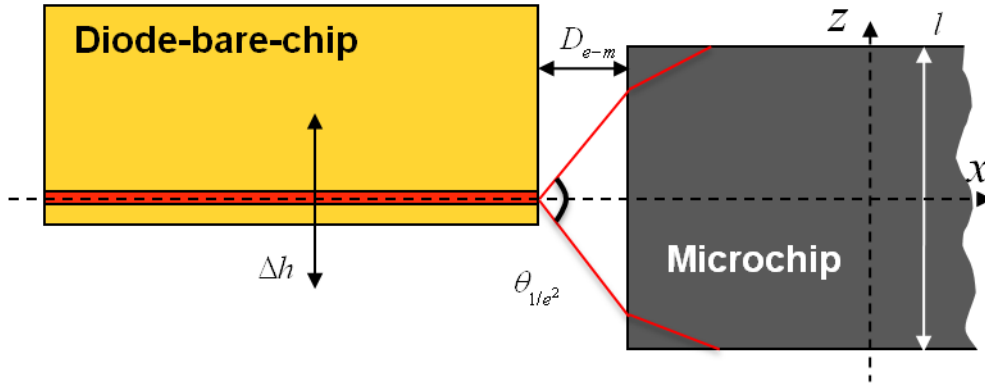
Figure 3.2 The lens-less pump scheme for directly coupling from diode chip to microchip

We experimently make it realized by overcoming some difficulties. Firstly, there is no suitalbe model of diode-chip package in the market; secondly, the commercial heat-sink for diode is too huge for our application; thirdly, the coupling needs the precision and carefulness. It costs time to fabricate our home-made diode heatsink with special shape of front edge, which is suitable for multi-direction pump shceme without blocking other componets. The micro-channel heat-sink is made by CuW10 material with similar thermal expansion coefficient of gallium arsenide, the cooling ability is very good that possible for over 100 W diode laser cooling. The thermal resistance is about 0.5 K/W under the codition of 0.28 MPa water pressure. The design planed to carry three diode chips on it with total pump power over 45 W. For the preliminary experiment, we only bond one diode chip on each heat sink. The coupling was done under the microscopy by measureing the distance D_{e-m} from the diode emitter surface to the edge of microchip. The heights difference of the diode chips and microchips also measured as the heights tolerences Δh as shown in Fig.3.2 the scheme of lens-less edge-pumped design.The fast axis divergence angle of diode is θ_{1/e^2} as methioned in chapter 2.

The heights tolerence Δh is about $\pm 25 \mu m$. The caculated coupling efficiency reasult is shown in Fig.3.3 without taking account into the pump window refecltion

(the value is 8.45% for polished surface and 0.05% for anti-refelction coated surface). We just study the distance dependents coupling efficiency to judege the availble diode coupling pricision.The result shows that from 0 to 127μmthe coupling efficiency is more than 99.9%. What we can realize is around 50-70μmwith the help of coupling tools.
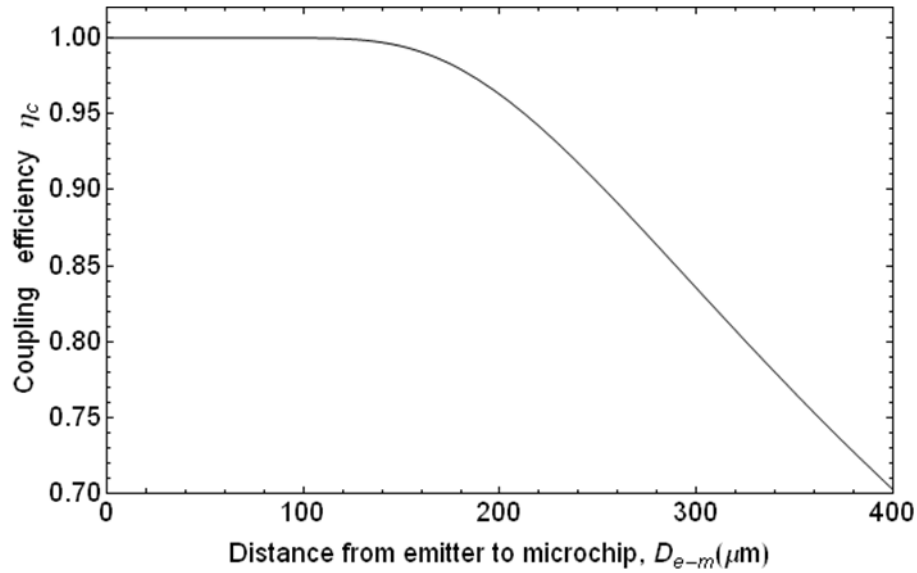

Figure 3.3 The coupling efficiency as a function of the distance from emitter to microchip.
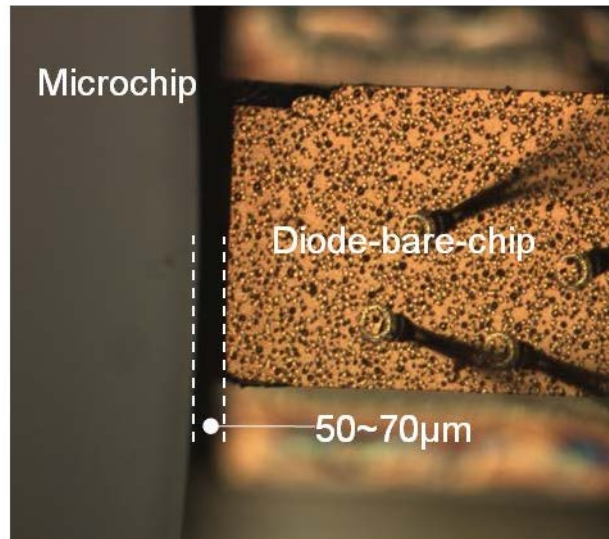

Figure 3.4 The experimental lens-less coupling taken by microscope. The focus surface is on the top metallization of the diode bare chip. The altitude of top surface of microchip is lower than it.

The experimetal result of lens-less coupling is shown in Fig.3.4. The distance from microchip (left) and diode chip (right) is between 50μm to 70μm as we tried for several times. The focus surface is on the top metallization of diode-bare chip. The altitude of top surface of microchip is lower than it.. The diode chipis dangous for any further colser to the microchip, it is easily damaged by microchip and the microchip is easily damaged by the heat-sink of diode. The demonstration of this lens-less method suggest a integrated heat-sink for both microchip and diode chips. In addition, Professional bonding machine will make it much easier like integrated circuit motherboard.
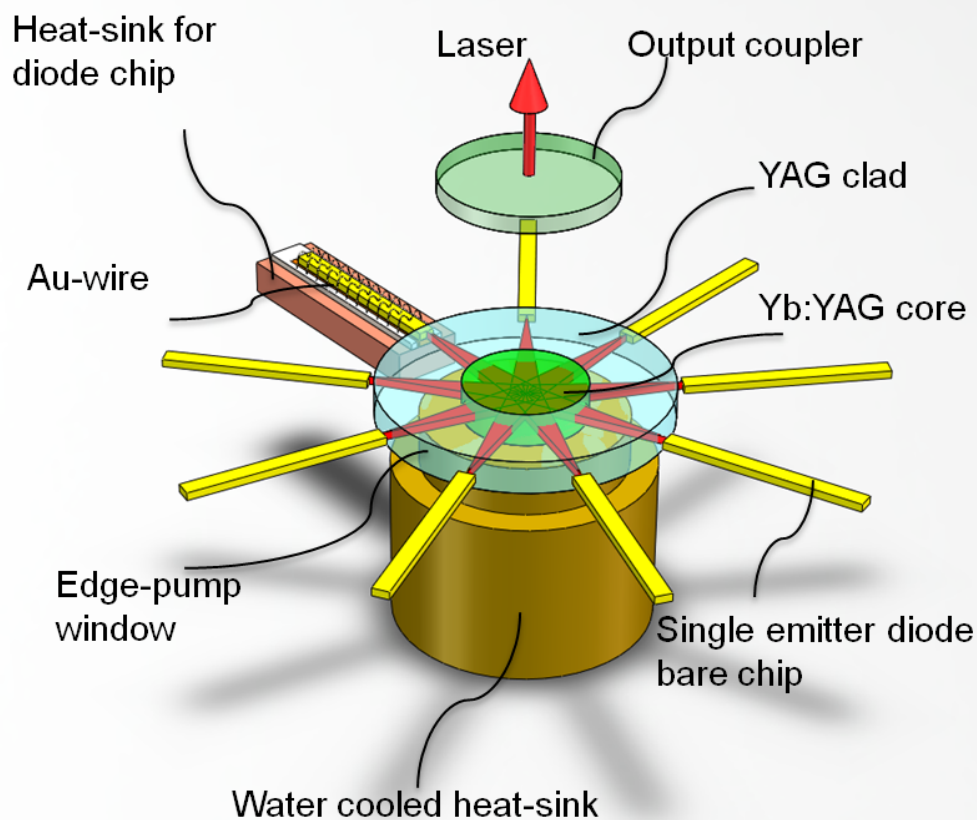

Figure 3.5 The schematic of lens-less edge pumped microchip laser
module. 9 diode chips pump from 9 directions radially.

3.4 Laser module assembling

Laser module is assembledfollowing the schematic in Fig.3.5. Firstly, composite Yb:YAG/YAG all ceramic microchip is bonded to the water-cooled CuW heat-sink by Au-Sn solder. In Fig.3.5 the thickness of microchip is exaggerated to give a clearly show. The 200-μm-thickness microchip has a 3-mm-diameter 9.8 at. % doped Yb:YAG core as the gain material and 8-mm-diameter undoped YAG clad as waveguide for pump light. Antireflection (<0.5%) and high refectlion (>99.5%) coatings for laing wavelength 1030 nm are deposited on the top and bottom surfaces, respectively. The edge aslo has an antireflection coating (<0.5%) for the pump wavelength 940 nm.

Figure 3.6 The front view of assembled 9 direction pumped edge-pumped laser module..

Secondly, the diode chips (by Optoenergy Inc., 15 W maxiumu output power) are bonded to home-made heatsink, followed by the golden wire connection. Then place radially around the microhip. The size of diode chip is6 mm long strip shape,

which can be a ruler of this schematic. The emitter is 100 μm width and 1μm height. The output beam of the diode chip propagate with far-field parallel and perpendicular FWHM divergence angle 10 deg.and 26 deg. The fix of diode module is applyied with the help of home-made coupling tools to realize a good precision.

Finally, the electrods for diodes and cooling water tubes are connected.

The real laser modual is shown in Fig.3.7. The size is around 60 mm diamter and the thickness is about 20 mm, which is very compact. The design for this laser modual is for 27 diode chips, now we only finished 9 diodes, there are two empty slots on the heat-sink for another two diodes bonding.
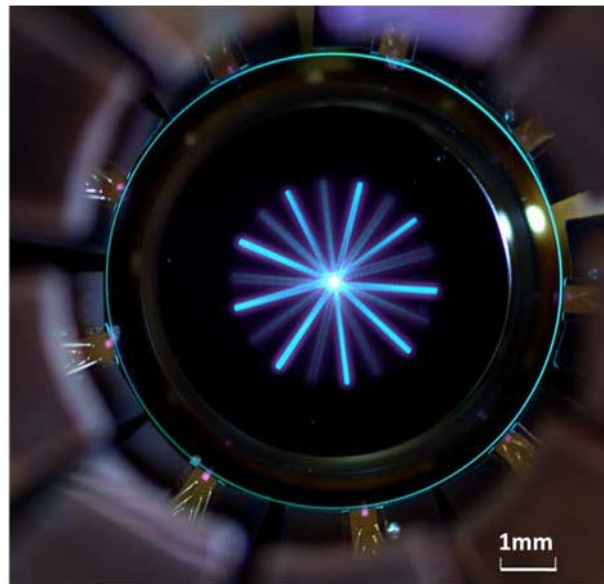

Figure 3.7 The front view of microchip when the diodes
pump near threshold

3.5 Experimental result

The diodes from 9 directions pump inside the microchip and the overlap at the centre. We test the pump around the diode thershold less than 1 W, the front view on microchip is shown in Fig.3.7. The bright lines are pump beam,the beam seems very narrow compared with caculation, but as the diode pump ower increse the pump power the beam will broaden.The central brighter point is overlap area. The small

circle is the core of microchip; the black circle area is the metalization aear where is bonded to the water-cooling heatsink; the blue circle is the edge of microchip. We can see nine diode chips next to the edge. Above the diode chips are the golden wires for electrical connection. Below the diode chips are heat-sink for microchip. The obscure part of the picture is protection cover of the diodes.
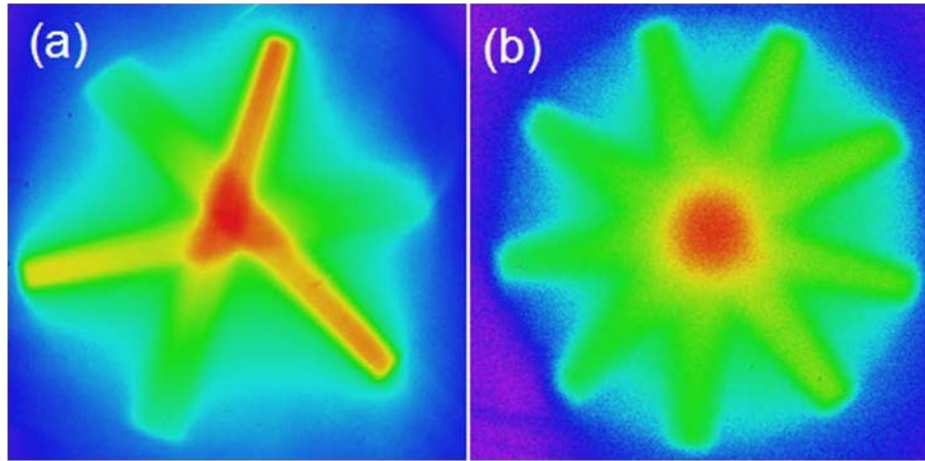

Figure 3.8The Fluorescence images taken by CCD camera, pumped by (a) 3 diode chips and (b) 9 diode chips

Te fluorescence images taken by a CCD camera are shown in Fig.3.8 when the pump power for each diode around 3 W. The absoption coefficient α is estimate to around 3~4 mm^{-1} by the wavelength measurement deponds on the cooling temperature. The fluorecnece for 3 diodes pump and 9 diodes pump are in good agreement with our simulation, it proves that the absorbed power density distribution is controllable by manipulating the pump scheme. To point out that, for the 3 diodes pump the collimation is not perfect as we see the central part overlap not in the same point. For the nine-direction pump, the overlap also not perfect, but we could not see clearly in the flourences figure, it also tells us more-pump beam is good for uniformity even if the overlap is not good.

The CW laser performance was evaluated with a 20 mm flat-flat cavity, using a 97% refectivity output coupler mirror. The microchip cooling water temperature was

15 deg. The threshold pump power was around 13 W. the maximum CW output power was 32.5 W for full multi-mode operation when the total incident power was 121 W, corresponding to 45% slope efficiency which was caculate from 5 times the threshold. By slightly adjusting the output coupler mirorr to suppress the small peak at the edge of the core, a good Gaussian shpe laser could be obtained in the short flat-flat cavity. Fig 3.18 shows the Gaussian shape output power versus incident pump ower, and maximu 27.2 W was availble. M^2 factor was 1.1, 3.2, 9.4, 16 and 19 when the output power is 0.32 W, 3.5 W, 11 W, 19.3 W, and 27.2 W. A CCD camera was applied to record the 2D and 3D beam patterns when the output power was 27.2 W, while the both 2D and 3D beam images show the radial fringes because of the non-uniform pumping by only 9 diodes.
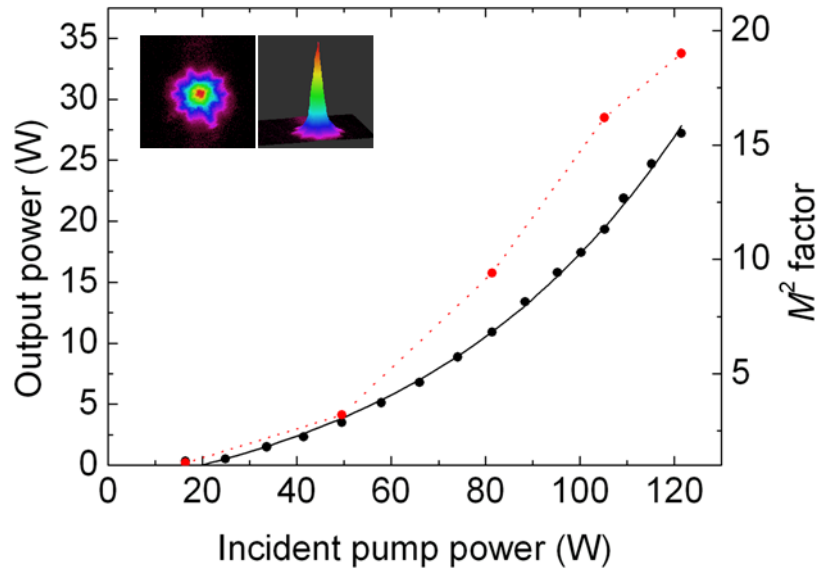

Figure 3.9 The output power (black) and M^2 factor (red) as a function of the incident pump power. The 2D and 3D beam patterns are taken by CCD camera when the maximum output power.

3.6 Optimization of pump shape

Although the nine direction pump seems enough for the uniformity, it is necessary to consider the better pump shape and increase more pump directions for power scaling. Followed the pump shape calculation in section 3.2, we fit pump

distribution $D(x, y)$ by 2D-Gauss equation to check the uniformity. The 2D-Gauss equation is written by:

$$D_{fit}(x, y) = D_0 + A \exp\{-\frac{2(x-x_0)^2}{w_1^2} - \frac{2(y-y_0)^2}{w_2^2}\} \qquad (3.3)$$

Where w_1 the major axis is beam waist and w_2 is the minor axis beam waist. D_0, A, x_0, y_0, w_1 and w_2 are regression parameters. We evaluate the fit by the Ajusted-R^2, often written as $\bar{R}^2$ see the Ref.2:

$$\bar{R}^2 = 1 - \frac{SS_{err}}{SS_{tot}} \cdot \frac{n-1}{n-p-1} \qquad (3.4)$$
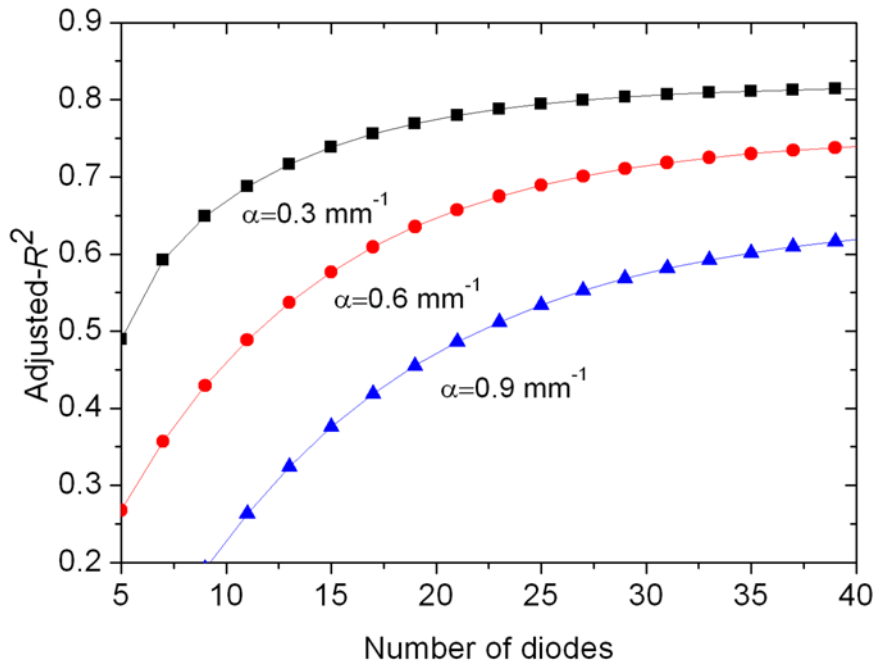

Figure 3.10 The Ajusted-R^2 as a function of the number of diodes depends on the different absorption coefficient .

Where the total sum of squares $SS_{tot} = \sum_{i=1}^{n} \{D(x_i, y_i) - \bar{D}(x, y)\}^2$, the residual sum of squares $SS_{err} = \sum_{i=1}^{n} \{D(x_i, y_i) - D_{fit}(x_i, y_i)\}^2$, and the mean of the observed data $\bar{D}(x, y) = \frac{1}{n}\sum_{i=1}^{n} D(x_i, y_i)$ .n is the sample size and p is the total number of regressors. $\bar{R}^2$ is one of the obvious metric to show how close the fitted curve from the actual

data points so called goodness of fit. If the fit is perfect, $\overline{R}^2$ should be equal to 1 and a value closer to 1 indicates that the fit is a better one. In our case, we suppose better pump shape with higher $\overline{R}^2$ number to help us evaluate how close the pump shape from the ideal fundamental Gaussian shape and optimize our pumping design. Fig 3.2 shows the relationship between $\overline{R}^2$ and the number of diodes with the absorption coefficient α as a parameter. The result shows that what number of diodes is sufficient for uniform pump shape, $\overline{R}^2$ will not increase shapely when the number of diodes is big enough for Gaussian shape manipulation. Besides, the increasing number of diodes increases the uniformity of the pump shape edge. The higher α performs worse and it needs more direction pump for uniformity, it is easily to
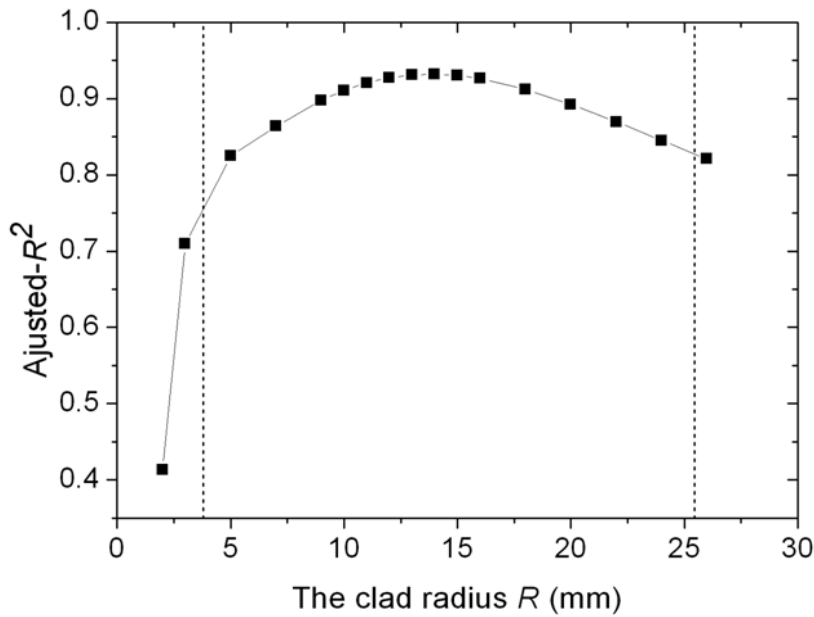

Figure 3.11 The Ajusted-R^2 as a function of clad radius when the core size r =1.9 mm under 27 diodes pump.

understand that the higher absorption coefficient leading to strong edge absorption, asking more pump beams to overlap in the central area against basin shape. The central peak strongly depends on the equation $w(x) \approx (R-x)\tan(\dfrac{\varphi_{1/e^2}}{2})$, which is the pump beam size when it reaches to the centre, a small size will lead to a sharp peak as

48

in Fig. 3.1. The bigger size needs a bigger R or φ_{1/e^2}. Instead of scaling R, we can use a bigger divergence angle φ_{1/e^2} diode chip to realize the same result.
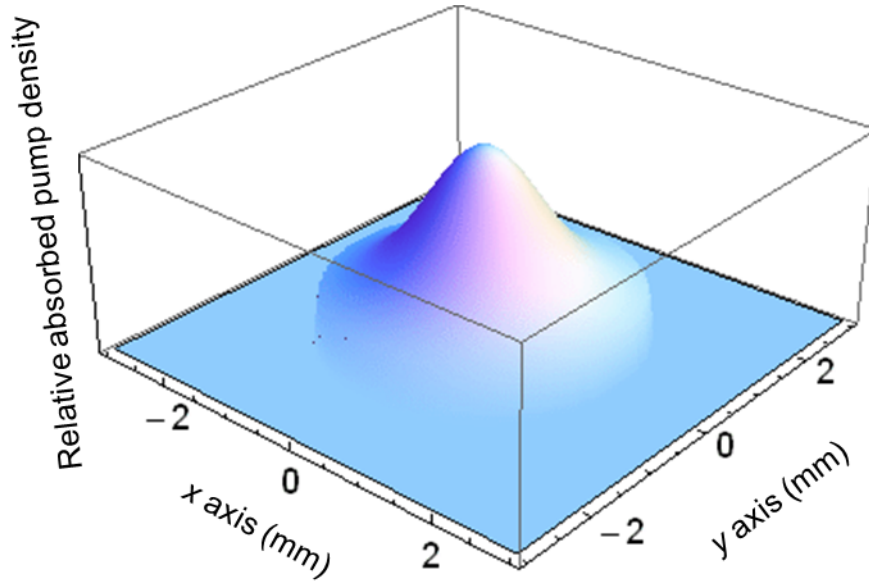

Figure 3.12 The optimized pump shape, when N=27, R=14 mm, r =1.9 mm, α=0.3 mm^{-1}

In order to optimize the Gaussian shape, the evaluation of $\overline{R}^2$ and the clad radius of microchip is shown in Fig.3.12 under the condition of N=27, core-radius r=1.9 mm. The $2r \leq R$ and $R \leq r/\tan(\varphi_{1/e^2}/2)$, corresponding to the left dashed line and right dashed line. The left prevents from parasitic oscillation and the right one prevents from pump beam outside the core range. The pump shape can be optimized to uniform Gaussian like shape. Fig.3.11 shows the pump shape when the N=27, r=1.9 mm, α =0.3 mm^{-1} and $\varphi_{1/e^2} = 8.54°$ and R=14 mm. As the reason of practical limitation, the R cannot be too big. The R bigger than 6 mm is enough for a uniform Gaussian pump shape. For high power laser, the sharp peak leads to thermal problems, we need a fatter one like in Fig 3.13, with the parameters: N=27, r=1.9 mm, α =0.9 mm^{-1} and $\varphi_{1/e^2} = 8.54°$ and R=14 mm. The pump shape keeps the central peak as well

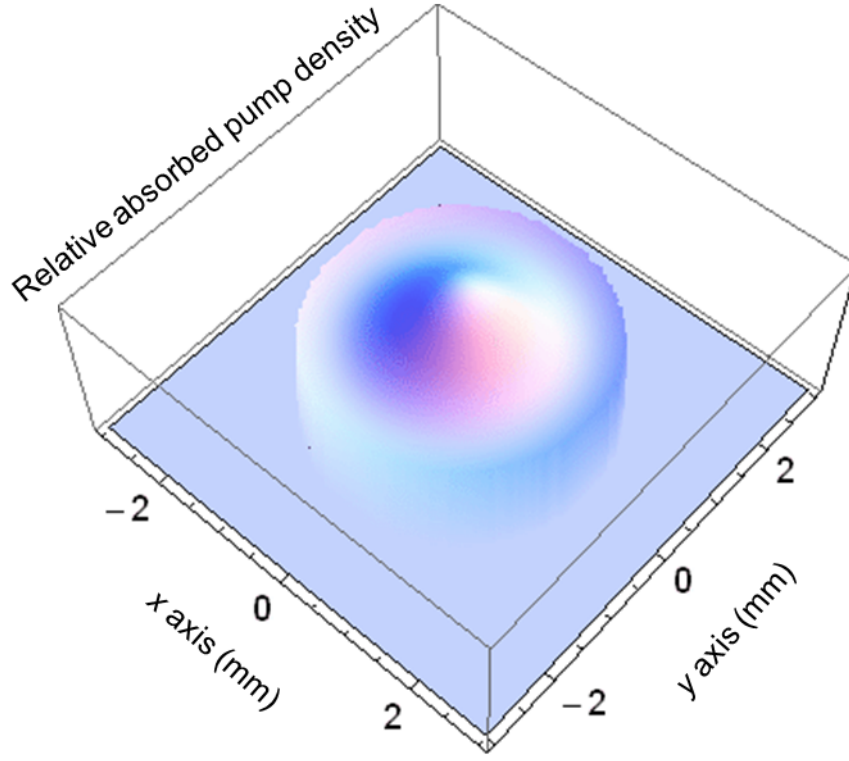as a fatter shape which could realize the similar pump shape of fiber coupled high power diodes.

Figure 3.13 The optimized pump shape, when *R*=14 mm, *r* =1.9 mm, α=0.9 mm⁻¹

The more practical method is to use the mini bar that mentioned in chapter 2.5 and equilateral polygon microchip with flat pumping widows; to keep the small propagation distance and transfer to Gaussian pump beam shape with bigger overlapping area than single emitter diode chip. As an example of 3 emitters diode mini bear with the $\varphi_{1/e^2} = 15.1°$. The calculation of the pump intensity of this kind diode bar with the different distance away from the emitter $x = 0.9 y_0$, corresponding to the distance 0.7 mm to become a uniform Gaussian pump, the overlapping area is more than three time compared with single emitter diode chip. For 7-emitters mini bare the distance to reach Gaussian pump beam is around 3 mm, which means 9 mm diameter microchip is enough for this setup.

By using the pump shape in Fig.3.12 and 3.13, the power scalability can be calculated numerically as shown in Fig.3.14, the parameters for calculation are same with last chapter. Solid line presents the pump shape in Fig.3.12 and dot line for Fig.3.13. The scalability is much improved compared with top-hat pump shape. The 10 times pump power scaling without TEM_{11} mode oscillation can be finished as r_{in} <1.in both case of Fig.3.12 and Fig.3.13. Although it is not as good as Gaussian or super-Gaussian pump shape, it is enough for several hundred watts output power of single fundamental mode. Especially for the compact 100-watt level laser module, it is much attractive.
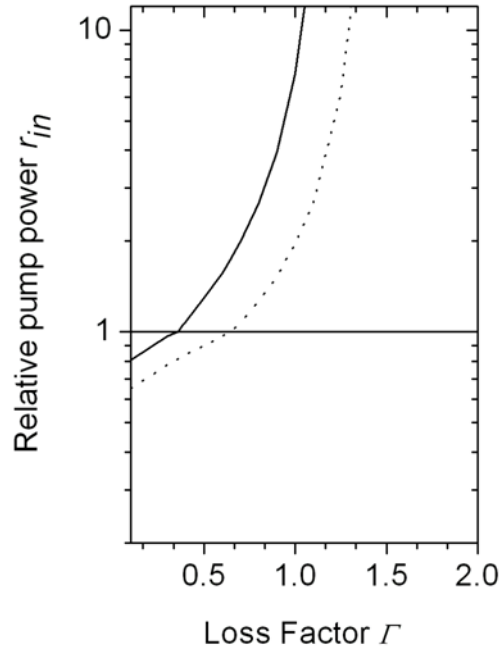
Figure 3.14 Relative pump power as a function of loss factor
under the pump shape in Fig.3.12 and Fig.3.13.

3.7 Thermal distribution and thermal effects

For high power laser, it is necessary to consider the thermal distribution and thermal effects: such as thermal induced stress, displacement and optical patch difference (OPD). In this section, we will present the thermal distribution depends on different pump shape. Basically, the pump distribution is applied to calculate the

thermal distribution, then by the thermal distribution, the stress, displacement and OPD can be addressed.

For any pump shape $D(x, y, z)$ is related with heat load $Q(x, y, z)$ distribution as: $Q(x, y, z) = P_h D(x, y, z)$, where P_h is total heat load including the heat from the quantum defect, the absorption of pump power and fluorescence by coatings and metallization. We assume P_h is percentage of total pump power and $\iiint\limits_{microchip} D(x, y, z) = 1$.

We calculate the temperature distribution by the steady state heat distribution equation and we assume the axis symmetric microchip and use polar coordinates[3]:

$$\frac{1}{r}\frac{\partial}{\partial r}(r\frac{\partial T}{\partial r}) + \frac{\partial^2 T}{\partial z^2} = -\frac{Q(r,z)}{K(T, c_{Yb})} \qquad (3.5)$$

Where $Q(r, z)$ is re-written heat load, also can be called heat source density in the microchip. $K(T, c_{Yb})$ is thermal conductivity which has relationship with temperature T and doping concentration c_{Yb} of Yb:YAG. We use the thermal and doping dependence $K(T, c_{Yb})$ as shown in the Ref.4:

$$K(T, c_{Yb}) = \rho C_p(T, c_{Yb})D(T, c_{Yb}) \qquad (3.5)$$

where ρ is density, C_p is isopiestic specific heat for unit mass and D is thermal diffusivity. They are given by:

$$C_p(T, c_{Yb}) = 3N_A k_B \frac{m}{M} f_D(\frac{T}{\Theta_D(c_{Yb})})$$
$$D(T, c_{Yb}) = \frac{A(c_{Yb})}{T} + B(c_{Yb}) \qquad (3.6)$$

N_A, k_B, m, M and f_D are Avogadro constant, Boltzmann constant, number of atoms in unit cell in host crystal, molecular mass and Debye function. A, B and Θ_D are fitting functions.

The parameters in Table 3.1 are applied for the simulation. We assume Type B for the shape of microchip. The internal heat generation is only inside the core area and along the z-axis it is uniform.

Table 3.1 The parameters for thermal simulation

Parameters	Units	Value
Core radius r	mm	1.5
Clad radius R	mm	4
Doping concentration $c_{\mathrm{Y}b}$	at.%	9.8
Heat fraction	%	10
Total pump power	W	324
Thickness of heat sink	mm	1
Cooling face area	mm^2	2.5×2.5×pi
Cooling ability	MW/m^{2}K	0.3
Cooling water	$^\circ C$	20
YAG refractive index		1.82

The parameters of materials are shown is Table 3.2.forthermal and structure calculation in finite element software ANSYS.

Fig.3.15 shows the temperature distribution of the top surface along the x-axis.The thermal distribution is caculated under different kind of pump shape: the idea top-hat shape and Gaussian shape, the pump shape in Fig.3.12 and Fig.3.13. The temperature distribution stronly deponds on the pump distribution and the constant temperature aear can be got when the top-hat pump shape. The radius of constant area is around 0.7r. The Gaussion shape pump has a peak of temperature at the very centre. The temperature gradiant is biggest compared with other Gaussian like pump shape. But the top-hat pump shape, at boundary of pump and unpumped area, the termperature gradiant is biggest. The termperature distribution of the pump shape in

Fig.3.12 is still very sharpe, the pump shape in Fig.3.13 exhibits an acceptable theraml distribution.

Table 3.2 the material thermal and structure parameters

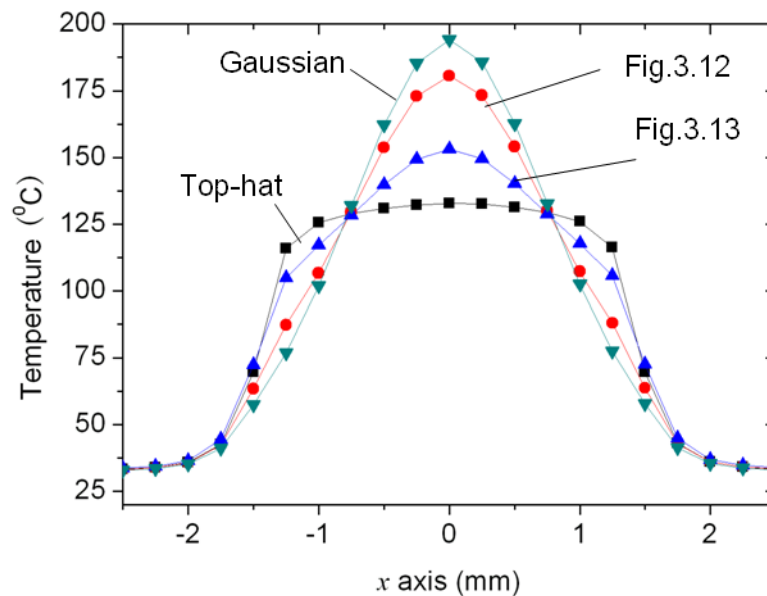| Parameter	Units	Material	
		Yb:YAG/YAG	CuW20
Thermal expansion coefficient	10^{-6}/K	8	8.3
Thermal conductivity	W/mK	Eq. 3.5/Eq. 3.6	230
Young's modulus	GPa	280	256
Poisson's coefficient		0.3	0.3

Figure 3.15 The temperature distribution under different pump shape. The idea top-hat shape, Gaussian shape, the pump shape in Fig.3.12 and 3.13

Other ANSYS thermal caculation results show that the cooling is important. The value of theraml heat exchange, bigger is better. The thickness of microchip, thinner is better. The potential that edge pumped schme can minize the thickness of microchip without worring about the abosrption efficiency.
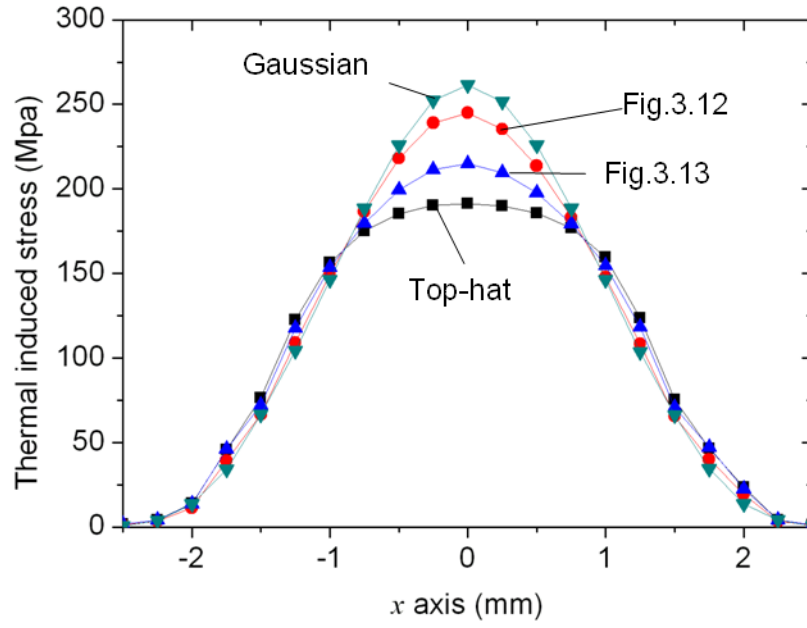
Figure 3.16 The stress distribution under different pump shape. The idea top-hat shape and Gaussian shape; the pump shape in Fig.3.12 and 3.13
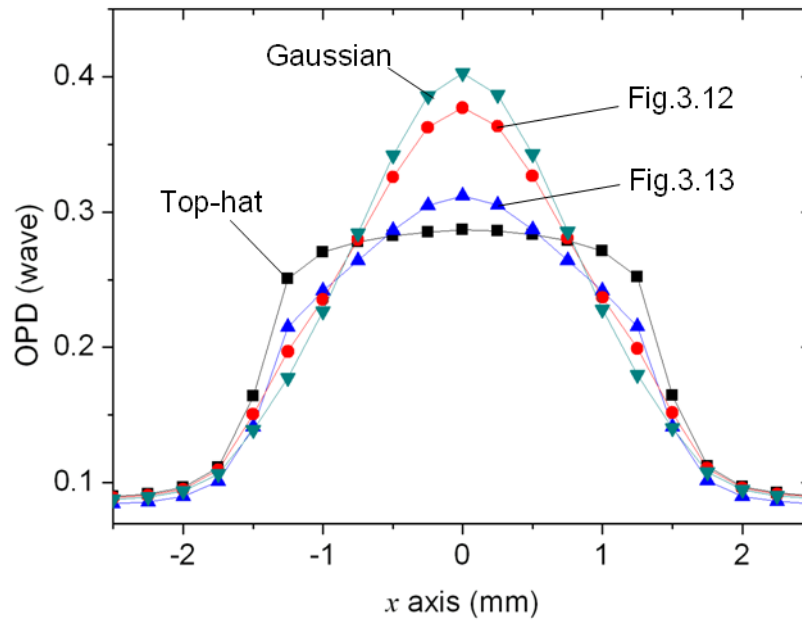

Figure 3.17 OPD distribution under different pump shape. The idea top-hat shape and Gaussian shape; the pump shape in Fig.3.12 and 3.13.

Follow the thermal distribution, we can do the caculation based on thermal-stress coupling in ANSYS softwar. The equation is written by: $\{\varepsilon\} = [C]\{\sigma\} + \{\varepsilon_T\}$. It shows

the realationship between elastic strain $\{\varepsilon\}$, thermal strain $\{\varepsilon_T\}$ and stress $\{\sigma\}$, where $[C]$ is the coeffecent matrix has relationship withPoisson's coefficient and Young's modulus. $\{\varepsilon_T\}$ is proportional to the coefficient of thermal expansion (CTE) and temperature difference given by: $\Delta T = T(r,z) - T(r,z_0)$, where (r,z_0) can be defined as the surface of heat-sink contacted with cooling water. Then the optical path difference (OPD) can be written as[5,6]:

$$OPD = \frac{2}{\lambda_l}\int_0^l \left\{ \frac{\partial n}{\partial T}\Delta T(r,z) + \sum_{i=r,z,\theta}\frac{\partial n}{\partial \varepsilon_i}\varepsilon_i(z,r) + T(r,z)C_{TE}(n-1) \right\}dz \qquad (3.7)$$

where, the 2 means two times pass in the microchip of laser, λ_l is the wavelength of laser, the first item of the integral indiacate the theraml inducedrefraction index change OPD, the second part is strain induced refraction index change OPD, the third part is thermal expasion OPD also can be thought as surface deformation of microchip, where C_{TE} is coefficient of thermal expasion. As the thickness far smaller then the pump radius, the caculated value of $\sum_{i=r,z,\theta}\frac{\partial n}{\partial \varepsilon_i}\varepsilon_i(z,r)$ is very small compared with the other two items, we can omit this part. It is easy to understand that the OPD distribution is similar with thermal distribution by understanding physics meaning of the equation.Then, the phase distortion is given by $2\pi \times OPD$ for laser wavelength.

Fig.3.16 shows the thermal stress distribution of the top surface along the *x*-axis.The thermal stress distribution is also caculated under different kind of pump shape: the idea top-hat shape and Gaussian shape; the pump shape in Fig.3.4 and 3.5. Now we can see that the ideal Gaussian pump is dangerous because of the central stress peak. It will easily break the microchip by the stress far beyond 384 MPa for Yb:YAG ceramic. Compared with single crystal, ceramic can suffer over twice of the stress, the high shock resistance can help us for higher power operation.For the optimized pump shape in Fig.3.5, the thermal stress is minimized compared with ideal

Gaussian pump shape and the shape in Fig 3.4. In this case, it shows the great flexibility of edge-pumped scheme for low power to high power fudmental mode ossilator or amplifier system. One should be addressed to the specific aim of the pump shape related to the demands.
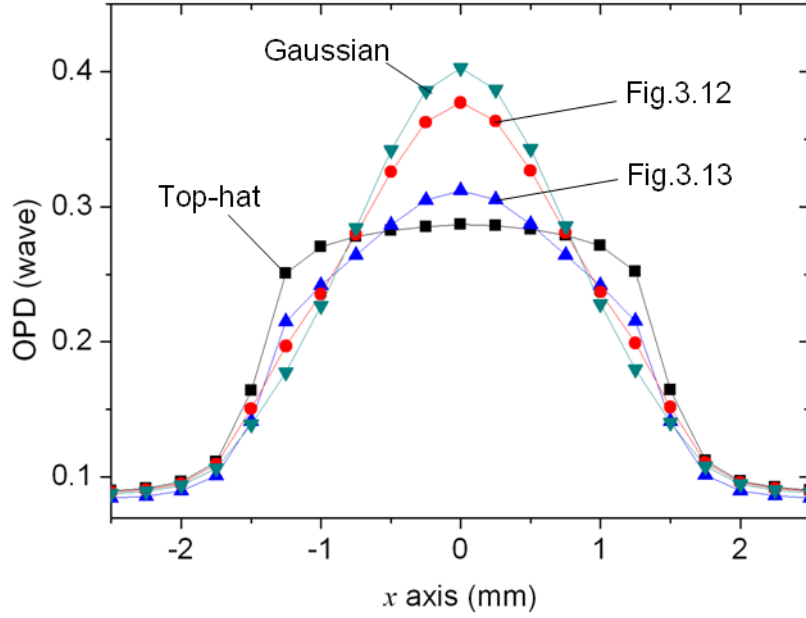

Figure 3.17 OPD distribution under different pump shape. The idea top-hat shape and Gaussian shape; the pump shape in Fig.3.12 and 3.13.

We also canculate the OPD for the optimization of pump design, the result of OPD along *x*-aixs is shown in Fig 3.17. The OPD has the units of wave corresponding to the laser wavelength. The peak to valley ratio in the pump area is 3.2, 2.9, 2,2, and 1.8 corresponding to the ideal Gaussian pump shape, the pump shape in Fig.3.12, the pump shape in Fig.3.13 and ideal top-hat pump shape. For the optimized pump shape in Fig.3.13 the OPD is only 0.27 wave.

In order to investigate edge-pumped tolerance the thermal induced displacement is caculated. The result is shown in Fig.3.10 under different pump shape. The biggest displayment happens at the edge of microchip, but it is almost same under different pump shape and it is less then 1μm. The central part of Guassion pump shape shows the biggest deformation, it is one important part of OPD generation. It is obvious in

microchip and disk laser media, taken big part of OPD value compared with rod type laser material.
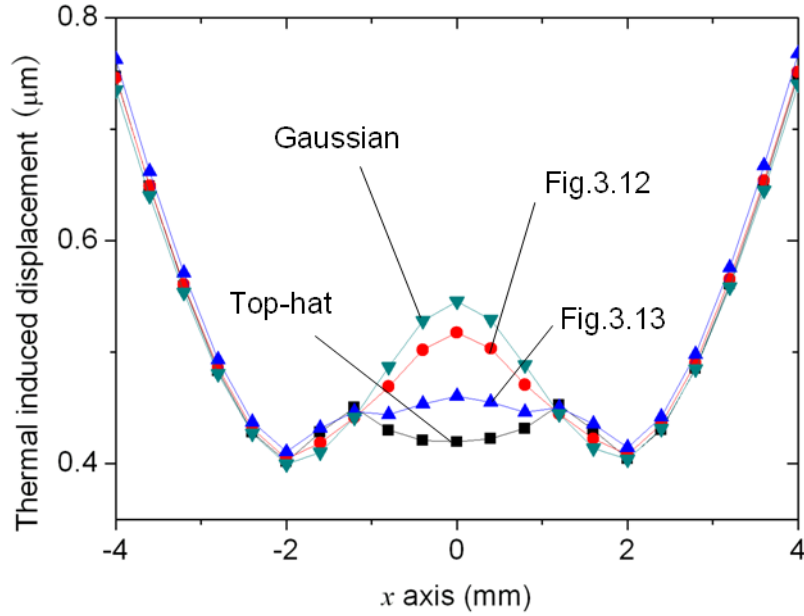

Figure 3.18 Displacement of microchip under different pump shape. The idea top-hat shape and Gaussian shape; the pump shape in Fig.3.12 and 3.13

3.8 Conclusion

In this section, we theoretically study the pump distibution design of multi-direction edge-pumped microchip laser. It shows the possiblity to achieve the central-peak to aviod edge-peak pump shape. The preliminary experiment was done by a 9-direction lens-less edge-pumped microchip laser. The flourence shows agreement with the simulation. The optimization of pump shape is theoretically simulated by using 27 diode chips and other parameters of microchip. The power sacling is available by increasing pump directions as well as use powerful pump diode. We also simulate the thermal, stress , OPD and displacement of microchip under different pump shape.

[1]Keller, Ursula. "Recent developments in compact ultrafast lasers." Nature 424.6950 (2003): 831-838.

[2]http://en.wikipedia.org/wiki/Coefficient_of_determination

[3]Najafi, M., et al. "Simulation of thin disk laser pumping process for temperature dependent Yb: YAG property." Optics Communications 282.20 (2009): 4103-4108.

[4]Sato, Yoichi, Jun Akiyama, and Takunori Taira. "Effects of rare-earth doping on thermal conductivity in $Y_3Al_5O_{12}$ crystals." Optical Materials 31.5 (2009): 720-724.

[5]Aminpour, Hamed, et al. "Dynamical stable cavity of side-pumped thin-disk laser with slanted sides." Applied Optics 50.6 (2011): 811-821.

[6]Copeland, Drew A., and John Vetrovec. "Gain tailoring model and improved optical extraction in CW edge-pumped disk amplifiers." SPIE LASE. International Society for Optics and Photonics, 2012.

Chapter 4

Mode selection and generation for high-order mode

Related paper:

4.1 Introduction

The edge-pumped scheme can achieve controllable pump shape as mentioned in last chapter. It is not only limited in Gaussian like shape, but also available for other shapes. The pump shape will strongly influence on the mode overlapping, so it is a good method to control high-order transverse mode generation by controlling the pump distribution. Until today, high-order modes generation are not so easy and not so powerful by traditional pump method like end-pump Nd^{3+} DPSSL. We propose in this chapter the mode-selection method and demonstrated it by experiment.

4.2 High-order transverse mode and laser resonator

Firstly, it is necessary to distinguish the longitudinal mode and transverse mode in laser cavity, the longitudinal modes are different by their oscillation frequency; transverse modes are different by their filed distribution in the plane perpendicular to the direction of propagation in most case, so called transverse, although they also

have difference in oscillation frequency. It is better to separate the transverse and axial field distribution to make the laser performance more clear. Because the spectral characteristics of laser are determined by the longitudinal modes; beam size, beam quality and energy distribution are determined by transverse modes. Generally speaking, lasers in certain cavity are multimode oscillation; people try to apply it to limited number of modes operation by specific method. For longitudinal modes, it is well known that mode-locking; for transverse mode people pay much attention to fundamental mode oscillation; while in the case of multi-mode operation, a large number of modes occupy the cross-section of laser martial and difficult to select a clean high-order single transverse mode.

Below, we will show the mathematical transverse mode expression. We begin with the free-space wave propagation by the paraxial wave equation approach. The paraxial wave equation can be written as[1]:

$$\nabla^2 \tilde{u}(s,z) - 2jk\frac{\partial \tilde{u}(s,z)}{\partial z} = 0 \quad (4.1)$$

Where $\tilde{u}(s,z)$ is the complex scalar wave amplitude to describe the transverse profile of the beam, $k = 2\pi/\lambda$ is the wave number, s is the transverse coordinate, for rectangular coordinate it is (x,y) and for cylindrical coordinate it is (r,θ). ∇^2 is the laplacian operator on these coordinates plane.

In rectangular coordinate, for easier calculation we separate the x and y parts as: $\tilde{u}_{nm}(x,y,z) = \tilde{u}_n(x,z) \times \tilde{u}_m(y,z)$. The equation for rectangular coordinate can be solved; then we get the solution of Hermite-Gaussian (HG) mode as[2]:

$$\tilde{u}_n(x,z) = (\frac{2}{\pi})^{1/4} \sqrt{\frac{\exp[-i(2n+1)(\psi(z)-\psi(0))]}{2^n n! w(z)}} \\ \times H_n(\frac{\sqrt{2}x}{w(z)})\exp[-i\frac{kx^2}{2R(z)} - \frac{x^2}{w^2(z)}] \quad (4.2)$$

Where $w(z) = w_0\sqrt{1+(z/z_R)^2}$ is the spot size depends on the z axis location, $\psi(z)$ is phase angle, also called Guoy phase shift term and the relationship is given by:

$\tan\psi(z) = z/z_R$, $z_R = \pi w_0^2/\lambda$ and $R(z) = z[1+(z_R/z)^2]$ is spherical curvature. H_n is Hermite polynomial of the order n.

Similarly, the solutions can be got in cylindrical coordinate, which called Laguerre-Gaussian modes written as:

$$\tilde{u}_{p,l}(r,\theta,z) = \sqrt{\frac{2p!}{\pi(1+\delta_{0l})(|l|+p)}}$$
$$\times\left[\frac{\sqrt{2}r}{w(z)}\right]^{|l|} L_p^{|l|}\left[\frac{2r^2}{w^2(z)}\right]\frac{w_0}{w(z)} \qquad (4.3)$$
$$\times\exp[i(2p+|l|+1)\psi(z)]\exp[-\frac{ikr^2}{2(z+iz_R)}+il\theta]$$

where δ_{0l} is the Kronecker delta. $L_p^{|l|}$ is the Laguerre polynomials, with the radial index order p, and azimuthal index order l.

In fact, another solution in elliptic coordinates, one can write the Ince-Gaussian (IG) modes as[3]:

$$\tilde{u}_{p,m}^e(\xi,\eta,z) = \frac{Cw_0}{w(z)}C_p^m(i\xi,\varepsilon)C_p^m(\eta,\varepsilon)\exp[\frac{-r^2}{w^2(z)}]$$
$$\times\exp[kz+\frac{kr^2}{2R(z)}-(p+1)\psi(z)] \qquad (4.4)$$

Where in the elliptic coordinate $x = f(z)\cosh\xi\cos\eta$ and $y = f(z)\sinh\xi\sin\eta$, with radial elliptic variable $\xi \in [0,\infty)$ and angular elliptic variable $\eta \in [0,2\pi)$. Semi focal separation $f(z) = f_0 w(z)/w_0$. The C is normalization constant, C_p^m is the even Ince polynomials with the order p and degree m. For odd ones, to replace C_p^m by S_p^m and different constant C. Other parameters are same with above.

For IG modes the most important parameters in physics for describe these transverse structure is the elasticity $\varepsilon = 2f_0^2/w_0^2$. The HG modes and LG modes can be connected by IG modes. As this dimensionless parameter ε change from 0 to ∞. The trends can be written as: $0 \leftarrow \varepsilon \rightarrow \infty$ leading to $LG \leftarrow IG \rightarrow HG$. This can be a physical shape or size change, which we can slightly know the importance of pump

shape as $Round \leftarrow Ellipse \rightarrow Strip$. The relationship becomes the key to generate different kinds of mode, so called shaped pump beam.

The x axis and y axis are symmetrical and trends towards strip shape for both axis. High-order HG_{n0} modes increase their diameters as the mode index n increases. By mathematic calculation from HG function, to define the spot size by a containing 90% of the energy for rectangular modes, then it gives us the result as:

$$w_n = w_0 \sqrt{2n+1} \qquad (4.5)$$

where w_0 is the TEM_{00} mode waist. This equation can help us estimate the HG index number n later in our experiment, which we change the type of it as:

$$n_{max} \leq \frac{(w_n / w_0)^2 - 1}{2} \qquad (4.6)$$

The stable laser resonator is applied for HG modes generation, for the most common one: the flat-concaved cavity. We define the resonator parameter as $g_1 = 1 - L / R_1$ and $g_2 = 1 - L / R_2$, where the L is cavity length and R is the radius of curvature of the cavity mirror. For stable cavity: $0 \leq g_1 g_2 \leq 1$, as in flat-concaved resonator, $R_1 = \infty$, thus $g_1 = 1$ which we only use $g_2 = g$. With the relationship between HG_{00} mode and high order HG_{nm} modes, we can firstly consider only the fundamental mode by this laser resonator. As soon as we get the specification of HG_{00} mode, all higher order modes can simply scale from it by Equ.4.5. For HG_{00} mode the beam waist on the mirror can be written as:

$$w_0^2 = \frac{L\lambda_l}{\pi} \sqrt{\frac{g}{1-g}} \text{ and } w_2^2 = \frac{L\lambda_l}{\pi} \sqrt{\frac{1}{g(1-g)}} \qquad (4.7)$$

For any location of z-axis, the beam size can be calculate by: $w(z) = w_0 \sqrt{1 + (z/z_R)^2}$.

In good alignment pure laser resonator, the diffraction loss is only decided by the mirror diameter $2a$ and cavity size L. Fresnel number is written by: $N_f = a^2 / (\lambda L)$. In most of the case, the cavity mirror is big enough; the difference of diffraction loss

between modes can be neglected. In the real laser cavity, the losses will strongly depends on the aperture of laser media or other apertures. This is the reason that why the big-aperture pumping is quite important for high-order mode generation to keep a large Fresnel number in the cross-section of laser material. In this case, the Fresnel number can change to $N_f = w_p^{\ 2}/(\lambda L)$, the diffraction loss can be neglected under the condition of the mode index number $n_{max} \leq [(w_p/w_0)^2 - 1]/2$.

4.3 Gain and loss control

The multi-mode laser can be generated easily, because the different kinds of modes which reach the threshold occupy the cross-section of the laser gain media, normally the gain shape is uniform or Gaussian like shape, a few numbers of modes reaches the threshold and begin to oscillate. To explain this in the common situation, we assume the two mirrors stable resonator with certain transverse TEM$_{nm}$ modes at the threshold:

$$R_1 R_2 \exp(2G_{nm}l - 2L_i) = 1 \qquad (4.8)$$

Where R_1 and R_2 are the reflectivity of the two cavity mirrors, l is the thickness of the laser media, L_i is the sum of single pass diffraction loss and other intrinsic cavity loss. We assume the Fresnel number N_f is big enough to let L_i independent on the mode index number *nm* as we discussed in last section. G_{nm} is the single-pass gain coefficient, defined by:

$$G_{nm} = \iiint \phi_0(x, y, z) \Delta N(x, y, z) \sigma dx dy dz \qquad (4.9)$$

The $\phi_0(x, y, z)$ is the normalized density distribution of TEM$_{nm}$ modes, $\Delta N(x, y, z)$ is the population inversion density, which we can be solved from the rate equation in chapter2 as[4]:

$$\Delta N(x, y, z) = \frac{(f_1 + f_2)\tau_f R r_p(x, y, z) - N_l^0}{1 + \frac{(f_1 + f_2)\tau_f c\sigma}{n}\Phi\phi_0(x, y, z)} \qquad (4.10)$$

The parameters are same as that in chapter.2, below threshold the inversion density is

$\Phi = 0$. In the equation, the term of $r_p(x, y, z)$ indicating the pump density

distribution is the gain control. This equation has the meaning that the non-pumped

area and below threshold area exhibit the re-absorption loss, where G_{nm} become

negative. This should be the loss mechanism decided by the material nature, different

from the hard aperture or other cavity loss. We can use it as loss control by manipulate

pump distribution in the *x-y* coordinate of microchip to change re-absorption term

$-N_l^0$ for preventing un-wanted mode reaching threshold. It is worthy to point out that,

in the case $\Phi = 0$ all of the modes suffer from re-absorption loss.

Without the transverse mode selection, several modes can satisfy equation 4.8.

By the method of gain and loss control, the modes TEM_{nm} which meets

$R_1 R_2 \exp(2G_{nm}l - 2\delta) < 1$, will fail to oscillate, it is possible for us to select the desired

single transverse mode in certain laser cavity.

4.4 Calculation for high-order HG modes selection

In the stable laser cavity, for a given pump position in the *x-y* coordinate of laser

media, pump size w_p and pump shape, the transverse mode with the minimum

threshold will break into oscillation at first. Followed by this judgment, it is necessary

for us to discuss the threshold at first, the threshold must be has relationship with the

pump position, pump size, pump shape and pump density. Turn back to the rate

equation in chapter 2, the solution of threshold is proportional to the effective mode

volume and total loss: $P_{th} \propto V_{eff}(L_i + T + 2N_l^0 \sigma l)$. The mode volume V_{eff} is related

with pump distribution $r_p(x, y, z)$ and laser mode $\phi_0(x, y, z)$. As shown in the

equations, if make a directly result of $P_{th,\text{TEM}nm} / P_{th,\text{TEM}n'm'}$ by uniform pump, the selectivity of pump threshold is independent on the loss term N_l^0, only related with the V_{eff}. As the pump distribution $r_p(x,y,z)$ can be manipulated in *x-y* coordinate, the N_l^0 becomes different after some place is pumped to transparent, the role of re-absorption loss now is effective when $\Phi > 0$ mainly for preventing from secondary mode to reach threshold. In order to make the discussion easier, firstly we separate the gain and loss terms. Only discuss the $P_{th} \propto V_{eff}$, the loss is assumed to be same for the limited index number of TEM_{nm} modes.

As the thickness of microchip is far less than the aperture of microchip, we neglect the z-axis variation only discuss in the *x-y* coordinate. Let us begin with the basic model of pump distribution. Fig.4.1 shows several pump method of traditional ones of end-pump scheme and news ones introduced by edge-pumped scheme. In the figure, the grey colour represents pump distribution $r_p(x,y)$ and red circle represents the TEM_{00} mode distribution $\phi_{00}(x,y)$. In Fig.4.1 (a), it is the most common pump scheme in end-pump and face-pump scheme for fundamental TEM_{00} mode generation, the pump shape could be Gaussian, top-hat or super-Gaussian; Fig.4.1 (b), it is the off-axis pump method for high-order transverse mode generation; (c) is shaped pump beam as well as off-axis for high-order transverse mode generation, the shaped beam is often made by special lens or prism pair; (d) is one dimensional strip pump for HG_{n0} mode generation, it can be easily realized in edge-pumped scheme, the pump source could be diode coupled fiber or diode chip directly; (e) is special shaped pump method for doughnut mode generation by using capillary or hollow laser material in end pump scheme, in edge-pump scheme it can be realized much easier by pump distribution manipulation or non-doped core composite ceramic laser material; (f) is two-dimensional strip pump for HG_{nm} mode generation as well as vortex arrays generation, because of the limited space of pump scheme, diode chip is the best

choice. Some researcher apply hard aperture by wires in the cavity to realize the line

shape loss instead of shaped gain can realize same effect.
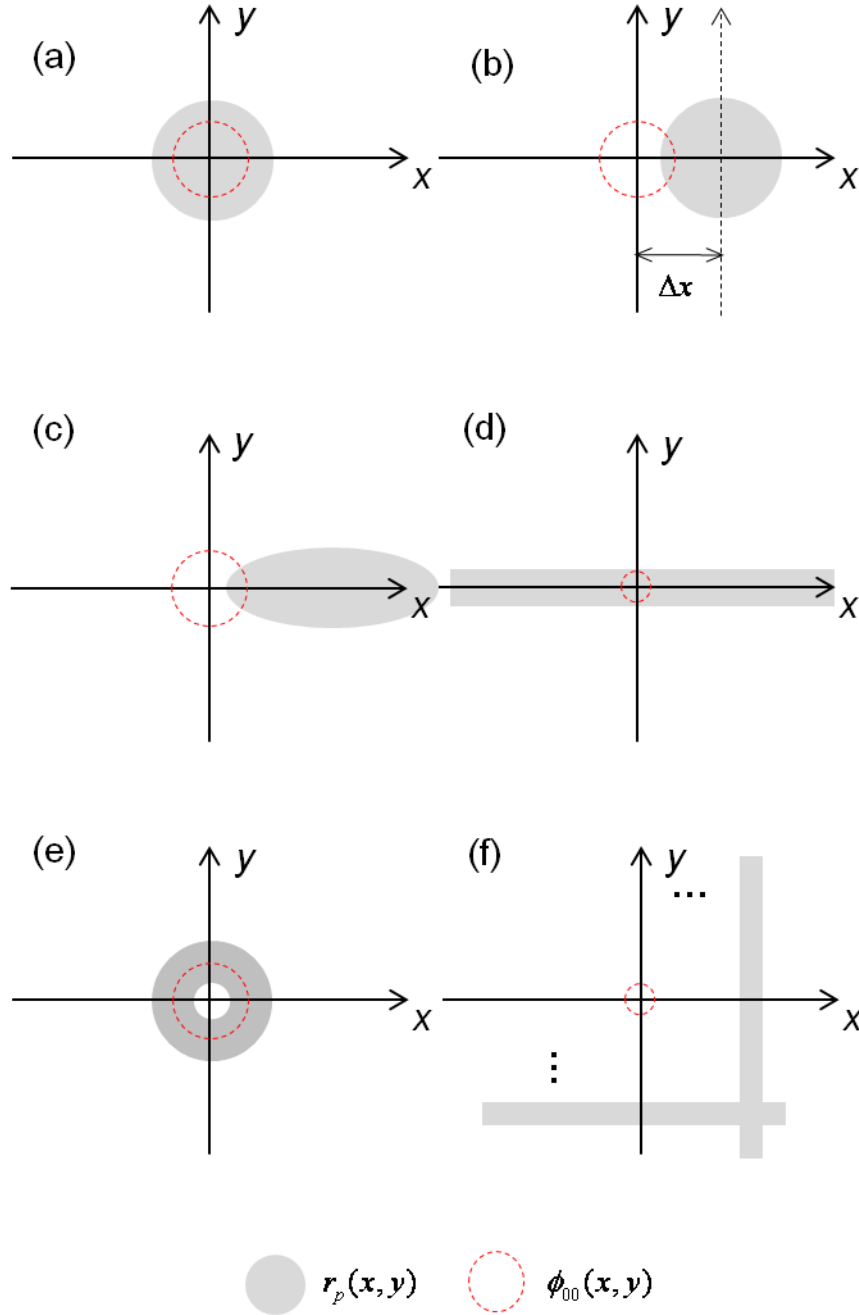

Figure.4.1 Several pump schemes (a) normal pump; (b) off-axis pump; (c) shaped off-axis pump; (d) 1-D strip pump; (e) doughnut pump; (f) 2-D strip pump

In order to analyse the mode selection mechanism, we give the mathematical expression of $\phi_{nm}(x,y)$ and $r_p(x,y)$. Because the symmetry of HG modes in x and y axis. We just analyse the HG_{n0} modes. And $\phi_{n0}(x,y)$ is given by:

$$\phi_{n0}(x,y) = \frac{2}{\pi w_l^2 2^n n! l} H_n^2(\frac{\sqrt{2}x}{w_l^2}) \exp[-\frac{2(x^2+y^2)}{w_l^2}] \qquad (4.11)$$

where w_l is the laser beam waist of TEM_{00} mode. The pump distribution $r_p(x,y)$ in Fig.4.1 (a) can be given by equation 2.13. Define the relationship of pump beam size and laser beam size as $w_p/w_l = a$. The calculation result of relative pump power $r_{in} = P_{th,TEM_{n0}} / P_{th,TEM_{00}}$ under the pump scheme in Fig.4.1 (a) is shown in Fig.4.2.The pump shape is Gausssian shape represents most of the pump case in end-pump scheme. The black dot means the threshold of HG_{00} mode is normalized as $r_{in} = P_{th,TEM_{00}} / P_{th,TEM_{00}}$ equal to 1 under any case of pump beam size. The red dots is under the condition of the same size of pump beam and fundmental beam, the fundmental beam size is decided by the laser cavity. Obviously, the HG_{00} mode with the lowest threshold will ossilate first, then it will extract energy from the active medium and preventing from other high order mode ossilation, it is impossible to select high order mode in this case, even negelecting diffraction loss and reabsorption loss for high-order modes.It is easy to undertand that the loss will not be helpful for high-order mode, as the loss of high-order modes always bigger than funmental mode. The blue dots are under the condition of $a = 1.2$, the pump beam size is a little bigger than the fundmental mode size. Although the relative pump power for HG_{n0} modes are modified slightly, the trend can not change. Even if the pump size change to 5 times more, shown by the gray dots, the threshold of HG_{00} mode still keeps the minimum, although the difference is much smaller. In this case, definatly it will be multi-mode osslation and the ossilated high-order modes number only desided by the

Fresnel number $N_f = w_p^2/(\lambda L)$, which means the diffraction loss of cavity will dominate the mode selection.
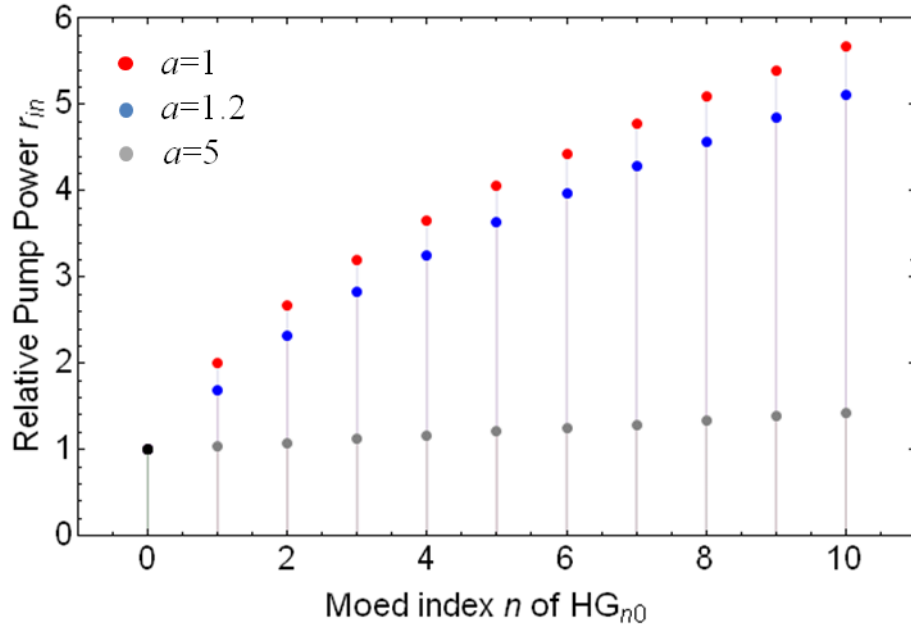

Figure.4.2 The relative pump power for different high-order HG$_{n0}$ under the traditional Gaussian pump shape
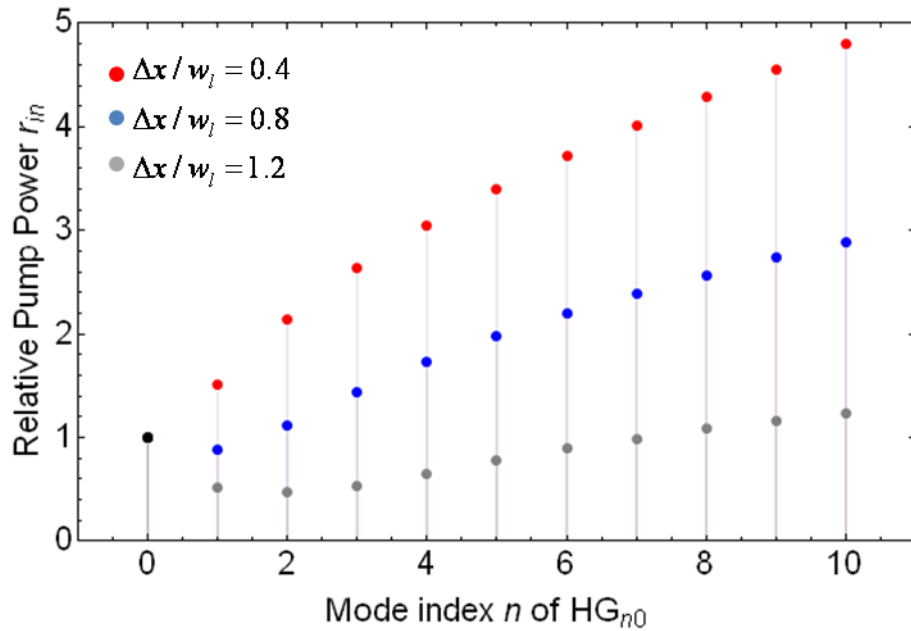

Figure.4.3 The relative pump power for different high-order HG$_{n0}$ under the condition of off-axis pump

In the case of off-axis pump in Fig.4.2 (b), the modified pump distribution of equation 2.13 can be written as:

$$r_G(x, y, z) = \frac{2}{\pi w_p^2 l} \exp[-\frac{2(x - \Delta x)^2 + 2y^2}{w_p^2}] \qquad (4.12)$$

Where the Δx is the length of off-axis as shown in Fig.4.1 (b). The calculated result of relative pump power for different high-order HG_{n0} modes under different Δx is shown in Fig.4.3. The red dots represent $\Delta x / w_l = 0.4$, which means a little bit off-axis cannot change the trend. The HG_{00} is still keeping the minimum threshold. The high-order modes cannot break into oscillation. With a little bigger off-axis $\Delta x / w_l$ =0.8, which is shown by the blue dots, the relative pump power is modulated. The HG_{10} mode now holds the minimum threshold and break into oscillate at first. The grey dots show the condition of relatively big off-axis $\Delta x / w_l = 1.2$. It is obvious that the amplitude of modulation becomes smaller, but still it can select the HG_{20} mode. We can easily judge the trends that for higher mode selection, just make the off-axis distance bigger, but it will finally failed by the small difference of gain, then re-absorption loss or diffraction loss will dominate, higher order mode failed in competition. In addition, the threshold is too big that we cannot bear. In this case we need another pump method like shaped one in Fig.4.1 (c) and (d), as the ellipse pump shape has the similar effect with the round one when they are off-axis. Next we will only discuss about the strip shape pump in Fig.4.1 (d).We define the strip pump shape as:

$$r_S(x, y, z) = \frac{1}{4\sqrt{2b+1} w_p^2 l}, \quad |x| \le \sqrt{2b+1} w_p, |y| \le w_p \qquad (4.13)$$

And assume the length of long side is $\sqrt{2b+1}$ times than the length of short side. In reality, the ideal uniform strip size cannot be realized; we neglect the divergence of pump beam, only consider the absorption coefficient α to re-write the equation 4.13 as:

$$r_{S'}(x,y,z) = \frac{\alpha \exp[-\alpha(x + \sqrt{2b+1}w_p)]}{2w_p l(1 - \exp[-2\alpha\sqrt{2b+1}w_p])}, \qquad (4.14)$$

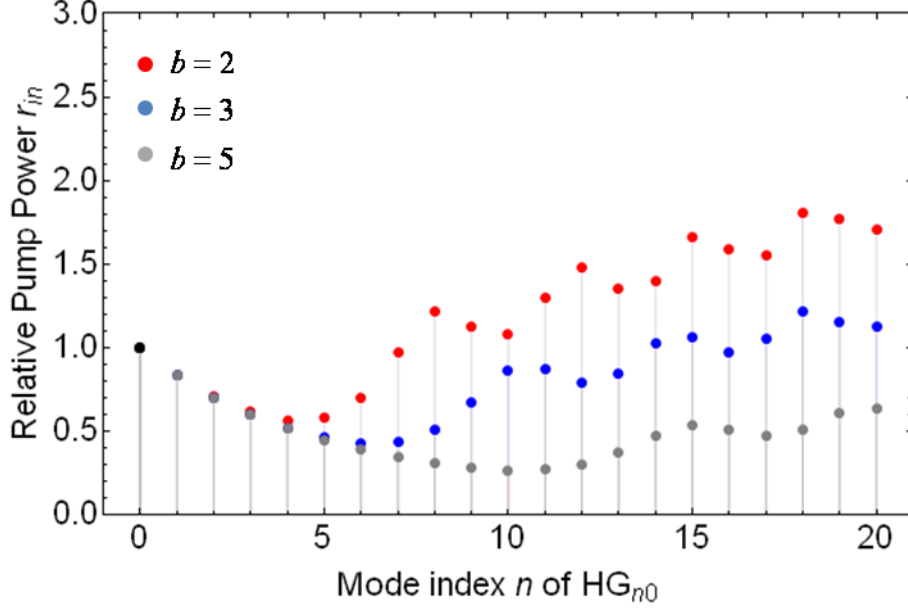$$|x| \leq \sqrt{2b+1}w_p, |y| \leq w_p$$

Figure.4.4 The relative pump power for different high-order HG_{n0} under the condition of strip size pump

Fig.4.4 shows the relative pump power for different high-order HG_{n0} under the condition of strip shape pump, assume $a=1$ and $\alpha = 9mm^{-1}$. The red dots are under the condition of $b=2$, the threshold of HG_{n0} modes are modulated strongly compared with the off-axis pump in Fig.4.4. the HG_{40} mode holds the minimum threshold and oscillate at first. The fundamental modes failed to compete with other HG_{n0} modes ($n \leq 7$). The modulation appear the wave type because the energy percentage of side peak for different HG_{n0} modes. The blue dots represent $b=3$ and gray dots represent $b=5$. The selected modes are $HG_{6,0}$ and $HG_{10,0}$ respectively. The selected mode index has the relationship with the b factor as $b = n/2$ if don't take account into the loss impact. The parameters a and α also influence on the result of selection but the trends is same.
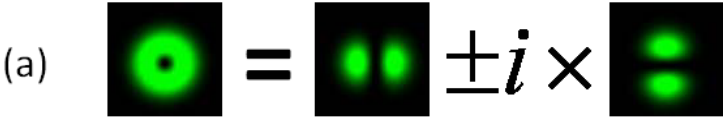
Fig.4.1 (e) shows a special pump shape aiming at the doughnut mode generation. We will discuss in next chapter for doughnut mode power scaling. Fig.4.1 (e) is the

2-dimentional strip pump for HG_{nm} mode generation. As we know that HG_{n0} can be easily generate by the off-axis end pump scheme, but only limited in HG_{n0}. Obviously, it is because the limitation of pump method. Edge-pumped scheme has the flexibility to make n_{max}^{x} bigger as well as the secondary dimensional n_{max}^{y}, so the generation of HG_{nm} mode is promised. As HG_{nm} modes were only realized in gas laser[5] and end-pumped opaque-wire method[6], the edge-pumped microchip lasers proposes both the new convenient pump scheme and power scalability.
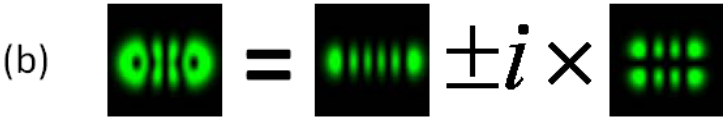
4.5 Vortex beam generation.

The vortex beam denotes the beam with doughnut intensity distribution and a spiral phase variation in its beam cross-section. For example, the LG modes have the spiral phase front $il\theta$ shown in equation 4.3 which corresponding to the orbital angular momentum $l\hbar$, where θ is the azimuthal angle. The $LG_{p,l}$ modes with radial order p and azimuthal order l is the solutions of paraxial wave equation in cylindrical coordinate. The fundamental mode LG_{00} is same as HG_{00}. Other higher order modes are different with HG_{nm} modes. When $|l| \geq 1$ the interference pattern with spherical wave is spiral shape so called "vortex beam"[7], for $l>0$ it is counter-clockwise spiral and for $l<0$ it is clockwise spiral shape. It is worthy to point out that the light is not propagating like a helical path; it is the phase of the light changing in such a way. The beam quality is defined as: $M^2 = 2p + |l| + 1$. So, the beam quality factor of LG_{01} mode is $M^2 = 2$.
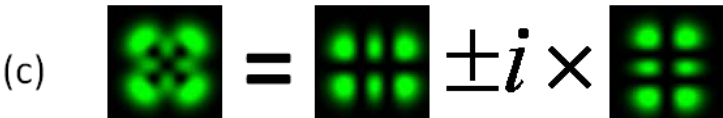
The generation of LG_{01} mode beam can be represented by HG pairs[6,8] as: HG_{01} and HG_{10} mode with a phase shift of $\pi/2$, which can be written as: $LG_{01} = HG_{10} \pm iHG_{01}$, the simulation prediction is shown in Fig.4.5. For vortex arrays (VA), similarly we can write as: $VA = HG_{nm} \pm iHG_{mn}$, which is shown in Fig.4.5 as VA. This can be experimentally demonstrated by a converting $HG_{n,n+1}$ mode to

(a)

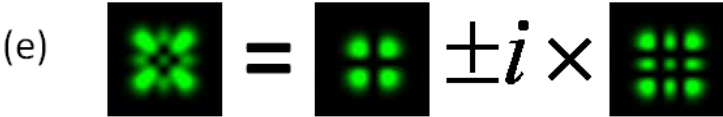$$\text{LG}_{01} = \text{HG}_{10} \pm i \times \text{HG}_{01}$$

(b)

$$\text{VA}_1 = \text{HG}_{n+k,0} \pm i \times \text{HG}_{n,1} \quad \begin{array}{l} n=3 \\ k=2 \end{array}$$

(c)

$$\text{VA}_2 = \text{HG}_{n+1,n} \pm i \times \text{HG}_{n,n+1} \quad n=1$$

(d)

$$\text{VA}_3 = \text{HG}_{n+k,n} \pm i \times \text{HG}_{n,n+k} \quad \begin{array}{l} n=1 \\ k=2 \end{array}$$

(e)

$$\text{VA}_4 = \text{HG}_{n,n} \pm i \times \text{HG}_{n+k,n+k} \quad \begin{array}{l} n=1 \\ k=1 \end{array}$$

Figure.4.5 Vortex array beams generated by different kinds of
HG mode pairs.

$\text{HG}_{n+1,n}$ mode and generation of square vortex array laser beams by the Dove prism-embedded unbalanced Mach-Zehnder interferometer. Mathematically, follow equation 4.2, applied $\text{HG}_{nm} = \tilde{u}_{nx}(x,z) \times \tilde{u}_{my}(y,z)$, HG_{nm} can be written by:

73

$$HG_{nm}(x,y,z) = \sqrt{\frac{1}{2^{nx+ny-1}nx!ny!\pi}} \frac{\exp[-i(nx+ny+1)(\psi(z)-\psi(0))]}{w(z)}$$
$$\times H_{nx}(\frac{\sqrt{2}x}{w(z)})H_{ny}(\frac{\sqrt{2}y}{w(z)})\exp[-i\frac{k(x^2+y^2)}{2}-\frac{x^2+y^2}{w^2(z)}] \quad (4.15)$$

the parameters are same as equation 4.2. The Guoy phase $\psi(z)$ item is controlled by propagation distance: $\psi(z) = \tan^{-1}(z/z(R))$. Different from what we will illustrate here, this method is operated outside laser cavity by $HG_{n,n+1}$ mode and interferometer. What we will discuss is that $HG_{n,n+1}$ and $HG_{n+1,n}$ mode pairs in laser cavity combining directly into VA beams. We will present an experimental demonstration for our casein experimental section later.

Fig.4.5 shows the different VA beam patterns by theory prediction. Beside LG_{01} and square vortex array VA_2. We also set example of other VA beams. VA_1 is one dimensional vortex array, there are 2 holes inside the beam pattern. The left of VA beams are the symmetry vortex array but a little different from each other. It is necessary to distinguish them by discussing the number of holes. The embedded holes can be calculated by the method of zero-point calculation of HG Polynomials. By omit the duplicate parts of equation 4.15 and let $H_{nx}H_{my} + iH_{mx}H_{ny} = 0$. Take an example of square vortex array VA_2 we could obtain[6]:

$$H_n(\frac{\sqrt{2}x}{w(z)})H_{n+1}(\frac{\sqrt{2}y}{w(z)}) = 0$$
$$H_{n+1}(\frac{\sqrt{2}x}{w(z)})H_n(\frac{\sqrt{2}y}{w(z)}) = 0 \quad (4.16)$$

Considering that the different order index cannot be zero at the same time. We separate them by two nodal point square-arrays calculation $n \times n$ and $(n+1) \times (n+1)$, so the total number of the holes is $n^2 + (n+1)^2$. For one-dimensional case VA_1 and $k = 2$, the holes number is 2. For two-dimensional case VA_3, as $k = 2$ the hole

number is always 2×2. For the case of VA_4, the holes number is calculated by $2n(n+1)$. For the specific cases in Fig.4.5 the holes number is VA_1=2, VA_2=5, VA_3=4 and VA_4=4. For higher number of *n*, it is possible to scale up the calculation by the same method.
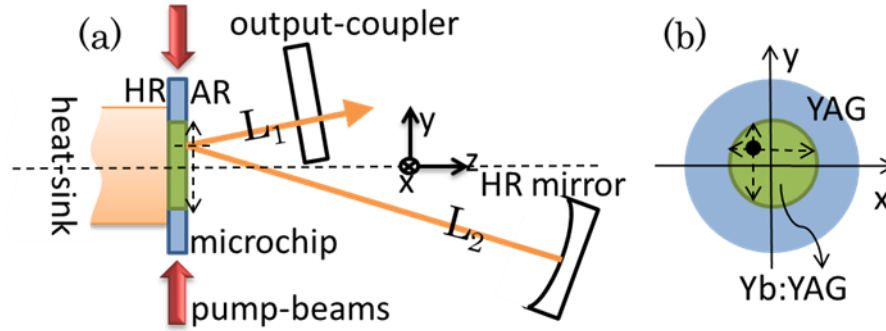

Figure.4.6 (a) Schematic diagram of 9-direction edged pumped Yb:YAG ceramic microchip laser with V-type cavity. (b) Front view of microchip; the black point indicates mode area on the microchip and arrow-lines indicate the 2D scan coordinate by misalignment of the microchip and cavity mirror.

4.6 Experimental setup and result

The experimental setup is shown in Fig.4.6. The laser module is same as Chapter 3. The composite Yb:YAG/YAG all-ceramic microchip is type B, with core radius of 1.9 mm. The nine diode chips are controlled by two power supplies, one power supply for 4 diodes and the other for five diodes. The diodes have the $1 \times 100 \, \mu m^2$ emitter size and relative low divergence angle about 8.45 deg after coupling inside the microchip. The beam widths is about 0.7 mm at the $1/e^2$ of the maximum at the center of the microchip under the maximum pumping power. A V-type cavity is applied instead of the normal plane-concaved cavity, we are going to apply misalignment between the microchip and end mirror to choose mode areas. The misalignment displacement can be calculated by the simple geometrical optics which we have discussed in section 4.2. By keeping good alignments of end mirror and misalignment of microchip, the mode area can scan on the core of microchip. The

mode size on the microchip can be controlled by changing the distance of L_1 and L_2.

We use the plano-concaved mirror with a curvature radius of 500 mm and 97% flat

output coupler, $L_1 = 50$ mm and $L_2 = 200$ mm for the experiment, corresponding to a

fundamental beam diameter of $2w_l = 0.58$ mm by the ABCD cavity calculation.

Compared with the beam width $2w_p = 0.7$ mm at maximum pump power, the ratio of

pump beam size and fundamental mode size is $a = w_p / w_l = 1.2$, when the pump

power is low, a is estimated around 1~1.1. The pump strip ratio of $b \approx 14$ and the
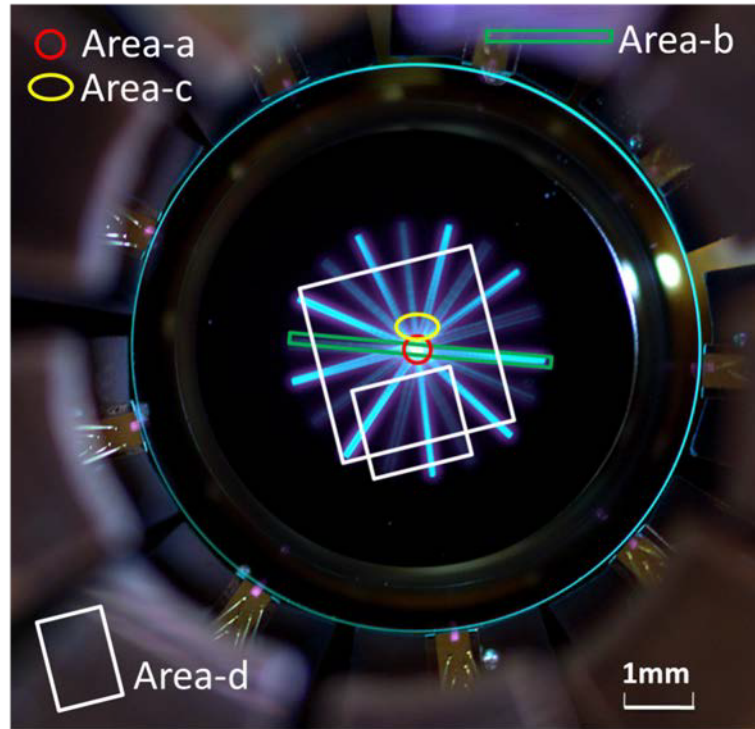
$n_{\max}$ is estimated about 21.

Figure.4.7 Front view of microchip laser and mode generation areas (marked by approximate shape): Area-a for HG_{00} mode, Area-b for HG_{n0} mode, Area-c for doughnut mode and HG_{11} mode, Area-d for HG_{mn} (m; $n > 1$) mode. The bright areas indicate the pump regions and the black area is the non-pumped regions and non-doped YAG regions.

Figure.4.7 shows the pumping shape on the microchip. The picture was taken

when the diode chips were around threshold (<1 W for each), so the beams seem very

narrow. As the pump power increase, the beam will become fatter and fatter. Nine beams are designed to overlap at the centre, which the initial aim is for fundamental mode generation. The overlap is not perfect due to technical limitation, but the resulted different kinds of overlap shape could help us select different kind of mode. Beside the central peak like Fig.4.1 (a) and strip shape like Fig.4.1 (d), many crossover shape exist, for example it appear the triangle pump shape which is similar like Fig.4.1(e). We mark the possible areas for the generation of different modes. Area-a (red circle mark) can easily generate HG_{00} mode with the highest output power, in Area-b (green strip mark); distinguished HG_{n0} modes can be generated from n=1 to n=22; Area-c (yellow ellipsoid mark) can generate doughnut mode and HG_{11} mode; Area-d (white rectangle mark) can generate HG_{nm} modes although it is not the perfect orthogonal pump like Fig.4.1 (f). When $1 < m, n < 7$ the modes are stable and clean, when $n, m \geq 7$, the modes become poor, the central part of the beam has the tendency to unite together, it is because the central pump is too strong to be suppressed as the pump power becomes higher and pump beam become fatter. If under the ideal condition of Fig.4.1 (f), it should be much better and could support higher order HG modes. We select several representative modes corresponding to the pump method in Fig.4.1 as visual explanation for gain loss control mode selection in Fig.4.8. We made this for experimental demonstration of HG modes selection and generation with relative high power compared with end pump scheme.
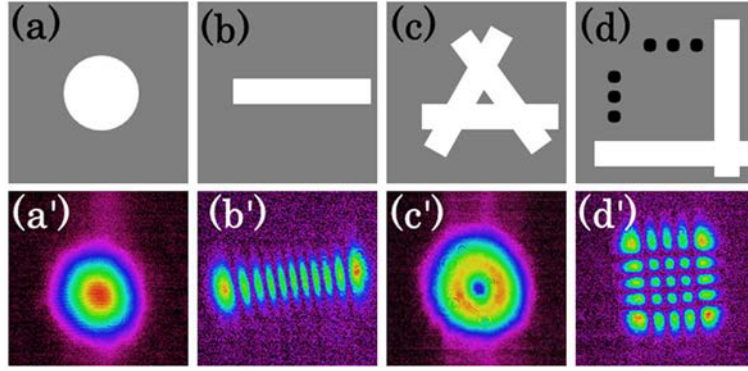
Figure.4.8 Different mode-gain and mode-loss distribution aim at (a) HG_{00} mode, (b) HG_{0n} modes, (c) doughnut (LG_{01}) modes, and (d) HG_{mn} modes. The gray color indicates non-pumped area as loss and white color indicates pumped area as gain. Different output beam pattern taken by CCD camera: (a') 0.94 W LG_{00} mode beam, (b') 0.33 W $HG_{10,0}$ mode beam, (c') 0.57 W doughnut shape beam, and (d') 1.3 W HG_{44} mode beam.
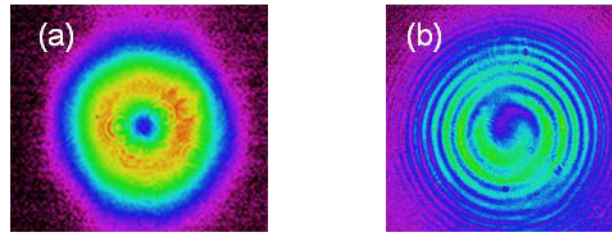

Figure 4.9 (a) Experimental doughnut mode beam pattern and (b) vortex interference pattern taken by CCD camera.

We also measured the out put power and the stable zone of different modes. Fig.4.9 shows the out put power of HG_{00} mode, doughnut mode (LG_{01}) and HG_{nn} modes versus input pumping power. The HG_{00} mode can be generated fro lasing thresholds around 13 W to 50 W of pump power. For higher pump power, HG_{00} is not available by current cavity, a mix mode appears, although it looks like a single-peak Gaussian shape. High-order HG modes appear after the lasing threshold. The HG_{01}, HG_{10} and HG_{11} modes can be attained easily under any pump power, but the dought mode only appears by good adjustment of the mode areas on the microchip, the balance between HG_{10} and HG_{01} is quite importance , this is the resason why we separate the power supply into two. From 300 to 620 mW, the doughnut mode can be attained sequentially without changing the location of the mode area, the beam quaility M^2 is around 2.0, which shows agreement with the theroy. The following

doughnut beams, we attained by changing the mode area for higher power with the M^2 around 2.1~2.2. It is worhy to point out that for a <1 W doughnut mode, the shape is perfect doughnut shape, for higher power doughnut beam, especail over 3 W, the shape turns out to be a little longer and stronger in the major axis, which should be attributed to the nonuniform pumping. Finally more than 7 W doughnut mode canbe attained, the M^2 is about 2.8. We confirmed the LG_{01} mode by checking the interference pattern as a vortex, the result was taken by CCD camera in Fig. 4.9. The output laser of doughnut was also passed though a polarizer, and we rotated the polarizer without any transmission mode structure changed. This suggested that the beam is not radial or azimuthal polarised but a radom one, because there is neither polarization selection mechanisms in laser material nor in laser caviy.
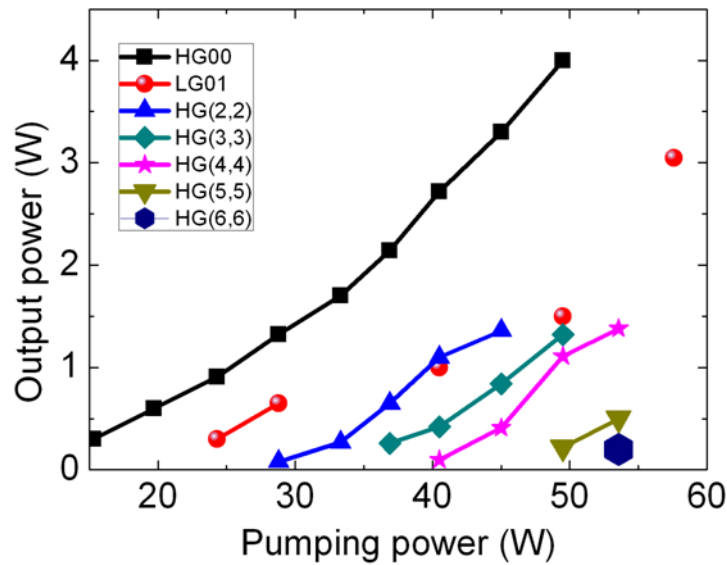

Figure.4.10 The output power of HG_{00} mode, LG_{01}, and HG_{nn} modes as a function of input pumping power.

We also generatd watt-level HG_{nn} modes as shown in Fig.4.10, for example 1.38 W HG_{44} mode under the pump power of 54 W. In Fig.4.10 we could find the HGnn modes appear and disappear regularly following the mode index n, it is because high order beam suffer a bigger diffraction loss and higher pump power support enough gain in the area far from the input edge. We do not show the data of HGmn mode here,

because too many of them, with the power from several hundred miliwatts to several watts.
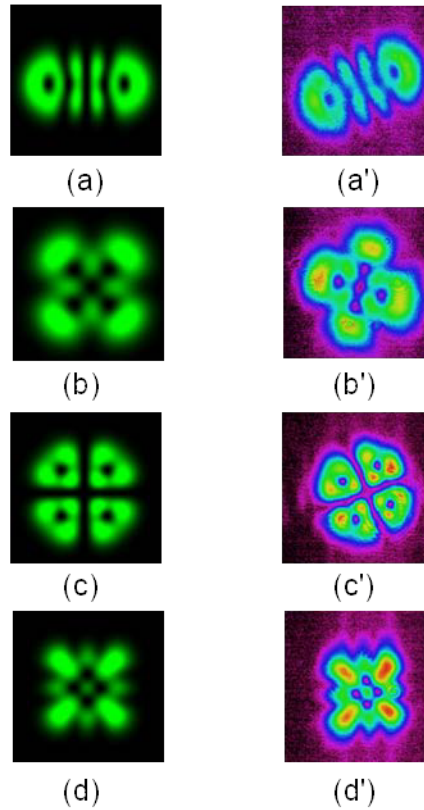

Figure.4.11 The simulation beam pattern of vortex arrays (a)~(d) compared with the experimental beam pattern (a')~(d') .

We shows the vortex array beams in Fig.4.11, the simulated beam pattern shows great agreement of generated beam pattern with about 500 mW power in the experimental result. For higher power, it is still possible for several watts. The method of HG mode pair generation in laser cavity has been demonstrated. The theory illustrated in last section can be approved simply by our experiment as below: when some kind of vortex array is attained after a good adjustment, decrease the pump power of four diode chips controlled by one power supply, until we can get one of the HG_{nm} mode. Then recover the pump power and decrease the other diode chips controlled by the second power supply, until we can get the other HG_{mn} mode. Finally recover all the pump power to get the initial vortex array beam. We also generated lot kinds of vortex array beams with different holes number. By understanding the HG_{n0} generation theory, it is easy to understand these results. The method is approved to be

useful for directly generation of vortex arrays. This demonstration also show us the advantage of edge-pumped scheme, it is possible to precisely adjust the intensity of *x*-axis and *y*-axis by different pump power to realize the uniform vortex beam. In many other high power vortex beam generation experiment, for example doughnut mode, the headache is always the imperfect doughnut beam shape that the intensity of one direction is far less than the other.

4.7 Conclusion

In this chapter, we study on the high-order transverse mode selection theory in edge-pumped microchip laser. The experiment demonstrated various predicted modes. The power is much higher compared with traditional end-pump scheme; the method is effective and convenient.

It is worthy to point out that power scalability and efficient high-order mode oscillation are limited in our current system due to the non-target pump scheme. We are going to study the theory and method here, as soon as we understand theory, we can design the specific laser module for high efficiency and high power certain mode generation.

---

[1]Siegman, Anthony E. "Lasers University Science Books." Mill Valley, CA 37 (1986).

[2]Senatsky, Yury, et al. "Laguerre-Gaussian modes selection in diode-pumped solid-state lasers." Optical Review 19.4 (2012): 201-221.

[3]Bandres, Miguel A., and Julio C Gutiérrez-Vega. "Ince Gaussian beams." Optics letters 29.2 (2004): 144-146.

[4]Taira, Takunori, William M. Tulloch, and Robert L. Byer."Modeling of quasi-three-level lasers and operation of cwYb: YAG lasers." Applied optics 36.9 (1997): 1867-1874.

[5]H. Kogelnik and T. Li, "Laser beams and resonators," Appl. Opt.5(10), 1550–1567 (1966).

[6]Shu-Chun Chu, Yun-Ting Chen, Ko-Fan Tsai, and Kenju Otsuka, "Generation of high-order Hermite-Gaussian modes in end-pumped solid-state lasers for square

vortex array laser beam generation," Opt. Express 20, 7128-7141 (2012)

[7]Padgett, Miles, and L. Allen."Light with a twist in its tail." Contemporary physics 41.5 (2000): 275-285.

[8]Koki Shimohira, Yuichi Kozawa, and Shunichi Sato, "Transverse mode control by manipulating gain distribution in a Yb:YAG ceramic thin disk," Opt. Lett. 36, 4137-4139 (2011)

Chapter 5

Power scaling and Future direction

Related paper:

5.1 Introduction

We have studied on mode-selection theory and above threshold power scaling of certain mode. We also experimentally demonstrated the high-order transverse mode generation and vortex beam generation. But the preliminary laser module was not targeted designed. In order to realize high-power and high efficiency, it is necessary to use the theory to design a specific laser module for certain mode. As mentioned before, the LG_{01} mode is attractive with a lot of interesting application. In this chapter we will theoretically calculate the LG_{01} mode-design towards high-power as an example of power scaling and our future direction.

5.2 High power and high efficiency design for vortex beam

In last chapter, we experimentally demonstrated the mode-selection of high-order transverse modes. But the experiment only aim to study the selection mechanism without thinking the efficiency. In this section we are going to discuss high efficiency

system design towards high power operation. We will apply vortex beam generation as our future plan towards hundreds watts average power.
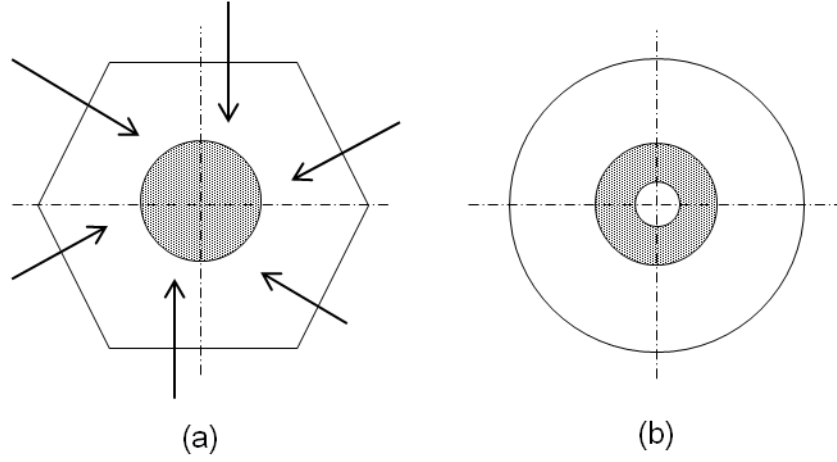

Figure 5.1 The method to realize doughnut pump shape by (a) off-axis edge-pumped scheme. And (b) double-core microchip. The shadow areas present doped Yb:YAG, the white areas are no-doped YAG. The arrows present pump beam by diodes.

The pump shape is defined following the Fig.4.2 (e). We assume the pump distribution as:

$$r_v(x, y, z) = \frac{1}{\pi w_p^2 l(p^2 - 1/q^2])} \qquad (5.1)$$

as $r \leq \sqrt{2p+1}w_p, r \geq w_p/q$,where p and q are the shape factor to make our discussion easier. We define this uniform doughnut pump shape although the real pump shape could be a little different. The method to realize the doughnut pump shape is quite easy by edge-pumped scheme. Fig.5.1 shows two of the methods to realize doughnut pump shape. Method (a) is off-axis pump without passing the centre, the scheme only show 6-direction pump and it is necessary for more-direction pump to realize uniformity and high pump power. Method (b) is based on double-core composite ceramic material the non-doped inner core makes it possible to realize the doughnut pump shape. It is also possible to make the other material of inner core to absorb laser wavelength but non-absorption of pump wavelength to increase the $L_i^{HG_{00}}/L_i^{LG_{01}}$. Apparently, method (b) is much easier in technique. But the method (a)

has another application in plural modes shift, as some application ask for two kinds of laser beam. By applying both on-axis and off-axis pumping controlled by different power supplies; it is possible to realize HG_{00} and LG_{01} modes fast switching without any adjustment of cavity mirror.
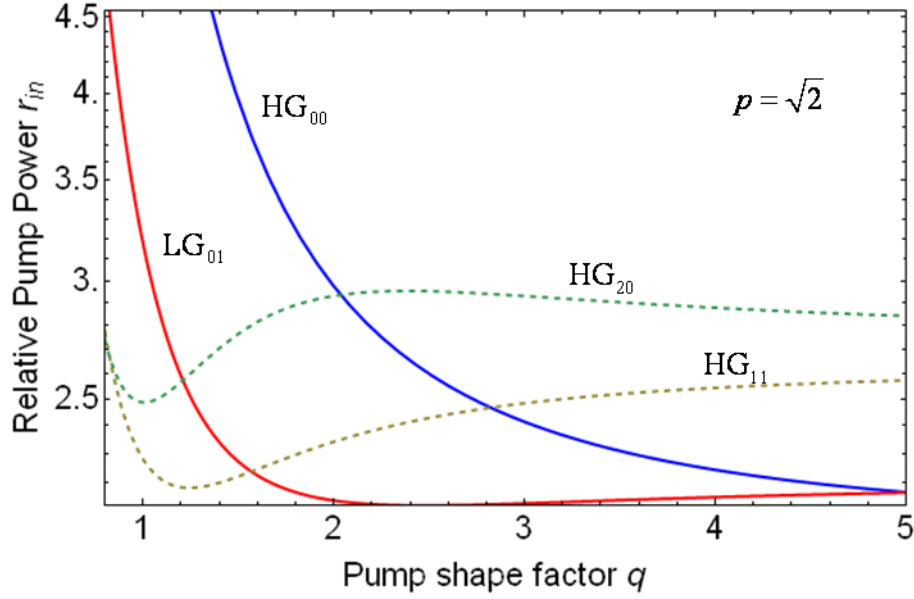

Figure 5.2 The relative pump power as a function of pump shape factor q for different kinds of modes.

In order to realize the lower threshold compared with HG_{00} mode, it is necessary to optimize the pump beam size at first. Follow the pump shape definition equation 5.1; it then turns out to study on the p and q shape factor. The beam radius of LG_{01} mode is $\sqrt{2}$ times larger than the HG_{00} mode[1]. Thus p can be easily decided to as $\sqrt{2}$ to let pump threshold be minimum. Then we need to determine the q value, we define the relative pump power as $r_{in} = P_{th,\text{mode}}^{doughnut-pump} / P_{th,\text{HG}_{00}}^{Gaussian-pump}$, which means the pump threshold of certain mode under the doughnut shape pump as in equation 5.1 normalized by the pump threshold of HG_{00} mode under the Gaussian-pump shape (assume $a = w_p / w_0 = 1$).

The calculated result is shown in Fig.5.2. The smaller q value means a bigger

non-pumped circle size, the bigger q value means a smaller non-pumped circle size. The blue line is the relative pump power of HG_{00} mode, written by $P_{th,HG_{00}}^{doughnut-pump}$. The red line is the relative pump power of LG_{01} mode, written by $P_{th,LG_{01}}^{doughnut-pump}$. The dashed lines are $P_{th,HG_{11}}^{doughnut-pump}$ and $P_{th,HG_{20}}^{doughnut-pump}$ modes respectively. The doughnut mode LG_{01} can hold the minimum threshold: $1.6<q<5$. The optimize q value should be around 2.8, as the pump threshold of LG_{01} keeps minimum and other modes keeps relative higher above it. Take $q=2.8$, the ratio of outer radius and inner radius of doughnut pump shape is $\sqrt{2}w_p/(w_p/2.8)\approx 4$. To be point out that, this calculation only show the gain aspect. It is also need to illustrate the loss for the pump power scaling. Assume the loss is all the same for different modes in Fig.5.2, when $p=\sqrt{2}$, $q=2.8$, the doughnut mode reach the threshold when $r_{in}=2.1$ at first, other modes keeps highest threshold compared with it, shown in Fig.5.2 as the crossing point of blue line and lower dashed line when $r_{in}=2.5$. It then need some loss mechanism to prevent from these mode reach threshold, which means to increase the loss ratio $L_i^{HG_{00}}/L_i^{LG_{01}}$, $L_i^{HG_{11}}/L_i^{LG_{01}}$ and $L_i^{HG_{20}}/L_i^{LG_{01}}$. For the high order mode HG_{11} and HG_{20}, it is easy to increase the diffraction loss by cavity design and using hard apertures, which means $L_i^{HG_{11}}/L_i^{LG_{01}}$ and $L_i^{HG_{20}}/L_i^{LG_{01}}$ could be bigger than 1. Now it is only need to consider how to suppress fundamental mode HG_{00}, because the diffraction loss of HG_{00} mode is always smaller than LG_{01} mode if not considering the cavity misalignment. The q number cannot be too small to make the pump threshold of LG_{01} mode too big. The acceptable range of q is 1.6~2.8 keeping pump threshold of other modes above pump threshold of LG_{01} mode.
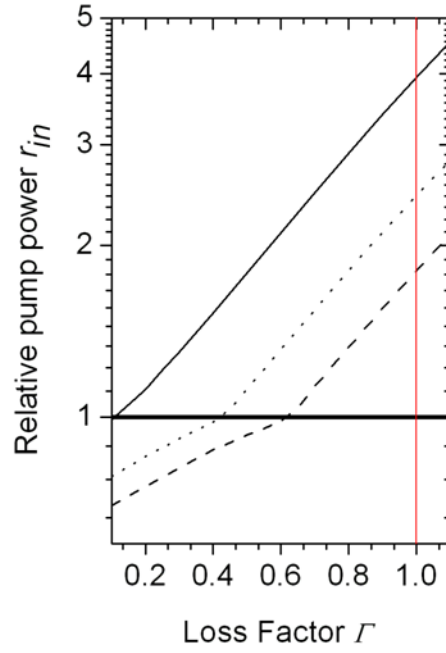
Figure 5.3 The relative pump power depends on pump shape factor *q*, the solid line is *q*=1.6, the dot line is *q*=2.2 and dash line is *q*=2.8. The red line is the loss factor limitation of 1.
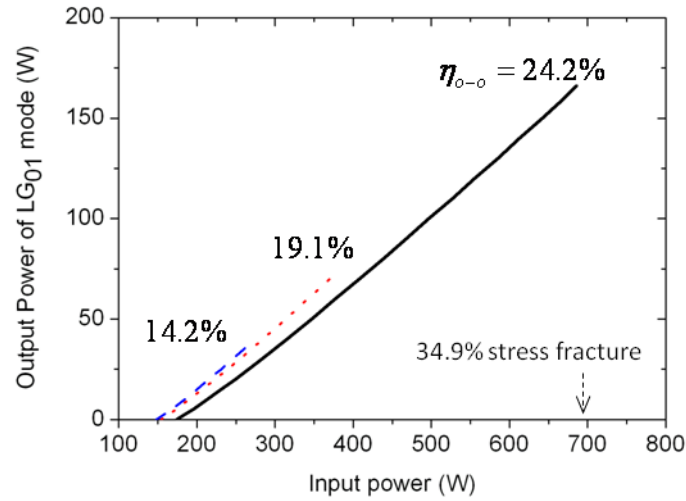

Figure 5.4 The input and output power of LG mode as $p=\sqrt{2}$. The solid line is *q*=1.6, the red dot line is *q*=2.2 and blue dash line is *q*=2.8. The lines of output power stop when HG_{00} begins to oscillate and become multi-mode output.

In Fig.5.3 we numerically calculate the *q* value and the power scaling under the condition of $p=\sqrt{2}$, $w_p = w_l = 1.5\,\text{mm}$, $\sigma = 3.3 \times 10^{-20}\,\text{cm}^{-2}$, $\tau_f = 0.951\,\text{ms}$, $f_u = 0.7$,

$f_l = 0.046$, $L_i^{LG_{01}} = 0.01$ and $L_T = 0.03$. The relative pump power is defined by

$r_{in} = P_{th,TEM_{00}}^{doughnut-pump} / P_{th,LG_{01}}^{doughnut-pump}$, the loss factor is $\Gamma = L_{i,T}^{HG_{00}} / L_{i,T}^{LG_{01}}$. The solid line is

q=1.6, the dot line is q=2.2 and dash line is q=2.8. The red line is the loss factor

limitation of $\Gamma = 1$. Apparently the scalability of q=1.6 is the best. When $\Gamma < 1$, it is

possible to scale to around 4 times of pump threshold. Even with a very low loss

factor, the doughnut mode keeps the minimum threshold compared with TEM$_{00}$

mode.

In order to achieve our design aim of 100 W CW output, we also calculate the

input and output power of LG$_{01}$ mode when $\Gamma = 1$ as shown in Fig.5.4.The solid line

is q=1.6with the optical to optical efficiency $\eta_{o-o} = 24.2\%$, the red dot line is q=2.2

with the optical to optical efficiency $\eta_{o-o} = 19.1\%$ and blue dash line is q=2.8 with

the optical to optical efficiency $\eta_{o-o} = 14.2\%$. The lines of output power stop when

HG$_{00}$mode begins to oscillate and become multi-mode output. The threshold is 174 W,

153 W and 148 W respectively. It is worthy to point out the importance of

re-absorption loss term $-N_l^0$, when q=1.6, $\Gamma = 1$ without $-N_l^0$ the threshold is 85

W, almost half of the condition with re-absorption loss. But the output power only can

scale to 92.5 W under 387 W pump power with the optical to optical efficiency

$\eta_{o-o} = 24\%$. It means with the re-absorption, the output power scale about 2 times,

the laser calculated performance comparison with re-absorption and without

re-absorption is shown in Fig.5.5.

It is clearly that with the help of pump distribution design and re-absorption loss.

166 W LG$_{01}$ mode output power is predicted in a compact diode edge-pumped laser

module. The maximum temperature on the top surface of microchip is calculated to be

120 deg, the maximum thermal induced equivalent stress is 134 Mpa, corresponding

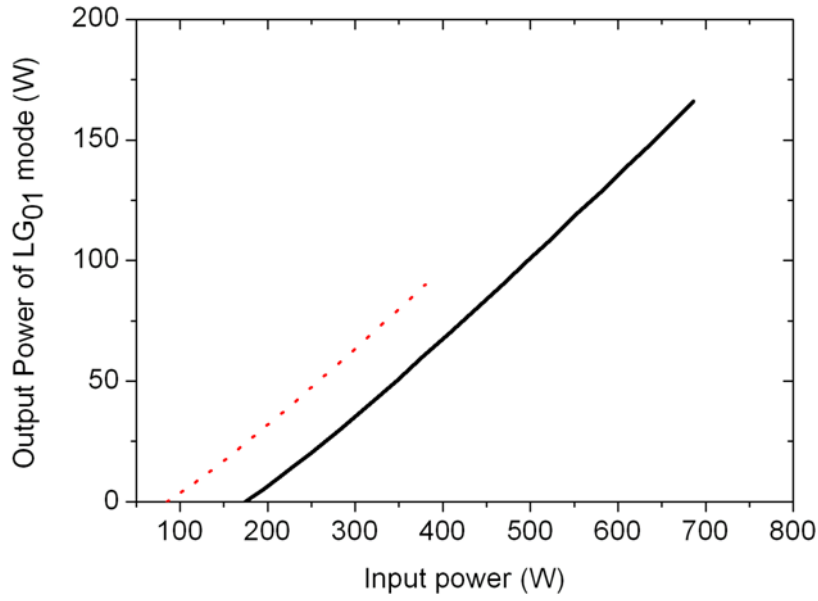to 34.9% stress fracture, if considering 384 Mpa is the ceramic YAG damage

threshold[2].

Figure 5.5 The input and output power of LG mode as p=$\sqrt{2}$ and q=1.6, the solid line is with reabsorption term. The dot line is no reabsorption term. The lines are stopped by HG$_{00}$ mode reaches the threshold and become multi-mode oscillation.

5.3 Conclusion

In this chapter, we propose the design of high power vortex mode based on mode-selection theory. We explain the power scalability influenced by pump shape. The re-absorption loss is considered to be useful for preventing from the secondary mode reaching threshold, thus it is helpful for power scaling. The high-average power is the foundation for pulsed operation. By achieving a stable and high power mode, the future towards pulsed operation should be promising.

---

[1]J. W. Kim, J. I. Mackenzie, J. R. Hayes, and W. A. Clarkson, "High power Er:YAG laser with radially-polarized Laguerre-Gaussian (LG01) mode output," Opt. Express 19, 14526-14531 (2011)

[2] Tsunekane, Masaki, and TakunoriTaira. "High-power operation of diode edge-pumped, composite all-ceramic Yb: YAlO microchip laser." Applied physics letters 90 (2007): 121101.

Chapter 6

Conclusion

While it was always a headache that the side- or edge- pump have the edge-peak pump shape, we have proposed the way to central peak Gaussian-like pump shape for fundamental mode generation as well as to become advantage in high-order modes generation. So far, the efficient high-power fundamental mode operation has only demonstrated in face-pumped thin disk laser. Since the current research has already figured out the pump shape and mode control theory, it is only the matter of time to solve several practical problems that mentioned in chapter 3. In future, the efficient high-power fundamental mode operation in edge-pumped Yb:YAG ceramic microchip laser module could be expected.

In addition, this research is also on high-order modes control and generation towards high power. The topic is attractive in recent years that related to high-order modes like HG modes, LG_{01} mode and vortex arrays. In Table 6.1, key index of reported research related with our topic of HG modes and vortex array modes are listed, most of the experiments in the table were carried out by using diode end-pump (e-p) scheme and Nd^{3+} doped gain material or side-pump (s-p) scheme and Yb^{3+} doped gain material. Our research is cited as the reference 9. Although our laser is the preliminary design for mode-selection, the results have obviously advantage both in the available modes type and output power.

The current research uses Yb:YAG as gain material, it is always effective for high peak power mode-locking and passive Q-switched operation by using saturable

absorber (SESAM and Cr:YAG). The edge-pump scheme supports such a configuration that the cooling is efficient and the pump will not be blocked.

Mentioned to practice applications[1] of DPSSLs, the good pointing stability, less power fluctuations and easy-operation of transverse modes are very important. The microchip laser has the advantage in heat management for mode stabilization, the edge-pump scheme makes the mode-selection as gain-guiding but not heat guiding. Besides, the laser system could be dramatically simplified by the diode pump lens-less design, that increase the reliability and reduce the cost from a practical perspective.

Table 6.1 Mode-selection in DPSSL

Gain material, pump scheme	Mode-selection method	Available modes	Laser properties	Ref.
HG modes selection ($n>1$)				
Nd:YAG, e-p	Off-axis pump	HG_{n0}, n=1-90	cw,mW, 1064 nm	2
Nd:YAG, e-p	Off-axis pump	HG_{n0}, n=1-12	cw,mW, 1064 nm	3,4
Nd:GdVO$_4$,e-p	Off-axis pump	HG_{n0}, n=1-4	cw, mW, 1064 nm	5
Nd:GdVO$_4$,e-p	Off-axis pump	HG_{n0}, n=1-9	3.5Ghz, 350-780mW, 20-25ps 1064 nm	6
Nd:GdVO$_4$,e-p	Off-axis pump Opaque-wire-inserted	HG_{nm}, n,m=1-5	cw, mW, 1064 nm	7
Yb:YAG, s-p	Gain-distribution	HG_{n0}, n=1-40	cw, mW, 1030 nm	8
Yb:YAG, s-p	Gain-distribution	HG_{n0}, n=1-22 HG_{nm}, n,m=1-6	cw, mW-several W, 1030 nm	9
Vortex arrays modes selection				
LiNdP$_4$O$_{12}$, e-p	Shaped pump	many kind of vortex arrays, with large vortex pixels	cw, mW, 1048 nm	10
Nd:GdVO$_4$,e-p	Outside-cavity interferometer	Square-vortex arrays	cw, mW, 1064 nm	7
Yb:YAG, s-p	Gain-distribution	many kind of vortex arrays	cw, mW-several W, 1030 nm	9
*Note: mW in the table generally less than 100 mW				

[1]Neuman, Keir C., and Steven M. Block. "Optical trapping." Review of scientific instruments 75.9 (2004): 2787-2809.

[2]Laabs, H., &Ozygus, B. (1996).Excitation of Hermite Gaussian modes in end-pumped solid-state lasers via off-axis pumping. Optics & Laser Technology, 28(3), 213-214.

[3]Y. F. Chen, T. M. Huang, C. F. Kao, C. L. Wang, and S. C. Wang, "Generation of Hermite–Gaussian Modes in Fiber-Coupled Laser-Diode End-Pumped Lasers," IEEE J. Quantum Electron.33(6), 1025–1031 (1997).

[4]Y. F. Chen, T. M. Huang, K. H. Lin, C. F. Kao, C. L. Wang, and S. C. Wang, "Analysis of the effect of pump position on transverse modes in fiber-coupled laser-diode end pumped lasers," Opt. Commun.136(5-6), 399–404 (1997).

[5]S.-C. Chu, T. Ohtomo, and K. Otsuka, "Generation of doughnut like vortex beam with tunable orbital angular momentum from lasers with controlled Hermite-Gaussian modes," Appl. Opt.47(14), 2583–2591 (2008).

[6]H. C. Liang, Y. J. Huang, Y. C. Lin, T. H. Lu, Y. F. Chen, and K. F. Huang, "Picosecond optical vortex converted from multi gigahertz self-mode-locked high-order Hermite-Gaussian Nd:GdVO4 lasers," Opt. Lett. 34, 3842-3844 (2009)

[7]Shu-Chun Chu, Yun-Ting Chen, Ko-Fan Tsai, and Kenju Otsuka, "Generation of high-order Hermite-Gaussian modes in end-pumped solid-state lasers for square vortex array laser beam generation," Opt. Express 20, 7128-7141 (2012)

[8]Koki Shimohira, Yuichi Kozawa, and Shunichi Sato, "Transverse mode control by manipulating gain distribution in a Yb:YAG ceramic thin disk," Opt. Lett. 36, 4137-4139 (2011)

[9] Weipeng Kong, Atsushi Sugita, and Takunori Taira, "Generation of Hermite–Gaussian modes and vortex arrays based on two-dimensional gain distribution controlled microchip laser," Opt. Lett. 37, 2661-2663 (2012)

[10]Kenju Otsuka and Shu-Chun Chu, "Generation of vortex array beams from a thin-slice solid-state laser with shaped wide-aperture laser-diode pumping," Opt. Lett. 34, 10-12 (2009)

Appendix A

Four-direction diode stacks edge-pumped microchip laser

In the chapter 1 and chapter 2, we mentioned the four-direction diode stacks edge-pumped microchip laser modules in our group; it was originally designed for the application of high-power laser processing. In 2007, we got 414 W output power at multi-mode CW operation by the type A all ceramic composite Yb:YAG microchip. In 2012, 1.0 μJ-pulse energy for 21W-average power mode-locked laser was obtained by a wedged composite microchip. Here we will introduce some details as appendix of main content.

In fig.A.1, we compare the (a) diode stacks pumped microchip scheme with (b) diode chips pumped microchip scheme.
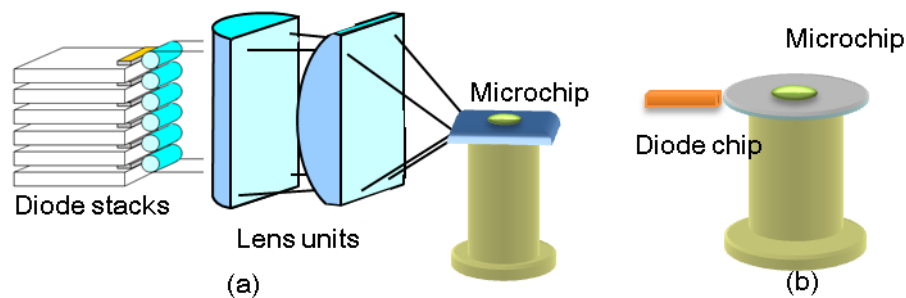

Figure A.1 (a) Diode stack pumped scheme and (b) diode chip pump scheme

Several key technologies we use in our laser system including: (a) partial metallization on composite microchip bottom; (b) micro-finger structure water-cooling heat sink; (c) precise die-bonding system for no defect Au-Sn bonding layer. (d) edge-pumped optical design and laser module design. They are shown in Figure A.2. To point out that, in diode chip pumped laser module, we use the same technologies as mentioned above.

It is obviously that the diode chip pump is more compact and simple, but so far the pump power cannot comparable with diode stacks, as diode stacks can give over 1000 W pump. For long time, we are focusing on these diode stacks pumped laser module because of the high pump power. The mutli-mode input and output compared with fundamental mode operation are shown in Fig A.3 with the microchip serial number #0704 (Type A microchip, wedged 0.1 deg.) The multi-mode laser cavity is plan-concaved cavity with 200 mm long and T=3%, R=250mm output coupler. The fundamental mode laser cavity is 3.1 m long and T=3% flat output coupler. The pump power is controlled below 450 W for safe operation. The output power of microchip

various from piece to piece with the range from multi mode 80~120W at the pump power of 450 W.
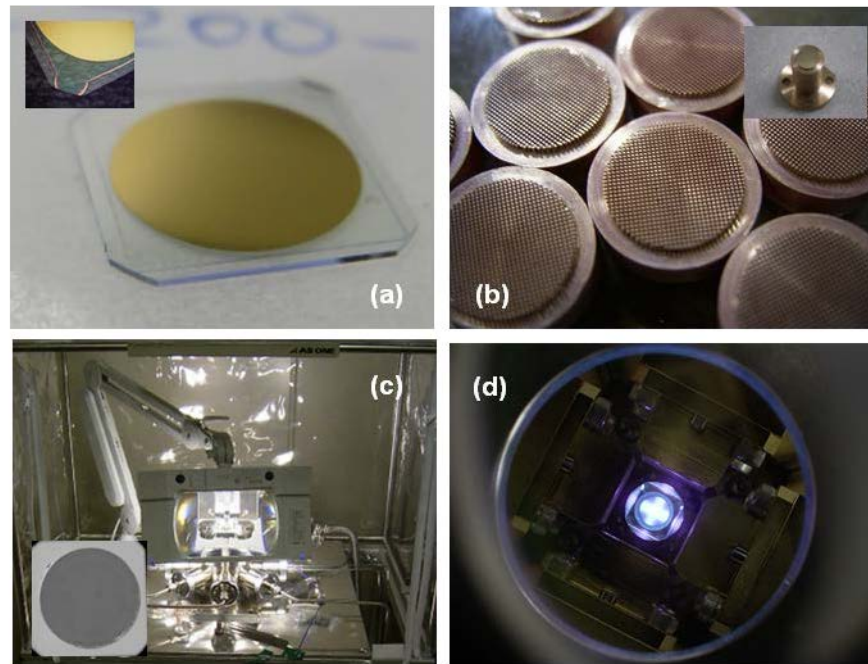

Figure A.2 Technologies we use in our laser system including: (a) partial metallization on composite microchip bottom; (b) micro-finger structure water-cooling heat sink; (c) precise die-bonding system for no defect Au-Sn bonding layer. (d) edge-pumped optical design and laser module design.
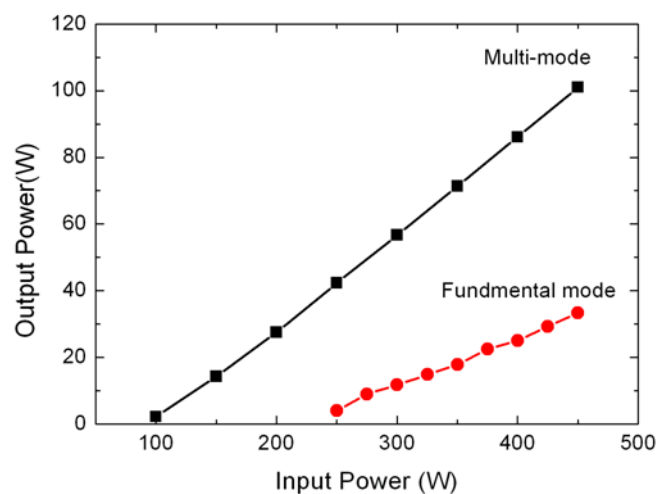

Figure A.3 The output power of multi-mode and single fundamental mode as a function of input power in diode stacks edge-pumped laser module with microchip #0704.

Appendix B

The pump shapes of theory simulation and real laser modules

In chapter 2-3, we use several ideal pump shapes for simulation, and we also simulate several pump shapes based on the edge-pumped microchip laser. Here, we will make a summary of these kinds of pump shapes. In Fig.B.1 we show the theory simulation pump shape of (a) ideal Gaussian; (b) ideal top-hat, (c-d) super-Gaussian (q=4, 6); (e-f) 4-direction diode stacks pump shape (absorption coefficient α=0.3 and 0.9 mm^{-1}); (g-h) optimized 27-direction diode bare chips pump shape (α=0.3 and 0.9 mm^{-1}).
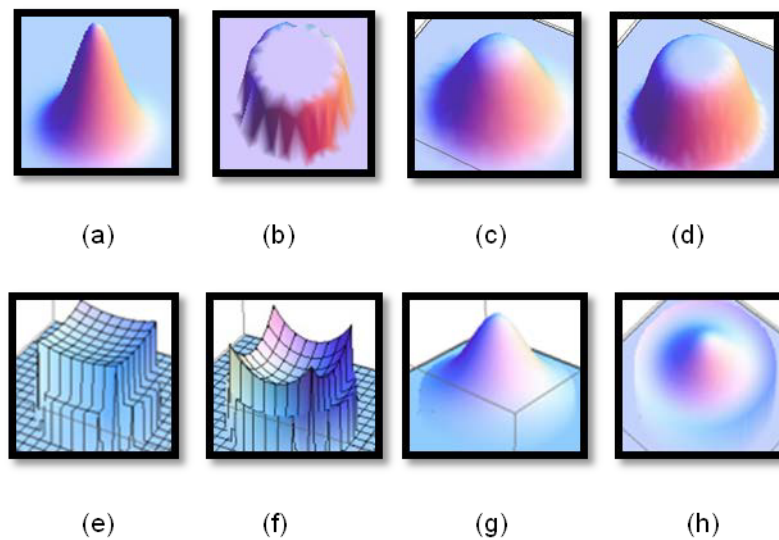

Figure B.1 theory simulation pump shape of (a) ideal Gaussian; (b) ideal top-hat, (c-d) super-Gaussian (q=4, 6); (e-f) 4-direction diode stacks pump shape (absorption coefficient α=0.3 and 0.9 mm^{-1}) ; (g-h) optimized 27-direction diode bare chips pump shape (α=0.3 and 0.9 mm^{-1}).

In the chapter 1 and 2, we mentioned the four-direction diode stacks edge-pumped microchip laser modules and the top-hat even basin pump shape. We also mention other pump shape in thin-disk mode-locking laser modules. Here we will show the pump shape of our edge-pumped laser module in Institute for Molecular Science (IMS) and the pump shape of thin-disk laser in Max-Plank-Institute fur Quantenoptik institute (MPQ) to see the difference of multi-mode aim designed pump shape and mode-locking aim designed pump shape. Both of the figures are fluorescence image taken by CCD camera. Fig. B.2 (a) The thin disk laser under 15 W pump power with the pump size of about 2.5 mm diameter and (b) the microchip laser

under 50 W pump power with the pump size of 3 mm. Obviously, the thin-disk mode-locking laser has a Gaussian peak in the center which are quite similar with the optimized pump shape in Fig.B.1 (h).
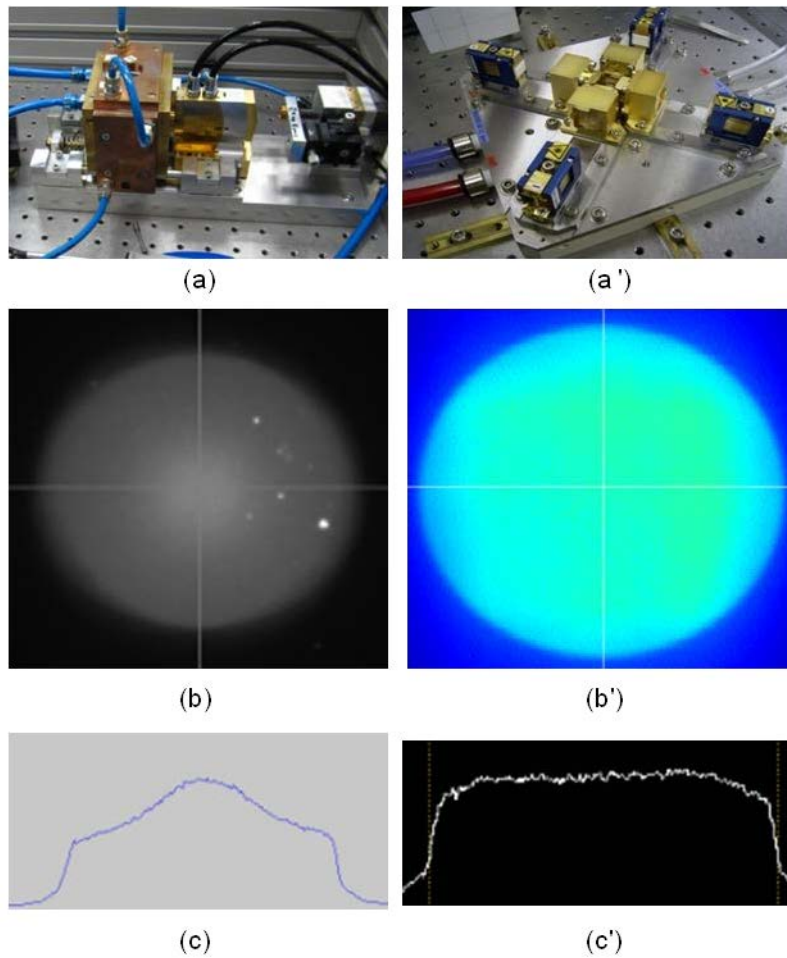

Figure B.2 (a) Thin disk mode-locking laser module in MPQ; (b,c) the 2-D and cross line profile of fluorescence in thin-disk laser; (b', c') the 2-D and cross-line profile of fluorescence in microchip laser

Appendix C

Diode bar edge-pumped passive Q-switched Nd:YAG microchip laser

As mentioned in the main content, the high-average power operation of transverse modes is promising in edge-pumped microchip laser system. As soon as the mode selection theory is clear, it is possible to design the efficient and compact high-average power laser module for fundamental mode or certain high-order mode generation. In addition, more than 150 W CW high power vortex mode laser module is predicted in chapter 5. It is the fundamental of high average power pulsed operation. The pulsed vortex mode has a lot of applications in material processing, super-resolution microscopes and plasma physics. Yb:YAG material is suitable for sub-ps to several ps mode-locking laser and several hundred ps passive Q-switched laser generation. Since intense pulsed optical vortex in ps range will be very useful. Here we introduce the Nd:YAG microchip laser as appendix for better understanding of diode bar edge-pumped scheme and as an example of pulsed high-order beam generation.

Figure C.1 shows the schematic of the diode edge-pumped Nd:YAG/Sm:YAG composite all-ceramic microchip laser. The central round shape core with a 2mm diameter is 1.5at% Nd doped ceramic YAG. To suppress the parasitic oscillation in the microchip, the core is surrounded by 5at% Sm doped ceramic YAG as an absorber at 1064nm which is often used as an ASE absorber. Sm:YAG strongly absorbs the laser light at 1064nm but is fully transparent for the pump light at 808nm. Then we can employ Sm:YAG not only as an absorber of parasitic oscillation but also as a pump waveguide. The thickness of the microchip is 0.25mm and bonded on a Cu-W heat-sink.

By using 80% transparence Cr:YAG inserted into the laser cavity, 90% output

coupler and 3.8 mm cavity length. We can get pulsed vortex mode (need to adjust the cavity mirror) output with 0.29 mJ pulse energy and 683 ps pulse duration. The beam shape and measured pulse duration are shown in Fig.C.2. In future, it could be quite interesting to use Yb:YAG replace current Nd material.
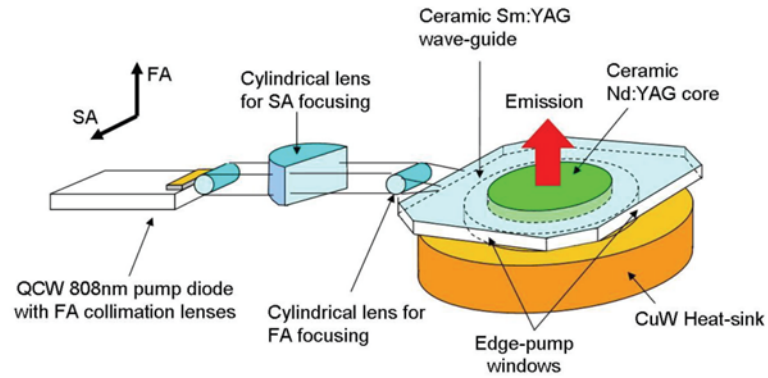

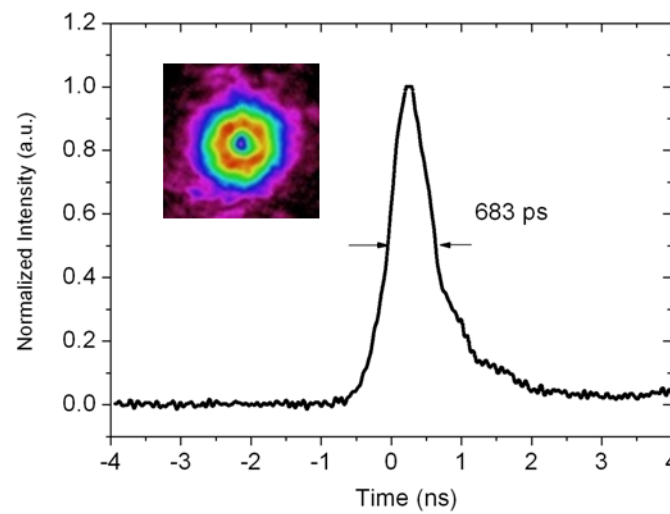Figure C.1 The schematic of diode bar edge-pumped passive Q-switched Nd:YAG microhip laser.

Figure C.2 The vortex beam pattern and pulse duration of edge-pumped passive Q-switched Nd:YAG microhip laser.